Title

Cold shock domain–containing protein E1 is a posttranscriptional regulator of the LDL receptor

Journal

Science Translational Medicine, 14(662)

ISSN

1946-6234

Authors

Smith, Geoffrey A
Padmanabhan, Arun
Lau, Bryan H
et al.

Publication Date

2022-09-14

DOI

10.1126/scitranslmed.abj8670

Peer reviewed

Science Translational Medicine AAAS

Submitted Manuscript: Confidential template updated: February 28 2012

Title: CSDE1 is a Post Transcriptional Regulator of the LDL Receptor

Authors: Geoffrey A. Smith[1†‡], Arun Padmanabhan[2,3,4†], Bryan H. Lau[5], Akhil Pampana[6,7], Li Li[8], Y. Clara Lee[4], Angelo Pelonero[4], Tomohiro Nishino[4], Nandhini Sadagopan[2,3,4], Vivian Q. Xia[3,9], Rajan Jain[8,10], Pradeep Natarajan[6,7,11], Roland S. Wu[2,3,5§], Brian L. Black[5], Deepak Srivastava[4,12,13], Kevan M. Shokat[1,14], John S. Chorba[3,9*]

Affiliations:

[1]Department of Cellular and Molecular Pharmacology, University of California, San Francisco CA

[2]Division of Cardiology, UCSF Health, San Francisco CA

[3]Department of Medicine, University of California, San Francisco CA

[4]Gladstone Institute of Cardiovascular Disease, San Francisco CA

[5]Cardiovascular Research Institute, University of California, San Francisco CA

[6]Cardiovascular Research Center, Massachusetts General Hospital, Boston MA

[7]Program in Medical and Population Genetics, Broad Institute of Harvard and MIT, Cambridge MA

[8]Department of Medicine and Penn Cardiovascular Institute, University of Pennsylvania, Philadelphia PA

[9]Division of Cardiology, Zuckerberg San Francisco General Hospital, San Francisco CA

[10]Department of Cell and Developmental Biology, Institute of Regenerative Medicine, and Penn Epigenetics Institute, University of Pennsylvania, Philadelphia PA

[11]Department of Medicine, Harvard Medical School, Boston MA

[12]Departments of Pediatrics, and Biochemistry and Biophysics, University of California, San Francisco CA

[13]Roddenberry Center for Stem Cell Biology and Medicine at Gladstone, San Francisco CA

[14]Howard Hughes Medical Institute, University of California, San Francisco CA

*To whom correspondence should be addressed: john.chorba@ucsf.edu

†Drs. Smith and Padmanabhan contributed equally.

‡Present Affiliation: Dana-Farber Cancer Institute, Boston MA

§Present Affiliation: Amgen, South San Francisco CA

One Sentence Summary: A genome-wide CRISPRi screen identifies CSDE1 as a key regulator of hepatic *LDLR* mRNA decay *in vivo*, making it a promising target for heart disease.

Abstract: The low-density lipoprotein receptor (LDLR) controls cellular delivery of cholesterol and clears LDL from the bloodstream, protecting against atherosclerotic heart disease, the

leading cause of death in the United States. We therefore sought to identify regulators of the LDLR beyond the targets of current clinical therapies and known causes of familial hypercholesterolemia. We show that Cold Shock Domain-Containing Protein E1 (CSDE1) enhances hepatic *LDLR* mRNA decay via its 3' untranslated region and regulates atherogenic lipoproteins *in vivo*. Using parallel phenotypic genome-wide CRISPR interference screens in a tissue culture model, we found 40 specific regulators of the LDLR left unidentified by observational human genetics. Among these, we show that, in HepG2 cells, CSDE1 regulates the LDLR at least as strongly as the targets exploited by the best available clinical therapies: statins and PCSK9 inhibitors. Additionally, we show that hepatic gene silencing of *Csde1* treats diet-induced dyslipidemia in mice similar to that of *Pcsk9* silencing. Our results suggest the therapeutic potential of manipulating a newly identified factor in the post-transcriptional regulation of the *LDLR* mRNA for the prevention of cardiovascular disease. We anticipate that our approach of modeling a clinically relevant phenotype in a forward genetic screen, followed by mechanistic pharmacologic dissection and *in vivo* validation, will serve as a generalizable template for the identification of therapeutic targets in other human disease states.

Introduction

The low-density lipoprotein receptor (LDLR) delivers cholesterol from low-density lipoprotein (LDL) to cells to maintain membrane homeostasis *(1)*. By clearing atherogenic LDL from the bloodstream, the hepatic LDLR protects against atherosclerotic heart disease *(2, 3)*. Despite successful therapies that upregulate the hepatic LDLR and reduce heart attacks *(4)*, cardiovascular disease remains the leading cause of death in Western countries *(5)*. Lowering LDL beyond that achieved by 3-hydroxy-3-methylglutaryl coenzyme A (HMG-CoA) reductase inhibitors (statins) improves clinical outcomes without adverse effects *(6, 7)*. Though there is a theoretical concentration at which LDL could get too low *(8)*, this has yet to be discovered in large randomized trials *(9, 10)*. Whether other LDLR regulatory mechanisms could be leveraged to further treat heart disease remains unknown.

The genetics of familial hypercholesterolemia (FH), which manifests as an isolated elevation in serum LDL, underlies the clinical success of LDLR upregulation by statins and proprotein convertase subtilisin/kexin type 9 (PCSK9) inhibitors. Estimates suggest that 20-40% of FH phenotypes remain unexplained outside of the four major causes: *LDLR*, *APOB*, *PCSK9*, and *LDLRAP1 (11, 12)*. Though polygenic causes drive some unexplained phenotypes *(13–15)*, additional regulators of the LDLR may still exist. Advances in forward genetics *(16–18)* can now enable searches for tissue and disease-specific effects across the entire genome that may elude the sporadic natural variants found in observational studies, which themselves require compatibility throughout the entire lifespan and in all cell types. Moreover, hepatic delivery of gene silencing agents is effective in the clinic *(19)*, providing a therapeutic modality against hits whose phenotypes are driven by expression in the liver. We therefore employed a genome-wide clustered regularly interspaced short palindromic repeats interference (CRISPRi) screen for

factors involved in hepatic LDLR regulation, both to understand the biology of this important receptor and to uncover potential therapeutic targets in cardiovascular disease.

Results

A Genome-Wide CRISPR Interference Screen for LDL Receptor Regulation

We engineered the HepG2 cell line, which models the regulation of the LDLR *(20–24)*, to constitutively express a dCas9-KRAB fusion protein, enabling the knockdown of any given gene with an appropriate single guide RNA (sgRNA, Fig. 1A) *(16, 17, 25)*. Because statins *(26, 27)* and PCSK9 inhibitors *(28–30)* increase cell surface LDLR, we scored surface LDLR abundance. To focus on factors that preferentially affect the LDLR over other receptors, we performed a parallel screen for regulators of the transferrin receptor (TFR). This critical player in iron metabolism shares a clathrin-mediated intake mechanism, but is otherwise orthogonally regulated from the LDLR *(31, 32)*. Prior to our screen, we confirmed both dCas9-KRAB activity and an appropriate dynamic range for both LDLR and TFR regulation by transduction with sgRNAs expected to alter receptor abundance in either direction (Fig. S1) *(33, 34)*.

We next performed our pooled screens in parallel by transducing a library encoding sgRNAs with 5-fold coverage of the entire protein-coding human genome *(17)*. We then selected the cells at the upper and lower third of receptor abundance by fluorescence-activated cell sorting (FACS) and quantified the sgRNAs for each population via deep sequencing (Fig. S2, Tables S1-S4). We compared the degree of enrichment of LDLR or TFR surface amounts in the high abundance to the low abundance cells (defined as ρ, Fig. 1B). We also compared the high and low receptor abundance cells to the unsorted population (defined as τ or γ, respectively) and included these results in our final hit count. This resulted in 130 total hits for the LDLR and 186

hits for the TFR (Tables S5-S6). We hypothesized that hits with shared phenotypes would likely have global effects on surface receptors, leaving us with 117 hits specific for LDLR regulation (Fig. 1C, Table 1). Gene ontology (GO) analysis *(35)* revealed a 15-fold enrichment for cholesterol metabolism as a biologic process (11 total hits, $p = 5.7 \times 10^{-10}$), providing confidence that we recapitulated our target biology. The hits also included 48 members of potentially druggable protein classes, including 29 with proposed enzymatic activity, and 22 hits were unclassified in GO databases (Fig. S3A).

Cross-referencing Human Genetic Datasets Identifies LDLR Regulators in vivo

We next compared genes associated with serum LDL cholesterol (LDL-C) from published genome-wide association studies (GWAS) *(36–38)* to our list of hits. Intriguingly, only 13 of these genes overlapped with our results (Fig. 1D), even when we relaxed our threshold for hit selection. To improve power for multiple hypothesis testing across the entire genome, we turned to 390,375 UK Biobank participants with genome-wide genotypes and known plasma lipids (Table S7) to search for variants associated with LDL-C amongst only our hits *(39)*. We filtered to nonsynonymous protein coding variants in these hits by a threshold minor allele frequency (>0.001) and minimum statistical significance ($p = 0.000427$, Table 2). For *BCAM*, we found both an association between higher LDL-C and a nonsense variant, along with bidirectional associations between LDL-C and missense variants, suggesting that this pathway may be tunable. We also found associations between elevated LDL-C and variants in *MSMO1*, *C6orf132*, *HNF4A*, and *TIMELESS*, suggesting that these hits may be functional in the human and warrant further evaluation. The results also suggest that the accessible "genomic space" of the CRISPRi and GWAS strategies is only partially overlapping.

Regulators of Surface LDL Receptor Abundance Affect Functional Uptake of LDL

To validate our screen results, we generated CRISPRi HepG2 cells harboring either of the two top-scoring sgRNAs for 77 of our hits as well as established controls. We preferentially tested hits with an increase in surface LDLR upon inhibition, as well as those with potentially druggable functions or lacking associated GO terms. Since surface receptor abundance might not necessarily correlate to increased function, we evaluated both LDLR and TFR surface phenotypes alongside LDL uptake *(40)*. This functional assay involves a pulse treatment of exogenous, fluorophore-labeled LDL followed by a similar flow cytometric readout. Lastly, as knockdowns could also cause growth phenotypes, we assayed the number of cells surviving to FACS analysis as a proxy for viability.

We recapitulated the phenotypes for receptor abundance for at least one of the guides in most of the hits (55 genes, 71% of those tested, Table S8). Moreover, for 40 of these genes, both sgRNAs independently validated, suggesting against an off-target effect. We visualized these hits based on their effects, at single cell resolution, on LDLR and TFR abundance, the LDLR/TFR ratio, functional LDL uptake and number of cells surviving to analysis (Figs. 2, S3B). Notably, in this tissue culture model, most knockdowns had independently validated effects on LDLR abundance and LDL uptake of similar or greater magnitude than our *HMGCR* or *PCSK9* controls.

Knockdown of hits expected to alter cellular cholesterol balance or transcriptionally regulate the LDLR showed directionally consistent effects between LDLR abundance and function (Fig. 2). For genes in the enzymatic pathway of cholesterol metabolism *(41)* (*HMGCS1* and *MSMO1*), this is consistent with activation of sterol regulatory element-binding protein 2 (SREBP2) mediated *LDLR* transcription. For genes encoding certain transcription factors (*HNF1A (42)*, *HNF4A (43)*, *ONECUT1 (44)*, and *ZEB1 (45)*), this is consistent with an effect on

LDLR transcription itself. Knockdowns of *SLC25A27*, which encodes a mitochondrial uncoupling protein *(46)*, and *ABCA4*, encoding a known lipid transporter *(47)*, both exhibited reductions in LDLR abundance and function (Fig. 2). These genes could plausibly induce a negative lipid balance, increasing LDL uptake via both LDLR-dependent and independent mechanisms.

Targeting of hits that either affect multiple transcriptional pathways or regulate endocytosis showed opposite effects on LDLR abundance and function. Knockdown of *TRIB1*, a GWAS hit *(36)* encoding a pseudokinase that regulates the constitutive photomorphogenic (COP1) E3 ligase *(48, 49)* and affects multiple transcription factors *(50)*, showed this phenotype. In the mouse, *TRIB1* overexpression lowers serum cholesterol, while the knockout has the opposite effect *(51, 52)*, consistent with our results. Knockdown of *AP2M1*, a TFR screen hit that encodes an adaptor protein required for endocytosis *(53)*, was similar, consistent with an accumulation of non-functional receptors at the cell surface. This phenotype, though specific to the LDLR, was also seen with knockdown of *BCAM*, which encodes a membrane cell adhesion molecule *(54)* identified by GWAS *(38)*, and *TMEM217*, which encodes an uncharacterized transmembrane protein (Figs. 2, S4). This suggests that these proteins could have a similar endocytosis adaptor function specific for the LDLR, akin to *LDLRAP1 (55)*, in which mutations cause a recessive form of FH.

Pharmacologic Inhibition of Clinically Relevant Pathways Provides Mechanistic Insight into Putative LDLR Regulators

We next turned to pharmacologic approaches to perturb specific pathways of LDLR regulation. We hypothesized that hits might alter cholesterol metabolism, LDLR recycling, or a yet unspecified pathway. By combining CRISPRi knockdown with either a statin, to inhibit

endogenous cholesterol biosynthesis *(56, 57)*, or a PCSK9 inhibitor, to arrest LDLR lysosomal degradation *(30)*, and assessing the combined effect, we inferred mechanistic information about the target gene. Furthermore, we hypothesized that either additive or potentiating effects between a clinically validated therapy and a hit gene might suggest promising therapeutic targets.

We evaluated the receptor abundance and function phenotypes for 29 of our validated hits in the presence or absence of a statin *(58)* or PF-846, a selective inhibitor of PCSK9 translation *(59, 60)* (Fig. 3, Table S9). We calculated a synergy score by subtracting the differential effects of CRISPRi knockdown, compared to the control, in the presence of compound from that with the dimethyl sulfoxide (DMSO) vehicle. A more positive value indicated synergy and a more negative value indicated antagonism.

Upon knockdown, regulators of cholesterol biosynthesis (*SREBF2*, *HMGCR*, *HMGCS1*, *MSMO1*, and *PMVK*) showed antagonism with the statin, but mild synergy with PCSK9 inhibition (Fig. 3). The antagonism with statins is expected, given that SREBP2 drives *LDLR* transcription. Because SREBP2 also induces *PCSK9* expression, knockdown of these genes raises total PCSK9, explaining both the synergy with PCSK9 inhibition we observe here and that observed with statins in the clinic *(61)*. The synergy phenotypes for knockdown of *MRPL16*, which encodes a structural component of the mitochondrial ribosome *(62)*, mirrored these cholesterol biosynthetic genes (Fig. 3), suggesting that MRP-L16 may play a role in the mitochondrial generation of metabolic precursors to sterol biogenesis. In contrast, *C6orf132* knockdown showed the opposite phenotype: mild synergy with a statin, and mild antagonism with PF-846 (Fig. 3). Given that C6orf132 localizes to the Golgi *(63)*, this suggests it may function by facilitating LDLR delivery to the cell surface, prior to any interaction with extracellular PCSK9. For some transcription factors, the synergy phenotypes can point to their

downstream targets. For example, synergy of *HNF1A* knockdown with a statin (Fig. 3) is consistent with disruption of hepatocyte nuclear factor 1-alpha (HNF1-α) mediated *PCSK9* transcription *(64)*.

CSDE1 Regulates the Stability of LDLR mRNA

One of our strongest hits, *CSDE1*, also known as upstream of N-ras (UNR), encodes an RNA binding protein with varied regulatory functions *(65–67)*, including mRNA decay *(68)*. As the *LDLR* 3' untranslated region (UTR) consists of adenylate-uridylate (AU)-rich elements (AREs) implicated in mRNA stability *(69)*, we hypothesized that CSDE1 could mediate the degradation of the *LDLR* transcript, thereby explaining its observed receptor abundance, function, and synergy phenotypes.

In the setting of *CSDE1* knockdown, we observed increased LDLR abundance in both sterol-replete and sterol-depleted conditions (Fig. 4A). Moreover, we observed progressively higher LDLR amounts with sterol-depletion and the addition of a statin (Figs. 4A, S5A-C), suggesting that the mechanism of *CSDE1* disruption is at least additive with SREBP2-mediated *LDLR* transcription and statin therapy. We reproduced our flow cytometry results with immunoblots against both total and surface LDLR, capturing the latter via a cell-surface biotinylation assay (Fig. S6). HepG2 cells transfected with *CSDE1*-targeting small interfering RNA (siRNA) exhibited similarly increased LDLR abundance and LDL uptake to the CRISPRi results (Fig. S7). siRNA against *CSDE1* increased both *LDLR* transcripts in Huh7 cells (Fig. S8) and LDL uptake in primary mouse hepatocytes (1.6-fold increase, $p = 0.0372$, Fig. S9A). Similar results were observed in primary mouse hepatocytes using adeno-associated virus serotype 8 (AAV8) delivered short hairpin RNA (shRNA) against *Csde1*, though these outcomes were not

statistically significant ($p = 0.373$, Fig. S9B). Together, these observations confirm that the effects of CSDE1 are not limited to a single cell line.

Returning to our CRISPRi HepG2 system, we generated a combined *CSDE1/LDLR* knockdown cell line harboring sgRNAs against each target *(70)*. As expected, the double knockdown had no additional effect on surface LDLR as compared with the *LDLR* knockdown alone (Fig. S10A&C). However, the double *CSDE1/LDLR* knockdown exhibited a small but significant increase in LDL uptake ($p < 0.0001$) compared with the single *LDLR* knockdown ($CSDE1^{nonLDLR}$, Figs. 4B, S10B&D). This LDLR-independent effect constituted about 40% of the total increase of LDL uptake driven by *CSDE1* knockdown in the *LDLR* sufficient background. Both LDLR-dependent ($CSDE1^{LDLR}$) and LDLR-independent components of CSDE1's effect on LDL uptake were additive with and unaffected by sterol-depletion and statin therapy ($SREBP2^{LDLR}$, Figs. 4B, S10B&D). Further, there was no significant difference in the magnitude of LDL uptake between that driven solely from the LDLR-dependent mechanism of CSDE1 and the sterol-depletion and statin ($p = 0.9002$, see pie chart, Fig. 4B). Yet in contrast to its equivalent effect on LDL uptake, *CSDE1* knockdown was less effective at upregulating surface LDLR than SREBP2 activation (Figs. S10A&C), raising the possibility that *CSDE1* knockdown may also result in a more functional LDLR. Taken together, these data suggest that the main effect of CSDE1 on LDL uptake is LDLR-dependent, with an additional but smaller LDLR-independent effect also present.

We next observed that overexpression of isoform 1 of CSDE1, but not isoforms 2 through 4, reduced surface LDLR in HepG2 cells (Figs. 4C, S11A-D). Overexpression of all four isoforms of CSDE1 downregulated LDLR abundance in the *CSDE1* CRISPRi knockdown cells, though isoform 1 showed the strongest effect (Fig. S11E-I). The opposing directional effects of

CSDE1 knockdown and overexpression suggest that, under physiologic expression conditions, isoform 1 of CSDE1 is a rate-limiting regulator of the LDLR.

Consistent with our mechanistic hypothesis, we noted over a 2-fold increase in steady-state *LDLR* mRNA (Fig. 4D), as well as depleted CSDE1 (Figs. 4D, S6A), in the *CSDE1* knockdown cells (Fig. 4D). Among control mRNA targets, we also observed significant increases in *MYLIP* and *KHSRP* mRNA ($p < 0.0001$), but not in *SREBF2*, *PCSK9*, *HMGCR*, or *TFRC* mRNA (Fig. 4D). The gene products of *MYLIP* and *KHSRP* downregulate the LDLR *(33, 71)*, which is the opposite of our observed phenotype, suggesting that the direct effect of *CSDE1* knockdown on the *LDLR* mRNA predominates in our tissue culture model. To specifically evaluate transcriptional decay, we treated cells with actinomycin D and measured *LDLR* transcripts over time. We observed significantly higher *LDLR* mRNA in the *CSDE1* knockdown cells at all subsequent timepoints ($p < 0.05$, Fig. 4E). The mRNA half-life, modeled by a single-phase decay equation, was nearly 1.5-fold longer for the *CSDE1* knockdowns compared to controls ($p = 0.0021$, Fig. 4E). Notably, *CSDE1* knockdown had no significant effect on *HMGCR*, *SREBF2*, or *TFRC* mRNA over time ($p > 0.05$, Fig. S12A-C). *CSDE1* knockdowns exhibited reductions in *PCSK9* and *KHSRP* mRNA at several timepoints, but the mRNA abundance over time did not fit a decay equation, suggesting against a CSDE1-mediated effect on transcript stability (Fig. S12D, F). By contrast, *CSDE1* knockdown showed a similar extension of transcript half-life on *MYLIP* mRNA as *LDLR* mRNA (Fig. S12E). This suggests that *MYLIP* may also be negatively regulated by CSDE1. Since the increase in *MYLIP* transcripts seen with *CSDE1* knockdown will downregulate the LDL receptor, the targeting of *MYLIP*, or its encoded protein inducible degrader of the LDL receptor (IDOL), could act synergistically with the targeting of CSDE1 in lowering LDL cholesterol.

To probe the relationship of CSDE1 to the *LDLR* 3' UTR, we transiently expressed luciferase constructs (Fig. 4F) under control of the native *LDLR* promoter in the *CSDE1* knockdown cells. The luciferase-only constructs showed appropriate physiologic upregulation by sterols, regardless of *CSDE1* knockdown (Fig. 4G). Constructs fused to the *LDLR* 3' UTR, but not those fused to the *LDLR* coding sequence alone, exhibited increased reporter activity with *CSDE1* knockdown (Fig. 4H). Notably, this increase in activity was attenuated by removing the first of four AREs *(69, 72)* from the 3' UTR (Fig. 4H). Activity of the 3' UTR-fused construct increased further with statin coadministration (Fig. 4I), suggesting that *CSDE1* knockdown may be synergistic with statins, consistent with our prior results (Fig. 3). Taken together, we conclude that under physiologic conditions, CSDE1 mediates decay of the *LDLR* mRNA through its 3' UTR, with the first ARE of the UTR required for its full effect.

Disruption of CSDE1 Upregulates Ldlr mRNA Expression and Protects from Cholesterol Loading in vivo

We then turned to an *in vivo* model in zebrafish, as the 3' UTR of its ortholog *ldlra* (XM_005163870.4) is highly AU-rich and contains at least two canonical ARE sequences for mRNA regulation *(73)*. The *ldlra* knockout in zebrafish results in hyperlipidemia and vascular lipid accumulation, and challenging larvae with a high cholesterol diet is sufficient to increase their overall cholesterol content *(74)*. We employed yolk microinjection of a Cas9-ribonucleoprotein (RNP) complex containing redundant guides to achieve near-saturation gene disruption *(75)*, followed with dietary cholesterol supplementation, and evaluated total cholesterol in the larvae *(74)*. Targeting of *csde1* protected against total cholesterol accumulation, with a modest (12%) but significant reduction ($p = 0.0017$) in total cholesterol in 8-day post fertilization (dpf) zebrafish, without any obvious phenotypic abnormalities (Fig. S13).

By contrast, targeting of *ldlra* showed the expected 1.4-fold increase in total larval cholesterol (Fig. S13), consistent with prior studies *(74)*.

To evaluate the *in vivo* effect of CSDE1 on lipoproteins more directly, we then turned to mouse models. We probed the effect of *Csde1* gene silencing in the mouse as a therapeutic proof-of-principle, given even greater homology between the 3' UTRs of the murine and human *LDLR* orthologs *(76)*. Using wild-type C57BL/6 mice, we delivered shRNA against *Csde1 (67)* or a scramble control via AAV8. One week after delivery of moderate dose AAV8 (3×10^{11} genomes/mouse), we harvested blood and tissue samples from the mice. We found that, compared to scramble controls, the *Csde1* targeted mice exhibited a ~30% reduction in hepatic *Csde1* mRNA and a ~1.8-fold increase in hepatic *Ldlr* mRNA (Fig. 5A) alongside robust expression of the enhanced green fluorescent protein (eGFP) reporter encoded by the AAV8 vector (Fig. S14). With *Csde1* knockdown, we also observed a corresponding reduction in hepatic CSDE1 protein (Fig. 5B). Intriguingly, however, steady-state hepatic LDLR protein amounts were not significantly different ($p = 0.826$, Fig. 5B). We also saw no differences in the hepatic lipoprotein receptors LDLR related protein 1 (LRP1) or scavenger receptor class B type 1 (SR-B1, Fig. 5B), hepatic PCSK9 protein (Fig. 5B), the appearance or behavior of the mice, plasma alanine or aspartate aminotransferase activity (Fig. S15A), total hepatic bile acids (Fig. S15B), or gross histologic appearance of the mouse liver (Fig. S14A-D). These observations argue against toxicity of either the *Csde1* shRNA or the gene knockdown.

To evaluate the functional effect of *Csde1* gene disruption, we turned to C57BL/6 mice on a Western-type (high-fat, high-cholesterol) diet (WD). We obtained baseline plasma samples on this diet and delivered a moderate dose (3×10^{11} genomes/mouse) of the AAV8-shRNA targeting either *Csde1*, *Pcsk9*, or a scramble control. Two weeks after transduction, we

reassessed total plasma cholesterol. We observed a significant decrease, compared to baseline, only for the mice transduced with *Csde1*-targeting shRNA (21% reduction, p = 0.0027, Fig 5C). The decrease observed with *Pcsk9*-targeting shRNA fell just above our prespecified cutoff for significance (p = 0.0592). Accordingly, lipoprotein fractionation of the post-transduction samples (Fig. S16A) revealed a 39% reduction in cholesterol in the LDL containing fractions between the *Csde1* knockdown mice and scramble controls (p = 0.0272, Fig. 5D), but no difference in the very low-density lipoprotein (VLDL) or high-density lipoprotein (HDL) fractions (Fig. S16B-C). Consistent with prior literature *(29)*, we observed an increase in total hepatic LDLR protein with *Pcsk9* knockdown, but as with chow-fed mice, we did not observe a significant difference between the scramble control and *Csde1* knockdowns (p = 0.744, Figs. S16D, S17).

To better assess the effects on non-HDL cholesterol, we also turned to C57BL/6 mice on the atherogenic, cholate-rich Paigen diet *(77–79)*. Here we delivered low dose (2×10^{10} genomes/mouse) AAV8-shRNA targeting either *Csde1*, *Pcsk9*, or a scramble control. Two weeks later, we observed a 25% reduction in fasting plasma cholesterol in the *Csde1* knockdown mice, which exceeded the effect of *Pcsk9* knockdown (p = 0.0497, Fig. 5E). We then re-dosed the *Csde1* and scramble AAV8-shRNA and, 2 weeks later, observed an even stronger phenotype (Fig. 5F). Despite the lower dose of AAV8 delivered, we observed the expected reduction in *Csde1* mRNA and an increase in *Ldlr* mRNA in the livers of the *Csde1*-targeted mice (Fig. S18A). Lipoprotein fractionation of the mouse plasma showed that *Csde1* knockdown mostly affected the VLDL-containing fractions (Fig. 5G), with immunoblots confirming a reduction in both apolipoprotein B100 (ApoB-100) and apoliproprotein B48 (ApoB-48), consistent with an increase in function of the murine LDLR on our dietary background *(80, 81)*. As with the chow-

fed mice, we observed no clear difference in the steady-state amount of LDLR protein in the liver (Fig. S18B), nor did we observe hepatotoxicity from the *Csde1*-targeting shRNA (Fig. S18C).

Last, we also employed a murine PCSK9 overexpression model to further assess the effects on atherogenic lipoproteins in a LDLR-depleted system. Again using C57BL/6 mice on the atherogenic, cholate-rich diet, we simultaneously delivered low-dose AAV8-*Pcsk9-D377Y* with low-dose AAV8-shRNA targeting either *Csde1*, *Pcsk9*, or a scramble control. We purposefully chose the sub-maximal dose (2×10^{10} genomes/mouse) for AAV8-*Pcsk9-D377Y* delivery *(82)* to reduce, but not completely ablate, the LDLR, given our hypothesis that CSDE1's effects on cholesterol are LDLR-dependent. Two weeks after AAV8 delivery, we observed a marked reduction (73%, $p = 0.0351$) in total plasma cholesterol in the shRNA-*Pcsk9* treated mice and a similar (57%) but nonsignificant ($p = 0.1013$) reduction in the shRNA-*Csde1* treated mice, both when compared to the scramble controls (Fig. S19). We therefore re-dosed the mice in the *Csde1* and scramble treatment arms with the corresponding AAV8. Two weeks after this second dose, which was also 8 weeks after the first dose, we again measured total plasma cholesterol and observed significant reductions for the *Csde1* (52%, $p = 0.0194$) and the singly-dosed *Pcsk9* (64%, $p = 0.0052$) knockdowns, both in comparison to the scramble controls (Fig. 5H). Given the results of these four independent mouse models, we conclude that hepatic CSDE1 downregulates *Ldlr* mRNA expression and reduces clearance of non-HDL lipoproteins *in vivo*.

The in vivo Effect of Hepatic CSDE1 Silencing on the Transcriptome

To gain further insight into the role of hepatic CSDE1, we performed bulk RNA sequencing (RNA-seq) on the liver tissue in our model with the strongest phenotype, the Paigen diet (Figs. 5I-J, S20, Table S10). We compared the *Csde1* knockdown to control (scramble)

mice, using the mice with the highest transcript counts of a vector-delivered eGFP reporter to control for variations in transduction efficiency. Since mice on the Paigen diet received a lower dose of AAV8 vector, we also filtered our results for the differentially expressed transcripts in the control mice at the extremes of eGFP expression to control for the effects of viral transduction alone. As expected, we found higher *Ldlr* expression in the *Csde1* knockdown mice ($log_2FC = 0.43$, $p = 0.0029$, Table S10). Consistent with our mechanistic hypothesis, GO enrichment analysis of the top differentially expressed genes ($log_2FC > |1|$, 745 genes total) revealed downregulation of genes involved in mRNA catabolic processes ($p = 4.9 \times 10^{-50}$) or encoding RNA binding functions ($p = 4.6 \times 10^{-29}$) and upregulation of genes involved in cholesterol homeostasis ($p = 2.5 \times 10^{-4}$, Figs. 5I-J, S20, Table S11). To remove the confounding effects of liver inflammation and steatosis induced by the cholate-containing diet *(83)*, we repeated the bulk RNA sequencing in the chow-fed mice. Compared to the Paigen diet model, we observed many fewer differentially expressed genes in the chow-fed *Csde1* knockdowns (43 genes total, any log_2FC, Fig. S21, Table S12), consistent with less homeostatic perturbation. In agreement with the results from the Paigen diet model, we observed a positive enrichment for genes promoting mRNA stability ($p = 4.9 \times 10^{-4}$) and a negative enrichment for genes encoding RNA binding functions ($p = 2.7 \times 10^{-3}$, Fig. S21, Table S13).

Discussion

The powerful biology of the LDLR is unquestioned in cardiovascular medicine *(84)*. Since their introduction, statins, which upregulate the LDLR, have become a major public health success, and with the discovery of PCSK9 and the therapeutic antibodies targeting it, patients can safely reach much lower LDL than is achievable by statins alone *(10)*. Together, this suggests that we can push further on this LDL-LDLR axis and still achieve a clinical benefit.

In this study, we modeled a clinically relevant phenotype of LDLR abundance and function, complementing the independent investigations of other groups *(85, 86)*. When synthesizing our screening and validation data together with large-scale genomics and additional pharmacologic perturbations, we produce an exploratory map of potential regulatory mechanisms for the LDLR (Fig. 6). These data represent not just promising targets but also pathways likely to be impacted by therapies already in use in the clinic.

We have shown that *CSDE1*, one of our strongest hits, regulates LDLR abundance in HepG2 cells by promoting *LDLR* mRNA decay via its 3' UTR. These data lay in concert with CSDE1's destabilizing effects on other transcripts, such as c-Fos *(68)*. We have also shown that *in vivo* knockdown of *Csde1* upregulates hepatic *Ldlr* mRNA expression and improves atherogenic lipid profiles in mice. This mimics the effect of deleting the 3' UTR *in vivo (87)* and phenocopies a human variant with a large deletion in the *LDLR* 3' UTR, the only gain-of-function *LDLR* mutation that markedly reduces LDL cholesterol *(88)*. These similarities illustrate the promise of targeting CSDE1 to lower LDL and protect against atherosclerosis. It is notable that several small molecules, including triciribine *(72)* and berberine *(76, 89)*, have stabilizing effects on *LDLR* mRNA, though whether their mechanisms directly involve CSDE1 remain to be elucidated. The magnitude of LDLR upregulation imparted by *CSDE1* knockdown mirrors or exceeds that of *HMGCR* and *PCSK9* in both tissue culture and mouse models, suggesting that a high-fidelity approach targeting CSDE1-mediated *LDLR* mRNA decay in the clinic could have similarly impressive effects. Additionally, our mechanistic data suggest that targeting CSDE1 would be at least additive with the use of statins.

Though upon *CSDE1* knockdown we observed an increase in hepatic LDLR protein in our human tissue culture models, we observed no change in total hepatic LDLR protein in our

mouse models despite a reduction in LDLR-cleared lipoproteins. Whether this difference between our models reflects hepatocyte physiology within an intact organism or instead a species-specific difference between the HDL-predominant mouse *(80, 81)* and the LDL-predominant human remains to be determined. Our data are consistent with metabolic labeling experiments demonstrating the homeostatic defense of steady-state hepatic LDLR in the mouse in response to cholesterol loading conditions and altered *LDLR* transcription *(90)*. Our data are also consistent with mouse experiments that markedly perturb *Ldlr* mRNA but have comparatively muted effects on LDLR protein *(76, 91)*. We hypothesize that inhibition of CSDE1 protects *LDLR* mRNA from CSDE1-mediated decay, upregulates LDLR synthesis, and induces *in vivo* homeostatic mechanisms that together increase LDLR function but maintain steady-state LDLR abundance in the mouse. The nature of these mechanisms will be important to uncover. Intriguingly, our tissue culture data show that compared to a statin, disrupting *CSDE1* has a disproportionately larger effect on LDL uptake than surface LDLR amounts, supporting the possibility that CSDE1 could also affect LDLR function, in addition to its abundance. Further, these data also show that *CSDE1* knockdown also increases *MYLIP* transcripts. Since the gene target of *MYLIP*, IDOL, induces post-translational degradation of the LDLR, this effect could help explain our *in vivo* findings. In support of this possibility, the transcriptomic profiling of the chow-fed *Csde1* knockdown mice revealed a negative enrichment in genes encoding ubiquitin ligase binding ($p = 5.9 \times 10^{-3}$, Fig. S21, Table S13), suggesting that ubiquitin-dependent regulators, such as IDOL, may be perturbed. Given our observation of increased LDL uptake with *CSDE1* knockdown in the *LDLR* deficient background, a separate LDLR-independent effect of CSDE1 on lipoproteins also may contribute. Further work is needed to investigate the potential contributions of these and other mechanisms, such as increased

endocytic turnover of existing LDLR and altered synthesis and secretion of non-HDL lipoproteins.

The degree to which CSDE1 inhibition affects other transcripts, or other tissues *(67, 92)*, also remains an important question. As an RNA chaperone, CSDE1 can have a variety of effects, from mRNA stabilization *(66)* to promotion or inhibition of translation *(93–96)*, dependent on the identity of the RNA it binds and the cofactors with which it interacts. Intriguingly, though CSDE1 was found to bind biotinylated *LDLR* 3' UTR transcripts in HepG2 cell lysates *(71)*, cross-linking immunoprecipitation approaches in both mouse brain and melanoma cells failed to identify *LDLR* mRNA as a CSDE1 binding partner *(97, 98)*. This suggests that the CSDE1-*LDLR* interaction is context dependent. Advances in liver-specific delivery of gene-silencing agents *(19, 99)*, novel gene editing technologies *(100)*, and small molecules *(101)* offer the possibility that selectively targeting hepatic CSDE1 for cholesterol lowering could avoid systemic toxicities.

We acknowledge several limitations in our study. First, outside of *CSDE1*, the validation of gene targets affecting both LDL receptor abundance and function is limited to a single cell line. Additionally, of our validated hits in tissue culture, we only confirmed CSDE1 in an *in vivo* mammalian model. Second, the fundamental differences in lipoprotein metabolism in the mouse may limit the translation of our conclusions surrounding CSDE1 to humans *(80, 81)*. Last, we have not directly assessed the effects of *CSDE1* disruption in non-hepatic tissues.

Nevertheless, we observed no ill effects from CSDE1 disruption in either our tissue culture or *in vivo* models and our transcriptional profiling suggests only a small number (43) of differentially affected transcripts under normal feeding conditions. This suggests that potential toxicities of hepatic CSDE1 disruption may be low, which will be important to confirm in future

studies that pursue CSDE1 as a therapeutic target for cholesterol lowering. Given that CSDE1 has such varied effects on other transcripts, further mechanistic dissection of the hepatic CSDE1-*LDLR* interaction could identify what makes this relationship unique and guide a potential therapeutic strategy. We expect that our transcriptomic analyses will guide subsequent investigations of both possible toxicities and mechanistic details of hepatic CSDE1 disruption. Combination therapies targeting interconnected pathways to disease can provide increased benefits without inducing extreme side effects, with angiotensin receptor blockade and neprilysin inhibition in heart failure a prominent clinical example *(102)*. To the extent hepatic CSDE1 utilizes specific factors to downregulate *LDLR* mRNA, simultaneous tissue-specific drugging of both CSDE1 and these factors could widen the overall therapeutic window. We anticipate that our study will serve as the seed for these and other further investigations.

Materials and Methods

Study Design

We designed the study as a discovery biology experiment to identify new regulators of the LDL receptor. We used an established tissue culture model, HepG2 cells, to evaluate for LDL receptor regulation. We used wild-type zebrafish (Ekwill) and wild-type mice (C57BL/6) to validate the contribution of our top hit, CSDE1, to LDL receptor regulation *in vivo*. We evaluated sufficient cells for the LDLR and TFR screens to provide adequate coverage for transduction and downstream sequencing of each sgRNA in the genome-wide library. Sample sizes for animal experiments were estimated to provide 80% power (two-tailed $\alpha = 0.05$) for a 25% difference in cholesterol compared to controls, based on effects in these models in the existing literature. The numbers of animals used in each experiment are noted in the figures and manuscript. Unless otherwise noted, all *in vitro* data are representative of multiple (≥ 3)

biological replicates to ensure robust outcomes. Experimental and control arms were randomly assigned at the outset of the experiment, with no exclusion criteria predefined. Experiments were not performed in a blinded fashion. All animal studies were performed in accordance with institutional animal care and use committee (IACUC) approved protocols at the University of California, San Francisco as well as the NIH Guide for the Care and Use of Laboratory Animals. Reporting of the animal studies is in compliance with ARRIVE guidelines 2.0 listed in the EQUATOR Network library.

Plasmids and Cloning

SFFV-dCas9-BFP-KRAB (Addgene 46911), CRISPRi/a v2 (Addgene 84832), pMD2.G, dR8.91, pLG_GI4 (Addgene 111595) and the hCRISPRi v2 top5 sgRNA library (Addgene 83969) were gifts from L. Gilbert and J. Weissman. Oligonucleotides of the protospacers of validated sgRNA sequences *(17)*, as well as those for polymerase chain reaction (PCR) amplification and isothermal assembly, were obtained from Elim Biopharmaceuticals (Hayward CA). Single protospacers were cloned into the CRISPRi/a v2 vector using restriction enzyme digest (BlpI and BstXI, ThermoFisher, Waltham MA) and ligation with 10× T4 ligase (NEB, Ipswich MA). Dual protospacers were cloned into the pLG_GI4 vector by PCR expansion of both the vector backbone and intra-protospacer sequences, using the 5' ends of the oligonucleotide primers to encode the desired protospacers, followed by gel purification (EZNA Gel Extraction Kit, Omega Bio-tek, Norcross GA) and isothermal assembly *(103)* of the resulting fragments. CSDE1 overexpression constructs were created by PCR expansion of *CSDE1* (HsCD00949797, DNASU, Tempe AZ) or AcGFP1 (vector control, pIRES2-AcGFP1, Clontech, Mountain View CA) and isothermal assembly into the pcDNA5/FRT/TO backbone (ThermoFisher), followed by site-directed mutagenesis to generate the four CSDE1 isoforms

(UniprotKB O75534 1 through 4). pLuc2-Prom$_{LDLR}$ was created by PCR expansion of the target luciferase from pGL4Luc-RLuc (Addgene 64034), custom gene synthesis of the LDLR promoter (NCBI Reference Sequence NG_009060.1, from -687 bp to the *LDLR* start codon, Twist Biosciences, South San Francisco CA) and isothermal assembly into the pcDNA5/FRT/TO backbone. pSS-NLuc was created by PCR expansion of the target luciferase from pNL1.1 (Promega, Madison WI) into a vector containing the PCSK9 signal sequence from the same backbone *(104)*. The remaining pLuc2-Prom$_{LDLR}$ constructs were created by PCR expansion of the coding region of *LDLR* (HsCD00004643, DNASU), custom gene synthesis of the 3' UTR of the *LDLR* mRNA (NCBI Reference Sequence NM_001252658.1, Twist Biosciences), or custom oligonucleotides to add the P2A ribosomal skipping linker *(105, 106)* and isothermal assembly into pLuc2-Prom$_{LDLR}$, as appropriate for each construct. All plasmids were confirmed by Sanger sequencing. Expansion of the top5 sgRNA library was as previously described *(16)*.

Cell Culture and Lentiviral Production

HepG2 (ATCC HB-8065) and derivatives and Huh7 cells (a gift from M. Ott, Gladstone Institutes/UCSF) were cultured in low-glucose Dulbecco's Modified Eagle Medium (DMEM, 1 g/L glucose, ThermoFisher) with 10% fetal bovine serum (FBS, Axenia BioLogix, Dixon CA), GlutaMax (ThermoFisher) and 1× penicillin-streptomycin (ThermoFisher). HepG2s and derivatives were sent thrice through a 21g needle during passaging to minimize cell clumping. Primary C57BL/6 hepatocytes (Cell Biologics, Chicago IL) were thawed directly from the manufacturer, plated on bovine-collagen coated plates (Millipore Sigma, Burlington MA), and grown in the same media as HepG2 cells but with daily replacement. HEK-293T (ATCC CRL-3216) were cultured in standard DMEM (ThermoFisher) with 10% FBS. All cell lines were cultured at 37 ºC at 5% CO_2, seeded for approximately 50% confluency at the time of

experiment, and were confirmed free of *Mycoplasma* contamination by the MycoAlert PLUS Mycoplasma Detection Kit (Lonza, Switzerland). Lentivirus was produced in 293T cells by transfection of dR8.91, pMD2.G, and the appropriate pLKO-derived vector (at ratios of 8 μg, 1 μg, and 8 μg, respectively, per 15 cm dish) with Trans-LT1 (Mirus Bio, Madison WI), according to the manufacturer's instructions. Viral harvest media was supplemented with Viralboost (Alstem, Richmond CA), collected 2-3 days after transfection, and filtered through 0.44 μm polyvinylidene difluoride filters and either frozen for storage at -80 ºC or used immediately for transduction.

Generation of CRISPRi Cell Lines

All cell lines were transduced using virus-containing supernatant in the presence of 8 μg/ml polybrene (Millipore-Sigma, St. Louis MO). HepG2 expressing dCas9-KRAB were derived by transduction with lentivirus harboring SFFV-dCas9-BFP-KRAB, followed by two rounds of FACS for blue fluorescent protein (BFP) positive cells on a Becton Dickson (BD) FACSAria II. dCas9-KRAB HepG2 with individual targeting sgRNAs were derived by transduction with lentivirus harboring the desired sgRNA, followed by 48 hrs of puromycin selection (2 μg/ml, InvivoGen, San Diego CA), prior to experiments.

Quantitative Reverse Transcription PCR (RT-qPCR)

dCas9-KRAB HepG2 stably expressing an appropriate sgRNA were harvested, lysed, and total RNA was extracted via the RNeasy Mini Kit (Qiagen, Germantown MD). RNA was converted into complementary DNA (cDNA) using qScript cDNA SuperMix (QuantaBio, Beverly MA) following the manufacturer's instructions. RT-qPCR was performed against indicated targets with PrimeTime qPCR primers (IDT, Coralville IA) using the SYBR Select Master Mix (ThermoFisher) according to the manufacturer's instructions on a CFX96 Touch

Real-Time PCR Detection System (BioRad, Hercules CA). Fold changes were calculated using ΔΔCt analysis, normalizing each sample to *B2M* controls, using CFX Maestro software (BioRad). RNA extracted from mouse liver from *in vivo* experiments was processed similarly but with additional *B2m*, *Actb*, and *Gapdh* housekeeping controls.

Receptor Abundance Analysis

1-2 days prior to analysis, dCas9-HepG2 cells and derivatives were cultured in low-glucose DMEM with 5% lipoprotein-deficient serum (LPDS, Kalen Biomedical, Germantown MD) unless otherwise noted. Prior to analysis, cells were dissociated with Accutase (Innovative Cell Technologies, San Diego CA), collected, washed in phosphate buffered saline (PBS, ThermoFisher), live-dead stained with Ghost Dye Red 780 (1:1000 dilution, Tonbo Biosciences, San Diego CA), washed, and then stained with the indicated antibody in FACS buffer (PBS with 1% FBS, 10 U/ml DNAse I, GoldBio, St. Louis MO) for 30 minutes on ice with gentle agitation. Cells were washed, resuspended in FACS buffer, filtered through 90 μm mesh (Elko Filtering, Miami FL) to give a single cell suspension, and placed on ice. Cells were then analyzed on either a BD Fortessa, BD LSRII, BD FACSAria II, or Beckman Coulter CytoFLEX, or sorted on a BD FACSAria II, depending on the experiment. In general, gating excluded cells positive for live-dead staining and included only the cells positive for the amount of BFP fluorescence induced by the CRISPRi/a v2 vector. FACS analysis and figure preparation was performed with FlowJo v10 (BD, Ashland OR).

Genome-Wide CRISPRi Screen

The screen was conducted similarly to prior descriptions *(16–18)*. Approximately 200 × 10^6 dCas9-KRAB HepG2 were transduced with hCRISPRi-v2 top 5 sgRNAs/gene lentivirus at an MOI of ~0.5, and with polybrene at 8 μg/ml, on day 1. Cells were grown on 15-cm dishes,

subdivided into four replicates immediately upon transduction (biological duplicate for each screen), and reseeded every 3-4 days as necessary to avoid overconfluence. Cells were selected with puromycin (2 mg/ml) from day 2 through day 6. On day 5, cells for the LDLR sort were placed in DMEM with 5% LPDS. On day 7, approximately 50×10^6 cells from 2 replicates were live-dead stained and stained for LDLR as described above, and then two-way sorted on a BD FACSAria II for the top and bottom 33% by LDLR abundance. Cells were spun down, washed in PBS and frozen at -80 ºC. On day 8, the sort was repeated except in one replicate, cells were stained for TFR instead of LDLR and then sorted as per above. Genomic DNA was isolated using a NucleoSpin Blood DNA extraction kit (Macherey-Nagel, Bethlehem PA). The sgRNA-containing region was PCR-amplified with NEBNext Ultra II Q5 MasterMix (NEB), acrylamide gel-purified, and size-selected by SPRI beads (Beckman Coulter, Indianapolis IN), all as previously described, prior to sequencing on an Illumina HiSeq 4000.

Screen Processing

Sequencing data were aligned to the top5 library, counted, and quantified using the ScreenProcessing pipeline (accessed from https://github.com/mhorlbeck/ScreenProcessing *(17)* 4/25/2019). Phenotypes and Mann-Whitney *P* values were determined as previously described *(17)*, with the phenotypes defined as follows: ρ indicated the comparison in high-abundance vs. low abundance cells, τ indicated the comparison in high-abundance vs. unsorted cells, and γ indicated the comparison in low-abundance vs. unsorted cells. Counts from 4 guides were removed from the final analysis as there was evidence of contamination from individually cloned plasmids (PCSK9_+_55505255.23-P1P2, HMGCR_+_74633053.23-P1P2, TFRC_-_195808987.23-P1P2, ACO1_-_32384733.23-P1P2). A hit threshold of 7 (normalized phenotype z score × -log10(p-value) ≥ 7) *(16)* was used to identify hits from ρ, τ, and γ phenotypes, which

were then compiled. Identical analysis of the TFR screen was used to prioritize hits unique to LDLR regulation. Gene ontology analysis was performed using the PANTHER Classification System database (v15) *(35, 107)*. For relaxation of the hit threshold for comparison to GWAS studies, a score of 6 was used. Cellular localization of hits was imputed by manual curation from UniProt *(108)* and the Human Protein Atlas *(63)*.

Human Genomic Analysis

Protein coding variants for hits validated with individual sgRNAs were assayed in the UK Biobank *(109)* for associations with LDL-C. In the setting of a statin medication, LDL-C was divided by 0.7 as before *(37)*. Genotyping and imputation was performed in the UK Biobank as previously described *(39)*, and nonsynonymous protein coding variants with minor allele frequencies greater than 0.001 were considered. Efficient linear mixed models adjusting for age, sex, genotyping array, and principal components of ancestry were employed, using BOLT-LMM *(110)*. Statistical significance was assigned at $\alpha = 0.05/117 = 0.000427$ to account for multiple hypothesis testing.

Validation Experiments of Individual sgRNAs

Cloning of protospacers, as described above, was performed in 96-well plate format until selecting individual colonies. For downstream phenotyping experiments, single sgRNA protospacers were chosen against CSDE1 (CSDE1_+_115300577.23-P1P2) or a negative control (Unassigned=negZNF335_-_44601297.24-all) *(17)*. Dual sgRNA protospacers were against CSDE1 (the same sequence as before), LDLR (LDLR_-_11200159.23-P1P2), and two separate negative controls (negative control-10016 and negative control-10029) *(70)*. Lentiviral production in HEK-293T, transduction of dCas9-KRAB HepG2 with lentiviral sgRNA vectors,

and receptor abundance and LDL uptake assays were similarly performed in 96-well plate format to maximize throughput.

LDL Uptake Assays

Assays were performed as previously described *(40)* with the following modifications. dCas9-HepG2 cells harboring appropriate sgRNAs were treated similarly to receptor abundance analysis, except that prior to harvest, cells were washed and then treated with 5 μg/ml 1,1'-dioctadecyl-3,3,3',3'-tetramethylindocarbocyanine perchlorate (DiI) labeled LDL (Kalen Biomedical) in low-glucose DMEM with 0.5% bovine serum albumin (BSA, MilliporeSigma) for 1 hr at 37 ºC. Cells were then washed, collected, and prepared for FACS analysis, as described above, but without antibody labeling. In dual sgRNA knockdown experiments, we defined the total effect of *CSDE1* knockdown as the difference in LDL uptake between *NegCtrl1/CSDE1* and *NegCtrl1/NegCtrl2* (WT) CRISPRi cells, the LDLR-independent component of *CSDE1* knockdown as the difference in LDL uptake between *LDLR/CSDE1* and *LDLR/NegCtrl2* CRISPRi cells, and the LDLR-dependent component of CSDE1 knockdown as the difference between the total effect of *CSDE1* knockdown and its LDLR-independent component.

Pharmacologic Synergy Experiments

Receptor and LDL uptake assays were performed as described, with cells treated overnight with either simvastatin (6 μM, MilliporeSigma), PF-6846 (10 μM, MilliporeSigma), or DMSO vehicle (final concentration of 0.5%) overnight prior to analysis. Synergy scores were calculated by the following equation:

$$\boxed{\left(LDLR_{sgRNA+compound} - LDLR_{NegCtrl+compound}\right) - \left(LDLR_{sgRNA+vehicle} - LDLR_{NegCtrl+vehicle}\right)}$$

with $\boxed{LDLR}$ obtained as the mean fluorescence, background subtracted from an unstained control and subsequently normalized to $\boxed{LDLR_{NegCtrl+vehicle}}$ within a given experiment.

Overexpression Experiments

HepG2 or engineered dCas9-HepG2 cell lines were seeded into 96 well plates at 5×10^4 cells per well in HepG2 growth medium. After 24 hrs, cells were washed and changed into low-glucose DMEM with 5% LPDS. Each well was transfected with 100 ng of the appropriate CSDE1 overexpression construct, or vector control, in a total of 10 µL OptiMEM (ThermoFisher) using Lipofectamine 3000 (ThermoFisher) according to the manufacturer's instructions. Cells were incubated at 37 ºC with 5% CO_2 for 72 hrs, and then harvested for LDL receptor expression analysis as above.

mRNA Decay Experiments

Engineered dCas9-HepG2 cell lines harboring appropriate sgRNAs were seeded into 12 well plates at 5×10^5 cells per well in HepG2 growth medium. After 24 hrs, cells were washed and changed into sterol-depleting media (low-glucose DMEM with 5% LPDS) supplemented with 6 µM simvastatin. After an additional 24 hrs, actinomycin D (MilliporeSigma) was added at 5 µg/ml, and cells were harvested as described at the indicated timepoints.

Immunoblots

Engineered dCas9-HepG2 cell lines harboring appropriate sgRNAs were grown in growth medium and harvested with 0.25% trypsin digestion. Cells were washed and lysed in lysis buffer on ice (50 mM Tris-HCl pH 7.4, 150 mM NaCl, 0.1% NP-40). Lysates were clarified at 21,000 × *g* for 10 min, and the supernatant was recovered. Equivalent amounts of lysates, as measured by BCA assay (ThermoFisher), were resolved on 4-12% Bis-Tris NuPAGE gels (ThermoFisher), transferred to nitrocellulose, probed with primary and secondary antibodies as

noted (see Key Resources Table) in 5% BSA in Tris-buffered saline with 0.1% Tween 20 (TBS-T, 20 mM Tris-HCl, pH 7.4, 150 mM NaCl), and visualized on an Odyssey imaging system (LI-COR, Lincoln NE).

Surface Biotinylation Assay

Surface biotinylation assays were performed as described in the literature *(24, 111)* with minor modifications. Engineered dCas9-HepG2 cell lines harboring appropriate sgRNAs cultured in 6 well plates were washed 3× with ice-cold PBS-CM (PBS with 1 mM $MgCl_2$ and 0.1 mM $CaCl_2$) on ice, and then treated with 0.5 mg/ml EZ-Link Sulfo-NHS-SS-Biotin (ThermoFisher) in PBS-C pH 8.0 (PBS with 2 mM $CaCl_2$) at 4°C for 30 min with gentle rocking. Biotin reagent was then quenched for 30 min at 4°C with PBS-CM containing 25 mH Tris-HCl pH 7.4 and 192 mM glycine. Cells were washed twice with PBS-CM and once with TBS-C (50 mM Tris-HCl, pH 7.4, 100 mM NaCl, and 2 mM $CaCl_2$), all on ice. Cells were collected by scraping in TBS-C, centrifuged at 1000 × *g* for 5 min at 4°C, and then lysed in biotin lysis buffer (50 mM Tris-HCl pH 7.4, 150 mM NaCl, 1% NP-40, 0.5% sodium deoxycholate, 5 mM ethylenediaminetetraacetic acid (EDTA), and 5 mM ethylene glycol-bis(β-aminoethyl ether)-*N,N,N',N'*-tetraacetic acid, (EGTA)) for 15 min on ice after brief (10 sec) sonication. Lysates were clarified at 12000 × *g* for 15 min at 4°C, with the supernatant recovered. Protein concentration was determined by bicinchoninic (BCA) assay (ThermoFisher). Biological replicates were then pooled to allow 150 µg of appropriate lysate to be added to 30 µL of Neutravidin Plus Ultralink Resin (ThermoFisher), equilibrated in 500 µL biotin lysis buffer, and incubated for 4 h at 4°C on a rotator. Beads were collected by centrifugation (500 × *g* for 5 min), washed 3× with biotin lysis buffer, 1× with high-salt buffer (50 mM Tris-HCl pH 7.4, 500 mM NaCl), 1× with low-salt buffer (10 mM Tris-HCl pH 7.4), and eluted directly into 30 µL 2X

Laemmli gel loading buffer with 5% β-mercaptoethanol at 95°C for 5 min. Samples were analyzed by immunoblot as described above.

siRNA and AAV8-shRNA Knockdowns in Tissue Culture

Appropriate cell types were transfected with Silencer Select siRNA (ThermoFisher) against *CSDE1* (Assay ID s15373) or control (Negative Control No. 1) at a final concentration of 25 μM with RNAiMAX (ThermoFisher) according to the manufacturer's instructions. For HepG2 cells, reverse siRNA transfections were performed, and for Huh7 cells and primary hepatocytes, forward transfections were performed. For primary hepatocytes, the transfection agent was removed and replaced with fresh media after 4 h. For AAV8-delivered shRNA, primary mouse hepatocytes were transduced with custom-generated AAV8 (Vector Biolabs, Malvern PA) at approximately 1×10^6 genomes/cell with 4 mM polybrene. Cells were incubated at 37°C with 5% CO_2 for 72 h, with daily media changes for primary hepatocytes, prior to downstream analyses (RT-qPCR, LDL receptor abundance, and LDL uptake as described).

Dual-Luciferase Assays

Engineered dCas9-HepG2 cells were seeded into opaque white 96 well plates, at 2.2×10^4 cells per well, in 100 μL growth medium the day prior to transfection. On day of transfection, medium was replaced or changed to sterol-depleted medium (low-glucose DMEM with 5% LPDS) with or without 6 μM simvastatin as appropriate. Each well was transfected with 100 ng of Luc2-$Prom_{LDLR}$ based construct and 1 ng of secreted nanoluciferase control construct (pSS-NLuc) in a total of 10 μL OptiMEM using Lipofectamine 3000 according to the manufacturer's instructions. 6 replicates were transfected per construct per experiment. After 48 hours at 37°C and 5% CO_2, 10 μL of medium was removed from each plate and aliquoted into a separate 384 well plate. Firefly luciferase activity was evaluated in the plates containing the cells

by adding an equal volume of a 2× firefly lytic assay buffer (100 mM Tris-HCl pH 7.7, 50 mM NaCl, 2 mM $MgCl_2$, 0.17% Triton X-100, 10 mM dithiothreitol (DTT), 0.4 mM coenzyme A, 0.3 mM adenosine triphosphate (ATP), and 0.28 mg/ml luciferin (Goldbio)) *(112)*. Nanoluciferase activity was evaluated from the conditioned medium using a non-lytic 2× coelenterazine (Goldbio) reagent as previously described *(104, 113)*. Raw luminescence was obtained on a SPARK plate reader (Tecan, San Jose CA) with 1 second integration time. Readout of firefly luciferase in each well was normalized to the corresponding secreted nanoluciferase control and data were visually inspected and cleaned to remove values from poorly transfected wells (formally defined by ROUT = 1%) during analysis.

Zebrafish Handling, Maintenance, and Cas9-Ribonucleoprotein Knockdowns

All zebrafish studies were performed as previously described *(75)* with minor modifications. Briefly, wild type zebrafish embryos were injected at the one-cell stage with Cas9-RNP complexes and raised at 28 ºC. Cas9-RNP complexes were prepared as previously described *(75)* using custom oligonucleotides against the indicated targets (Elim Biopharmaceuticals). Targeting of tyrosinase, which results in larval albinism, was used as an injection control. Larvae were fed a high-cholesterol diet *(74)* of Golden Pearls (5-50 micron, Brine Shrimp Direct, Ogden UT) supplemented (4% w/w) with cholesterol (MilliporeSigma) 3× daily from 4 dpf, fasted on 7 dpf to clear intestinal cholesterol, and harvested at 8 dpf. Larvae were collected, extensively washed, anesthetized in tricaine, and collected in groups of 10 per sample prior to storage at -80 ºC.

Cholesterol Analysis of Zebrafish Homogenates

Total cholesterol was analyzed as previously described *(74)* with minor modifications. Briefly, frozen larvae were homogenized in PBS with a plastic pestle, and then clarified at

18,000 × *g* for 15 min. Supernatants were recovered and total protein content was analyzed by BCA assay. Homogenates were then analyzed, in duplicate, at the appropriate dilution (typically 1:12 in PBS) for total cholesterol content using a commercial fluorometric assay (Cayman Chemical, Ann Arbor MI). Fluorescence outputs were measured on a Tecan SPARK plate reader, and cholesterol concentrations were interpolated from a regression line calculated from a standard curve. Cholesterol was normalized to total protein content for analysis and subsequently to the scramble control for comparison between experiments.

Mouse Handling, Maintenance, and shRNA Knockdowns

8-10 week old male C57BL/6 mice (The Jackson Laboratory, Bar Harbor ME) were maintained on a normal chow diet and then placed on the Western diet (0.15% cholesterol, 21% fat, D12079Bi, Research Diets, New Brunswick NJ) or atherogenic "Paigen" diet (1.25% cholesterol, 15% fat, 0.5% cholate, D12336i, Research Diets) *(77)* at the beginning of the appropriate experiment (week 0). After 2 to 4 weeks on the appropriate diet, AAV8-packaged expression vector encoding *Pcsk9-D377Y* or eGFP, or AAV8-packaged shRNA against mouse *Csde1* (NM_144901), *Pcsk9* (NM_153565), or scramble control (Vector Biolabs, Malvern PA), were diluted in sterile PBS to a concentration of either 2×10^{11} (low dose) or 3×10^{12} (moderate dose) genomes/ml. 100 µL of diluted AAV8 (2×10^{10} or 3×10^{11} genomes/mouse) harboring the appropriate construct shRNA was administered to each mouse via tail vein injection. Two weeks after AAV8 injection, mice were fasted overnight and then underwent blood sampling via submandibular vein puncture. Approximately 50 µL of blood was collected into an EDTA-coated tube, centrifuged at 2000 × g for 10 min at 4 °C, and the plasma recovered and stored at -20 °C until further analysis. Total cholesterol of the plasma, after approximately 1:200 to 1:400 dilution in assay buffer, or 1:4000 dilution for *Pcsk9-D377Y* boosted mice, was evaluated by

commercial fluorometric cholesterol assay (Cayman) as described above. Mouse plasma was evaluated for alanine and aspartate aminotransferase activity using commercial assays (Cayman) according to the manufacturer's instructions. For mice on the Paigen diet, 6 weeks after initial AAV8 injection, mice from the same exposure arm were re-dosed with AAV8-shRNA targeting either *Csde1* or scramble control. At the time of sacrifice, the mice were again fasted overnight and then euthanized after CO_2 narcosis followed by cervical dislocation. The abdominal cavity was opened with a ventral midline incision, the inferior vena cava was cannulated, and plasma was collected as described above. The liver and vasculature were perfused with PBS, and the samples of the liver were harvested. Tissue samples for RNA evaluation were placed in TRIzol (ThermoFisher) and those for protein analysis were flash frozen in liquid N_2 and stored at -80 ^{o}C.

Preparation and Analysis of Mouse Liver Lysates

Frozen mouse liver tissue was homogenized in a tissue homogenizer. For immunoblots, 50 mg of liver tissue was homogenized in 1 mL radioimmunoprecipitation assay (RIPA) lysis buffer and immunoblots performed as described above. For bile acid assays, 70 mg of liver tissue was homogenized in 700 μL PBS. Samples were then clarified at 10,000 × *g* for 10 min at 4 ^{o}C, the supernatant recovered, and then diluted 1:4 in H_2O for analysis of total bile acids using a commercial assay according to the manufacturer's instructions (Cell Biolabs, San Diego CA).

Mouse Liver Histology and Immunohistochemistry

Livers were fixed in 2% paraformaldehyde at 4 ^{o}C overnight, dehydrated through an ethanol series, embedded in paraffin, and sectioned as previously described *(114)*. Antibodies and their dilutions used for immunohistochemistry were as noted in the Key Reagent Table. Hematoxylin & eosin staining was performed using standard protocols. Slides were imaged on a Leica Dmi8 microscope.

Lipoprotein Fractionation

Plasma samples were thawed and centrifuged at 2000 × *g* for 10 min at 4 °C, and the supernatant recovered. 100 µL of individual mouse plasma was loaded onto a Superose 6 Increase 10/300 GL column (Cytiva, Marlborough MA) and eluted with PBS with 1 mM EDTA at 0.5 ml/min on an AKTA Pure chromatography system (Cytiva). Fixed 0.5 ml fractions were collected from 0.2 to 1 column volumes along the isocratic elution. Fractions were subjected to total cholesterol analysis and immunoblots as described above.

RNA-seq Library Preparation

Total RNA was extracted from frozen liver samples using the Qiagen RNeasy Plus Universal mini kit followed by Manufacturer's instructions (Qiagen). RNA samples were quantified using Qubit 2.0 Fluorometer (ThermoFisher) and RNA integrity was checked using Agilent TapeStation 4200 (Agilent Technologies, Palo Alto CA). Purified RNA was used for mouse RT-qPCR experiments as described above. RNA sequencing libraries were prepared via polyA selection using the NEBNext Ultra RNA Library Prep Kit for Illumina using manufacturer's instructions (NEB). Briefly, mRNAs were initially enriched with Oligod(T) beads. Enriched mRNAs were fragmented for 15 minutes at 94 °C. First strand and second strand cDNA were subsequently synthesized. cDNA fragments were end repaired and adenylated at 3'ends, and universal adapters were ligated to cDNA fragments, followed by index addition and library enrichment by PCR with limited cycles. The sequencing library was validated on the Agilent TapeStation (Agilent) and quantified by using Qubit 2.0 Fluorometer (Invitrogen) as well as by quantitative PCR (KAPA Biosystems, Wilmington, MA, USA). The sequencing libraries were clustered on a single lane of a flowcell. After clustering, the flowcell was loaded on the Illumina HiSeq instrument (4000 or equivalent) according to manufacturer's

instructions. The samples were sequenced using a 2 × 150 bp Paired End (PE) configuration. Image analysis and base calling were conducted by the HiSeq Control Software (HCS). Raw sequence data (.bcl files) generated from Illumina HiSeq was converted into fastq files and de-multiplexed using Illumina's bcl2fastq 2.17 software. One mismatch was allowed for index sequence identification. RNA library preparation and sequencing were conducted by GENEWIZ, LLC (South Plainfield, NJ).

RNA-seq Analysis

All raw sequencing data underwent quality control checks with FastQC (v 0.11.8). Reads were mapped to the mm10 mouse reference genome using Rsubread (v 2.4.3) and assigned to Ensembl gene IDs. Ensemble gene IDs were then mapped to org.Mm.eg.db (v3.12.0) gene symbols using AnnotationDBI (v1.52.0). Gene expression was quantified using raw counts and differential expression gene testing was performed on the scramble-shRNA samples comparing the groups (n=3 in each group) at the highest and lowest amounts of raw eGFP expression in the Paigen diet model with EdgeR *(115, 116)* (v.3.32.1) using the glmQLFit method, default settings *(117)*. Statistical significance was set at 5% false discovery rate (FDR; Benjamini-Hochberg). Differential expression gene testing was then performed on the *Csde1*-shRNA and scramble-shRNA at the highest amounts of eGFP expression with the overlap of differentially expressed genes identified between these two analyses subsequently removed. Functional enrichment gene-set analysis for GO (Gene Ontology) terms was performed using Enrichr *(118)* via the enrichR R package (v.3.0). Heatmaps were generated using the Bioconductor package ComplexHeatmap *(119)* (v.2.6.2) using log2-transformed CPM values (counts-per-million; values shown are log2-transformed and row-normalized). Volcano plots were generated using the Bioconductor package EnhancedVolcano (v.1.8.0).

Statistical Analysis

Fluorescence values from gated populations in flow cytometry experiments were background corrected by unstained controls and normalized to the values of the cell line harboring negative control sgRNA when appropriate. Normalized data were then grouped by the Cochrane method *(120)*, and values for cell lines transduced with individual sgRNAs were compared those of the negative control by t-test with Holm-Sidak correction. For comparison of one-phase decay regression curves in mRNA decay experiments, the extra sum-of-squares F test was used. Pairwise testing to controls was performed in all other experiments using Welch's t-test with Holm-Sidak correction unless otherwise noted. For comparison across more than two groups, one-way analysis of variance (ANOVA) with Tukey's multiple comparisons test or two-way ANOVA with Sidak's multiple comparisons test were used unless otherwise noted. When parametric tests were used, data was tested for normality by the D'Agostino-Pearson or Kolmogorov-Smirnov tests. Adjusted p values < 0.05 (two-sided testing) were considered significant. Unless otherwise noted, error bars indicate 95% confidence intervals. In figures, n.s. = non-significant at $p > 0.05$, * = $p < 0.05$, ** = $p < 0.01$, *** = $p < 0.001$, and **** = $p < 0.0001$. Statistical analysis was performed using Prism 7 (GraphPad Software, San Diego CA). All experiments were biologically replicated thrice unless otherwise noted.

Key Resources Table

Antibodies				
Target	**Fluorophore**	**Clone**	**Source**	**Dilution and Final Conc.**
Human LDL Receptor	Alexa Fluor 647	472413	R&D Systems	1:100, 2 µg/ml (FACS)
Human Transferrin Receptor	Alexa Fluor 647	29806	R&D Systems	1:100, 2 µg/ml (FACS)
Human Transferrin Receptor	Alexa Fluor 488	29806	R&D Systems	1:100, 2 µg/ml (FACS)

Human β-Actin	None	8H10D10	Cell Signaling Technology	1:2000 (WB)
Human & Mouse CSDE1	None	62328	Cell Signaling Technology	1:1000 (WB)
Human & Mouse LRP1	None	EPR3724	Abcam	1:20000-1:50000 (WB)
Human & Mouse SR-B1	None	NB400-104	Novus Biologicals	1:2000 (WB)
Mouse ApoA-I	None	2G4	Santa Cruz Biotechnology	1:1000 (WB)
Mouse ApoB	None	2G11	Millipore Sigma	1:1000 (WB)
Mouse LDLR	None	C7	Santa Cruz Biotechnology	1:200 (WB)
Mouse LDLR	None	PA5-81434	ThermoFisher	1:200 (IHC)
Mouse PCSK9	None	AF3985	R&D Systems	1:200 (WB)
Mouse β-Actin	None	8H10D10	Cell Signaling Technology	1:10000 (WB)
GFP	None	6673	Abcam	1:250 (IHC)
Rabbit IgG	IRDye 800CW	926-32211	LI-COR	1:5000, 0.1 µg/ml (WB)
Mouse IgG	IRDye 800CW	926-32210	LI-COR	1:5000, 0.1 µg/ml (WB)

RT-qPCR Primers				
Target	**Ref. Sequence**	**Assay ID**	**Source**	**Conc.**
B2M	NM_004048(1)	Hs.PT.58v.18759587	IDT	300 nM
LDLR	NM_000527(6)	Hs.PT.58.2004261	IDT	300 nM
HMGCR	NM_000859(2)	Hs.PT.58.41105492	IDT	300 nM
CSDE1	NM_001007553(6)	Hs.PT.58.40309152	IDT	300 nM
PCSK9	NM_174936(1)	Hs.PT.58.20317141	IDT	300 nM
MYLIP	NM_013262(1)	Hs.PT.58.39124976	IDT	300 nM
TFRC	NM_003234(1)	Hs.PT.39a.22214826	IDT	300 nM
HNRNPD	NM_031369(4)	Hs.PT.58.3757916	IDT	300 nM
KHSRP	NM_003685(1)	Hs.PT.58.555216	IDT	300 nM
Actb	NM_007393(1)	Mm.PT.39a.22214843.g	IDT	300 nM
B2m	NM_009735(1)	Mm.PT.39a.22214835	IDT	300 nM
Gapdh	NM_008084(1)	Mm.PT.39a.1	IDT	300 nM
Ldlr	NM_001252658(3)	Mm.PT.58.9930556	IDT	300 nM
Csde1	NM_001161854(2)	Mm.PT.58.8160050	IDT	300 nM
eGFP	n/a	Custom Primers Fwd: GAACCGCATCGAGCTGAA Rev: TGCTTGTCGGCCATGATATAG	IDT	300 nM

Supplementary Materials

Table S10: Differentially Expressed Genes in Paigen Diet-Fed Mice by *in vivo* RNA Seq *(provided as an Excel file)*

Table S11: Enriched GO Terms in Paigen Diet-Fed Mice by *in vivo* RNA Seq *(provided as an Excel file)*

Table S12: Differentially Expressed Genes in Chow-Fed Mice by *in vivo* RNA Seq *(provided as an Excel file)*

Table S13: Enriched GO Terms in Chow-Fed Mice by *in vivo* RNA Seq *(provided as an Excel file)*

References

1. M. S. Brown, J. L. Goldstein, A receptor-mediated pathway for cholesterol homeostasis, *Science* **232**, 34–47 (1986).

2. J. L. Goldstein, M. S. Brown, A Century of Cholesterol and Coronaries: From Plaques to Genes to Statins, *Cell* **161**, 161–172 (2015).

3. J. L. Goldstein, M. S. Brown, The LDL receptor, *Arterioscler. Thromb. Vasc. Biol.* **29**, 431–438 (2009).

4. M. G. Silverman, B. A. Ference, K. Im, S. D. Wiviott, R. P. Giugliano, S. M. Grundy, E. Braunwald, M. S. Sabatine, Association Between Lowering LDL-C and Cardiovascular Risk Reduction Among Different Therapeutic Interventions, *JAMA* **316**, 1289–1297 (2016).

5. K. D. Kochanek, J. Xu, E. Arias, Mortality in the United States, 2019, *NCHS Data Brief* **395**, 1–8 (2020).

6. G. G. Schwartz, P. G. Steg, M. Szarek, D. L. Bhatt, V. A. Bittner, R. Diaz, J. M. Edelberg, S. G. Goodman, C. Hanotin, R. A. Harrington, J. W. Jukema, G. Lecorps, K. W. Mahaffey, A. Moryusef, R. Pordy, K. Quintero, M. T. Roe, W. J. Sasiela, J. F. Tamby, P. Tricoci, H. D. White, A. M. Zeiher, L. B. Schiavi, M. Garrido, A. F. Alvarisqueta, S. A. Sassone, A. P. Bordonava, A. E. Alves De Lima, J. M. Schmidberg, E. A. Duronto, O. C. Caruso, L. P. Novaretto, M. A. Hominal, O. R. Montaña, A. Caccavo, O. A. Gomez Vilamajo, A. J. Lorenzatti, L. R. Cartasegna, G. A. Paterlini, I. J. Mackinnon, G. D. Caime, M. Amuchastegui, O. R. Codutti, H. O. Jure, J. O. E. Bono, A. D. Hrabar, J. A. Vallejos, R. A. Ahuad Guerrero, F. Novoa, C. A. Patocchi, C. J. Zaidman, M. E. Giuliano, R. D. Dran, M. L. Vico, G. S. Carnero, P. N. Guzman, J. C. Medrano Allende, D. F. Garcia Brasca, M. H. Bustamante Labarta, S. Nani, E. D. S. Blumberg, H. R. Colombo, A. Liberman, H. L. Luciardi, G. D. Waisman, M. A. Berli, R. O.

Garcia Duran, H. G. Cestari, H. A. Luquez, J. A. Giordano, S. S. Saavedra, J. H. Waites, N. Collins, A. Soward, P. E. Aylward, C. L. S. Hii, J. Shaw, M. A. Arstall, J. Horowitz, J. F. Rogers, D. Colquhoun, R. E. Oqueli Flores, P. Roberts-Thomson, O. Raffel, S. J. Lehman, S. G. M. Coverdale, P. J. Garrahy, G. Starmer, M. Sader, P. A. Carroll, R. Zweiker, U. Hoppe, H. Drexel, K. Huber, R. Berger, F. Weidinger, D. Faes, K. Hermans, B. Pirenne, A. Leone, E. Hoffer, P. Sinnaeve, M. C. M. Vrolix, L. De Wolf, B. Wollaert, M. Castadot, K. Dujardin, C. Beauloye, G. Vervoort, H. Striekwold, C. Convens, J. Roosen, E. Barbato, M. Claeys, F. Cools, I. Terzic, F. Barakovic, Z. Midzic, B. Pojskic, E. Fazlibegovic, M. Dilic, A. Durak-Nalbantic, D. Vulic, A. Muslibegovic, G. Reis, L. Sousa, J. C. Nicolau, F. E. Giorgeto, R. P. Silva, L. Nigro Maia, R. Rech, P. R. F. Rossi, M. Cerqueira, N. Duda, R. Kalil, A. Kormann, J. A. M. Abrantes, P. Pimentel Filho, A. P. Soggia, M. O. N. de Santos, F. Neuenschwander, L. C. Bodanese, Y. L. Michalaros, F. G. Eliaschewitz, M. H. Vidotti, P. E. Leaes, R. V. Botelho, S. Kaiser, E. R. F. Fernandes Manenti, D. B. Precoma, J. C. Moura Jorge, P. G. M. de B Silva, J. A. Silveira, W. Saporito, J. A. Marin Neto, G. S. Feitosa, L. E. F Ritt, J. A. de Souza, F. Costa, W. Souza, H. J. L. Reis, R. D. Lopes, L. Machado, J. C. Aidar Ayoub, G. V. Todorov, F. P. Nikolov, E. S. Velcheva, M. L. Tzekova, H. O. Benov, S. L. Petranov, H. S. Tumbev, N. S. Shehova-Yankova, D. T. Markov, D. H. Raev, M. N. Mollov, K. N. Kichukov, K. A. Ilieva-Pandeva, N. N. Gotcheva, R. Ivanova, V. M. Mincheva, P. V. Lazov, B. I. Dimov, M. Senaratne, J. Stone, J. Kornder, S. Pearce, D. Dion, D. Savard, Y. Pesant, A. Pandey, S. Robinson, G. Gosselin, S. Vizel, G. Hoag, R. Bourgeois, A. Morisset, E. Sabbah, B. Sussex, S. Kouz, P. MacDonald, N. Michaud, D. Fell, R. Leung, T. Vuurmans, C. Lai, F. Nigro, R. Davies, G. Nogareda, R. Vijayaraghavan, J. Ducas, S. Lepage, S. Mehta, J. Cha, R. Dupuis, P. Fong, J. Rodes-Cabau, H. Fadlallah, D. Cleveland, T. Huynh, I. Bata, A. Hameed, C. Pincetti, S. Potthoff, J. C. Prieto, M.

Acevedo, A. Aguirre, M. Vejar, M. Yañez, G. Araneda, M. Fernandez, L. Perez, P. Varleta, F. Florenzano, L. Huidobro, C. A. Raffo, C. Olivares, J. Chen, Y. Dong, W. Huang, J. Wang, S. Huang, Z. Yao, L. Cui, W. Lin, Y. Sun, J. Li, X. Zhang, H. Zhu, D. Chen, L. Huang, S. Dong, G. Su, B. Xu, X. Su, X. Cheng, J. Lin, W. Zong, H. Li, Y. Feng, D. Xu, X. Yang, Y. Ke, X. Lin, Z. Zhang, Z. Zheng, Z. Luo, Y. Chen, C. Ding, Y. Zheng, X. Li, D. Peng, Y. Li, M. Wei, S. Liu, Y. Yu, B. Qu, W. Jiang, Y. Zhou, X. Zhao, Z. Yuan, Y. Guo, X. Xu, X. Shi, J. Ge, G. Fu, F. Bai, W. Fang, X. Shou, N. Jaramillo, G. Sanchez Vallejo, D. C. Luna Botia, R. Botero Lopez, D. I. Molina De Salazar, A. J. Cadena Bonfanti, J. Diego Higuera, S. I. Barrera Silva, H. J. Garcia Lozada, J. A. Coronel Arroyo, J. L. Accini Mendoza, R. L. Fernandez Ruiz, A. M. Fernandez, F. G. Manzur Jatin, A. Sotomayor Herazo, J. Castellanos Parada, M. A. Urina Triana, M. Strozzi, S. Car, D. Miličić, M. L. Benčić, H. Pintarić, D. Prvulović, J. Šikić, V. Peršić, D. Mileta, K. Štambuk, Z. Babić, J. Spinar, D. Horak, J. Stasek, D. Alan, V. Machova, A. Linhart, V. Novotny, V. Kaucak, R. Rokyta, R. Naplava, Z. Coufal, V. Adamkova, I. Podpera, J. Zizka, Z. Motovska, I. Marusincova, P. Svab, P. Ostadal, P. Heinc, J. Kuchar, P. Povolny, S. H. Poulsen, B. Raungaard, P. Clemmensen, L. E. Bang, O. May, M. Bøttcher, J. D. Hove, L. Frost, G. Gislason, J. Larsen, P. B. Johansen, F. Hald, J. Jeppesen, T. Nielsen, K. S. Kristensen, P. M. Walichiewicz, J. D. Lomholdt, I. C. Klausen, P. K. Nielsen, F. Davidsen, L. Videbaek, M. Viigimaa, M. Soots, V. Vahula, A. Hedman, U. Soopõld, K. Märtsin, M. R. Taskinen, K. Porthan, J. K. Airaksinen, M. Juonala, T. Kiviniemi, S. Vikman, P. Posio, J. Taurio, H. Huikuri, K. Kaikkonen, P. Coste, E. Ferrari, N. Danchin, O. Morel, G. Montalescot, G. Barone-Rochette, J. Mansourati, Y. Cottin, F. Leclercq, A. Belhassane, N. Delarche, F. Boccara, F. Paganelli, J. Clerc, F. Schiele, V. Aboyans, V. Probst, J. Berland, T. Lefèvre, V. Chumburidze, I. Khintibidze, T. Shaburishvili, Z. Pagava, R. Ghlonti, Z. Lominadze, G. Khabeishvili, R. Hemetsberger, U. Rauch-Kröhnert, M. Stratmann,

K. F. Appel, E. Schmidt, H. Omran, C. Stellbrink, T. Dorsel, E. Lianopoulos, R. Marx, A. Zirlik, D. Schellenberg, T. Heitzer, U. Laufs, N. Marx, S. Gielen, B. Winkelmann, S. Behrens, K. Sydow, G. Simonis, T. Muenzel, N. Werner, S. Leggewie, D. Böcker, R. Braun-Dullaeus, N. Toursarkissian, M. Jeserich, M. Weißbrodt, T. Schaeufele, J. Weil, H. Völler, J. Waltenberger, M. Natour, S. Steiner, L. Heidenreich, U. Gremmler, H. Killat, S. Patsilinakos, A. Kartalis, A. Manolis, D. Sionis, E. Liberopoulos, I. Skoumas, V. Athyros, P. Vardas, F. Parthenakis, D. Alexopoulos, G. Hahalis, J. Lekakis, A. Xatzitolios, S. R. Fausto Ovando, P. C. Montenegro Valdovinos, J. L. Arango Benecke, E. R. Rodriguez De Leon, B. P. Y. Yan, D. C. W. Siu, T. Turi, B. Merkely, R. G. Kiss, I. Ungi, G. Lupkovics, L. Nagy, A. Katona, I. Édes, G. Müller, I. Horvath, T. Kapin, J. Faluközy, M. Kumbla, M. Sandhu, S. Annam, N. R. Proddutur, R. K. Premchand, A. Mahajan, A. D. Abhyanakar, P. Kerkar, R. A. Govinda, A. Oomman, D. Sinha, S. N. Patil, D. Kahali, J. Sawhney, A. B. Joshi, S. Chaudhary, P. Harkut, S. Guha, S. Porwal, S. Jujjuru, R. B. Pothineni, M. R. Monteiro, A. Khan, S. S. Iyengar, J. S. Grewal, M. Chopda, M. C. Fulwani, A. Patange, V. K. Chopra, N. K. Goyal, R. Shinde, G. V. Manakshe, N. Patki, S. Sethi, V. Munusamy, S. Karna, S. Adhyapak, U. Pandurangi, R. Mathur, S. Kalashetti, A. Bhagwat, B. Raghuraman, S. K. Yerra, P. Bhansali, R. Borse, S. Das, J. Abdullakutty, S. Saathe, P. Palimkar, S. Atar, M. Shechter, M. Mosseri, Y. Arbel, C. Lotan, U. Rosenschein, A. Katz, Y. Henkin, A. Francis, M. Klutstein, E. Nikolsky, Y. Turgeman, M. Halabi, R. Kornowski, M. Jonas, O. Amir, Y. Rozenman, S. Fuchs, O. Hussein, D. Gavish, Z. Vered, Y. Caraco, M. Elias, N. Tov, G. Piovaccari, A. De Pellegrin, G. Guardigli, G. Licciardello, C. Auguadro, C. Cuccia, A. Salvioni, G. Musumeci, P. Calabrò, S. Novo, P. Faggiano, N. B. De Cesare, S. Berti, C. Cavallini, E. Puccioni, M. Galvani, M. Tespili, P. Piatti, M. Palvarini, G. De Luca, R. Violini, A. De Leo, P. Perrone Filardi, M. Ferratini, K. Dai, H. Kamiya, K. Ando, Y. Takeda, Y. Morino, Y. Hata, K.

Kimura, K. Kishi, I. Michishita, H. Uehara, T. Higashikata, A. Hirayama, K. Hirooka, S. Sakagami, S. Taguchi, A. Koike, H. Fujinaga, S. Koba, K. Kozuma, T. Kawasaki, Y. Ono, M. Shimizu, Y. Katsuda, A. Wada, T. Shinke, T. Kimura, J. Ako, K. Fujii, T. Takahashi, T. Sakamoto, Y. Furukawa, H. Sugino, T. Mano, N. Utsu, K. Ito, T. Haraguchi, Y. Ueda, A. Nishibe, K. Fujimoto, J. H. Yoon, S. H. Kim, H. S. Park, I. H. Chae, M. H. Kim, M. H. Jeong, S. Rha, C. Kim, H. S. Kim, T. Hong, A. Busmane, N. Pontaga, A. Strelnieks, I. Mintale, I. Sime, Z. Petrulioniene, R. Kavaliauskiene, R. Jurgaitiene, G. Sakalyte, R. Slapikas, S. Norkiene, N. Misonis, A. Kibarskis, R. Kubilius, S. Bojovski, S. Kedev, N. Lozance, A. Kjovkaroski, S. Doncovska, T. K. Ong, S. Kasim, O. Maskon, B. Kandasamy, K. Yusoff, H. B. Liew, W. M. I. Wan Mohamed, A. García Castillo, G. A. Ramos López, J. Carrillo Calvillo, P. Fajardo Campos, J. C. Núñez Fragoso, E. A. Bayram Llamas, M. A. Alcocer Gamba, J. Carranza Madrigal, L. G. González Salas, E. López Rosas, B. González Díaz, E. Salcido Vázquez, A. Nacoud Ackar, G. A. Llamas Esperón, C. R. Martínez Sánchez, M. Guerrero De Leon, R. Suarez Otero, G. Fanghänel Salmón, J. A. Pérez Ríos, J. A. Garza Ruíz, M. Alings, R. W. Breedveld, P. A. M. Hoogslag, H. Suryapranata, A. Oomen, J. J. Wiersma, R. M. A. Van Der Wal, P. S. Hooft Van Huysduynen-Monraats, I. Karalis, G. J. E. Verdel, B. R. G. Brueren, R. P. T. Troquay, E. P. Viergever, N. Y. Y. Al-Windy, G. L. Bartels, J. H. Cornel, W. R. M. Hermans, J. P. R. Herrman, R. J. Bos, R. Groutars, C. C. Van Der Zwaan, R. Kaplan, E. Ronner, B. E. Groenemeijer, P. N. A. Bronzwaer, A. A. H. Liem, B. Rensing, M. Bokern, R. Nijmeijer, F. Hersbach, F. F. Willems, A. T. M. Gosselink, J. Elliott, G. Wilkins, R. Fisher, D. Scott, H. Hart, R. Stewart, S. Harding, I. Ternouth, N. Fisher, D. Aitken, R. Anscombe, T. Tomala, O. Nygård, J. A. Sparby, K. Andersen, L. Gullestad, J. Jortveit, P. S. Munk, S. Halvorsen, U. Hurtig, R. M. Correa Flores, J. R. Calderon Ticona, J. R. Durand Velasquez, S. A. Negron Miguel, E. S. Sanabria Perez, J. M.

Carrion Chambilla, C. A. Chavez Ayala, R. P. Castillo Leon, R. J. Vargas Gonzales, J. D. Hernandez Zuniga, L. A. Camacho Cosavalente, J. E. Bravo Mannucci, N. C. Llerena Navarro, Y. M. Roldan Concha, V. E. Rodriguez Chavez, H. A. Anchante Hernandez, C. A. Zea Nunez, A. Ferrolino, R. A. G. Sy, L. Tirador, R. G. Sy, G. Matiga, R. M. Coching, A. Bernan, G. Rogelio, D. D. Morales, E. Tan, A. Wlodarczak, K. Jaworska, G. Skonieczny, L. Pawlowicz, P. Wojewoda, B. Busz-Papiez, J. Bednarski, A. Goch, P. Staneta, E. Dulak, A. Budaj, K. Saminski, W. Krasowski, W. Sudnik, A. Zurakowski, M. Skorski, R. Lysek, B. Miklaszewicz, J. Kubica, J. A. Lipko, E. Kostarska-Srokosz, M. Piepiorka, A. Drzewiecka, R. Sciborski, A. Stasiewski, T. Blicharski, L. Bystryk, M. Szpajer, M. Korol, T. Czerski, E. Mirek-Bryniarska, J. Gniot, A. Lubinski, J. Gorny, E. Franek, P. Monteiro, J. Mesquita Bastos, H. H. Pereira, D. Martins, J. Morais, F. Seixo, C. Mendonça, A. Botelho, B. Minescu, O. Istratoaie, D. N. Tesloianu, M. Dorobantu, G. Cristian, C. G. C. Podoleanu, M. C. A. Constantinescu, C. M. Bengus, C. Militaru, D. Rosu, I. R. Parepa, A. V. Matei, T. M. Alexandru, Y. Shvarts, O. Orlikova, Z. Kobalava, O. L. Barbarash, V. Markov, N. Lyamina, A. Gordienko, K. Zrazhevsky, A. Y. Vishnevsky, V. Gurevich, R. Stryuk, N. V. Lomakin, I. Bokarev, S. Shalaev, L. Khaisheva, P. Chizhov, I. Viktorova, N. Osokina, E. Akatova, G. Chumakova, I. Libov, M. I. Voevoda, T. V. Tretyakova, E. Baranov, S. Shustov, S. Yakushin, I. Gordeev, N. Khasanov, O. Reshetko, T. Sotnikova, O. Molchanova, K. Y. Nikolaev, L. Gapon, E. Baranova, Z. Shogenov, E. Kosmachova, Y. Karpov, A. Povzun, L. Egorova, V. V. Tyrenko, I. G. Ivanov, D. Simic, N. Ivanovic, G. Davidovic, N. Tasic, M. R. Asanin, S. Stojic, S. R. Apostolovic, S. Ilic, B. Putnikovic, A. Stankovic, A. Arandjelovic, S. Radovanovic, A. D. Ristic, J. Balinovac, D. V. Dincic, P. Seferovic, S. Dodic, S. Dimkovic, T. Chua, K. K. Poh, H. Y. Ong, K. Micko, J. Nociar, D. Pella, P. Fulop, M. Hranai, J. Palka, J. Mazur, I. Majercák, A. Dzupina, F. Fazekas, J.

Gonsorcik, V. Bugan, J. Murin, J. Selecky, G. Kamensky, J. Strbova, R. Smik, A. Dukat, I. Žuran, J. Oklukar, N. C. Šuligoj, M. Cevc, L. Lipar, H. P. Cyster, N. Ranjith, C. Corbett, J. Bayat, E. M. Makotoko, I. E. Kapp, M. M. V. Basson, H. Lottering, L. J. Van Zyl, P. J. Sebastian, T. Pillay, J. A. Saaiman, P. J. Commerford, S. Cassimjee, I. O. Ebrahim, M. Sarvan, J. H. Mynhardt, A. J. Dalby, H. Reuter, R. Moodley, M. Vida, A. R. Cequier Fillat, V. Bodí Peris, F. Fuentes Jimenez, F. Marín, J. M. Cruz Fernández, B. Gil-Extremera, F. W. Diz, D. Garcia-Dorado, A. Iñiguez, J. Tuñón Fernández, J. R. Gonzalez-Juanatey, J. Fernandez Portales, F. Civeira Murillo, L. Matas Pericas, J. L. Zamorano, M. De Mora Martin, J. Bruguera Cortada, J. J. Alonso Martin, J. R. De Berrazueta Fernández, J. F. Díaz Fernández, J. A. García Lledó, J. Cosín Sales, J. Botas Rodriguez, G. Gusi Tragant, A. Benedicto, C. Gonzalez-Juanatey, M. Camprubí Potau, I. Plaza Perez, C. M. De La Tassa, P. Loma-Osorio Rincon, J. Balaguer Recena, J. M. Escudier, G. Constantine, R. Haniffa, N. Tissera, S. Amarasekera, N. Fernando, J. Jayawardena, W. Santharaj, R. Ekanayaka, S. Mendis, V. Senaratne, G. Mayurathan, T. Sirisena, A. Rajapaksha, J. I. Herath, N. Amarasena, S. Berglund, G. Rasmanis, E. Hagström, N. Witt, G. Mourtzinis, P. Nicol, O. Hansen, S. Romeo, S. A. Jensen, I. Torstensson, U. Ahremark, T. Sundelin, T. Moccetti, C. Müller, F. Mach, R. Binder, C. E. Chiang, W. C. Tsai, K. C. Ueng, W. T. Lai, M. E. Liu, J. J. Hwang, W. H. Yin, I. C. Hsieh, W. H. Lin, J. Y. Kuo, T. Y. Huang, C. Y. Fang, P. Kaewsuwanna, W. Soonfuang, W. Jintapakorn, A. Sukonthasarn, P. Sritara, N. Wongpraparut, K. Sastravaha, N. Sansanayudh, W. Kehasukcharoen, D. Piyayotai, A. Camsari, H. Kultursay, S. Guneri, B. Mutlu, M. Ersanli, M. Demirtas, C. Kirma, E. Ural, L. Koldas, O. Karpenko, A. Prokhorov, I. Vakaluyk, H. Myshanych, D. Reshotko, V. Batushkin, L. Rudenko, I. Kovalskyi, M. Kushnir, V. Tseluyko, Y. Mostovoy, M. Stanislavchuk, Y. Kyiak, Y. Karpenko, Y. Malynovsky, A. Klantsa, O. Kutniy, E. Amosova, V. Tashchuk, O. Leshchuk, A.

Parkhomenko, M. Rishko, M. Kopytsya, A. Yagensky, M. Vatutin, A. Bagriy, O. M. Barna, O. Ushakov, G. Dzyak, B. Goloborodko, A. Rudenko, J. Trevelyan, A. Zaman, K. Lee, A. Moriarty, R. K. Aggarwal, P. Clifford, Y. K. Wong, S. M. R. Iqbal, E. Subkovas, D. Braganza, D. Sarkar, R. Storey, H. Griffiths, S. Mcclure, R. Muthusamy, J. Kurian, T. Levy, C. Barr, H. Kadr, R. Gerber, A. Simaitis, H. Soran, A. Mathur, A. Brodison, R. Oliver, T. Mudawi, T. Reynolds, D. Sharman, R. Butler, P. Wilkinson, G. Y. H. Lip, J. Halcox, G. Vardi, D. Baldari, D. Brabham, C. Treasure, C. Dahl, B. Palmer, A. Wiseman, S. Puri, A. E. Mohart, C. Ince, E. Flores, S. Wright, S. C. Cheng, M. Rosenberg, W. Rogers, E. Kosinski, L. Forgosh, J. Waltman, M. Khan, M. Shoukfeh, G. Dagher, I. Lieber, P. Kumar, C. East, P. Krichmar, L. White, T. Knickelbine, T. Haldis, E. Gillespie, D. Suh, I. Arif, F. Akhter, E. Carlson, M. D'Urso, F. El-Ahdab, W. Nelson, B. Harris, S. Cohen, L. Carter, K. Sabatino, T. Haddad, A. Malik, S. Rao, A. Mulkay, I. Jovin, K. Klancke, V. Malhotra, S. K. Devarapalli, M. Koren, H. Chandna, G. Dodds, M. Janik, J. Moran, A. Sumner, J. Kobayashi, W. Davis, S. Yazdani, J. Pasquini, M. Thakkar, A. Vedere, W. Leimbach, J. Rider, N. Singh, A. V. Shah, P. M. Moriarty, D. Janosik, C. Pepine, B. Berman, J. Gelormini, C. Daniels, F. Keating, N. I. Kondo, S. Shetty, W. Waider, T. Takata, M. Abu-Fadel, V. Shah, R. Aggarwal, M. Izzo, A. Kumar, B. Hattler, C. Link, A. Bortnick, G. Kinzfogl, A. Ghitis, J. Larry, E. Teufel, P. Kuhlman, B. Mclaurin, W. Zhang, S. Thew, J. Abbas, M. White, N. Ranadive, C. Gring, D. Henderson, T. Schuchard, N. Farhat, G. Kline, S. Mahal, J. Whitaker, S. Speirs, R. Andersen, N. Daboul, P. Horwitz, Z. Jafar, J. Mcgarvey, V. Panchal, S. Voyce, T. Blok, W. Sheldon, M. M. Azizad, C. Schmalfuss, M. Picone, W. Herzog, J. Lindsey, R. Nowins, N. Lepor, M. El Shahawy, H. Weintraub, A. Irimpen, W. May, T. Galski, A. Chu, F. Mody, Z. Hodes, J. Fairlamb, C. Lambert, A. Raisinghani, A. Abbate, M. King, C. Carey, J. Gerber, L. Younis, H. T. Park, M. Vidovich, T. Knutson, D. Friedman, F. Chaleff, A. Loussararian, C.

Kimmelstiel, K. Silver, M. Foster, G. Tonnessen, M. Amlani, A. Wali, C. Malozzi, K. Wattanakit, P. J. O'Donnell, D. Singal, N. Jaffrani, S. Banuru, D. Fisher, M. Xenakis, N. Perlmutter, R. Bhagwat, J. Strader, A. Akyea-Djamson, A. Labroo, H. J. Marais, E. Claxton, M. Berk, P. Rossi, P. Joshi, A. S. Khaira, G. Kumkumian, S. Lupovitch, J. Purow, S. Welka, D. Hoffman, S. Fischer, E. Soroka, D. Eagerton, S. Pancholy, M. Ray, M. Farrar, S. Pollock, W. J. French, S. Diamantis, L. Gimple, S. Schwartz, E. Pereira, D. Spriggs, J. Strain, A. Vo, M. Chane, J. Hall, N. Vijay, K. Lotun, F. M. Lester, A. Nahhas, T. Pope, P. Nager, R. Vohra, R. Bashir, H. Ahmed, M. Berlowitz, R. Fishberg, R. Barrucco, E. Yang, M. Radin, D. Sporn, S. Eisenberg, J. Landzberg, M. Mcgough, S. Turk, M. Schwartz, P. S. Sundram, D. Jain, M. Zainea, C. Bayron, R. Karlsberg, H. Lui, W. Keen, D. Westerhausen, S. Khurana, H. Agarwal, J. Birchem, W. Penny, M. Chang, J. M. Gilbert, G. Chalavarya, C. Eaton, J. F. Schmedtje, S. Christenson, D. Denham, A. Macdonell, P. Gibson, A. Rahman, T. Al Joundi, G. Conrad, P. Kotha, M. Love, G. Giesler, H. Rubenstein, L. Akright, B. Schifferdecker, J. Krawczyk, T. Wells, J. Welker, R. Foster, R. Gilmore, J. Anderson, D. Jacoby, G. Gardner, R. Dandillaya, K. Vora, J. Kostis, J. Hunter, D. Laxson, E. Ball, Alirocumab and cardiovascular outcomes after acute coronary syndrome, *N. Engl. J. Med.* **379**, 2097–2107 (2018).

7. M. S. Sabatine, R. P. Giugliano, A. C. Keech, N. Honarpour, S. D. Wiviott, S. A. Murphy, J. F. Kuder, H. Wang, T. Liu, S. M. Wasserman, P. S. Sever, T. R. Pedersen, FOURIER Steering Committee and Investigators, Evolocumab and Clinical Outcomes in Patients with Cardiovascular Disease, *N. Engl. J. Med.* **376**, 1713–1722 (2017).

8. C. Ma, M. E. Gurol, Z. Huang, A. H. Lichtenstein, X. Wang, Y. Wang, S. Neumann, S. Wu, X. Gao, Low-density lipoprotein cholesterol and risk of intracerebral hemorrhage, *Neurology* **93**, e445–e457 (2019).

9. M. S. Sabatine, S. D. Wiviott, K. Im, S. A. Murphy, R. P. Giugliano, Efficacy and safety of further lowering of low-density lipoprotein cholesterol in patients starting with very low levels: A meta-analysis, *JAMA Cardiol.* **3**, 823–828 (2018).

10. R. P. Giugliano, T. R. Pedersen, J.-G. Park, G. M. De Ferrari, Z. A. Gaciong, R. Ceska, K. Toth, I. Gouni-Berthold, J. Lopez-Miranda, F. Schiele, F. Mach, B. R. Ott, E. Kanevsky, A. L. Pineda, R. Somaratne, S. M. Wasserman, A. C. Keech, P. S. Sever, M. S. Sabatine, FOURIER Investigators, Clinical efficacy and safety of achieving very low LDL-cholesterol concentrations with the PCSK9 inhibitor evolocumab: a prespecified secondary analysis of the FOURIER trial, *Lancet* **390**, 1962–1971 (2017).

11. A. Taylor, D. Wang, K. Patel, R. Whittall, G. Wood, M. Farrer, R. D. Neely, S. Fairgrieve, D. Nair, M. Barbir, J. L. Jones, S. Egan, R. Everdale, Y. Lolin, E. Hughes, J. A. Cooper, S. G. Hadfield, G. Norbury, S. E. Humphries, Mutation detection rate and spectrum in familial hypercholesterolaemia patients in the UK pilot cascade project, *Clin. Genet.* **77**, 572–580 (2010).

12. A. Garg, S. Fazio, P. B. Duell, A. Baass, C. Udata, T. Joh, T. Riel, M. Sirota, D. Dettling, H. Liang, P. D. Garzone, B. Gumbiner, H. Wan, Molecular Characterization of Familial Hypercholesterolemia in a North American Cohort, *J. Endocr. Soc.* **4**, bvz015 (2019).

13. D. Klarin, S. M. Damrauer, K. Cho, Y. V Sun, T. M. Teslovich, J. Honerlaw, D. R. Gagnon, S. L. DuVall, J. Li, G. M. Peloso, M. Chaffin, A. M. Small, J. Huang, H. Tang, J. A. Lynch, Y.-L. Ho, D. J. Liu, C. A. Emdin, A. H. Li, J. E. Huffman, J. S. Lee, P. Natarajan, R. Chowdhury, D. Saleheen, M. Vujkovic, A. Baras, S. Pyarajan, E. Di Angelantonio, B. M. Neale, A. Naheed, A. V Khera, J. Danesh, K.-M. Chang, G. Abecasis, C. Willer, F. E. Dewey, D. J. Carey, J. Concato, J. M. Gaziano, C. J. O'Donnell, P. S. Tsao, S. Kathiresan, D. J. Rader, P. W. F. Wilson, T. L. Assimes, G. L. G. Consortium, M. I. G. (MIGen) Consortium, T. G.-R. D. Collaboration,

T. V. A. M. V. Program, Genetics of blood lipids among ~300,000 multi-ethnic participants of the Million Veteran Program, *Nat. Genet.* **50**, 1514–1523 (2018).

14. P. J. Talmud, S. Shah, R. Whittall, M. Futema, P. Howard, J. A. Cooper, S. C. Harrison, K. Li, F. Drenos, F. Karpe, H. A. W. Neil, O. S. Descamps, C. Langenberg, N. Lench, M. Kivimaki, J. Whittaker, A. D. Hingorani, M. Kumari, S. E. Humphries, Use of low-density lipoprotein cholesterol gene score to distinguish patients with polygenic and monogenic familial hypercholesterolaemia: a case-control study, *Lancet* **381**, 1293–1301 (2013).

15. M. T. Oetjens, M. A. Kelly, A. C. Sturm, C. L. Martin, D. H. Ledbetter, Quantifying the polygenic contribution to variable expressivity in eleven rare genetic disorders, *Nat. Commun.* **10**, 4897 (2019).

16. L. A. Gilbert, M. A. Horlbeck, B. Adamson, J. E. Villalta, Y. Chen, E. H. Whitehead, C. Guimaraes, B. Panning, H. L. Ploegh, M. C. Bassik, L. S. Qi, M. Kampmann, J. S. Weissman, Genome-Scale CRISPR-Mediated Control of Gene Repression and Activation, *Cell* **159**, 647–661 (2014).

17. M. A. Horlbeck, L. A. Gilbert, J. E. Villalta, B. Adamson, R. A. Pak, Y. Chen, A. P. Fields, C. Y. Park, J. E. Corn, M. Kampmann, J. S. Weissman, Compact and highly active next-generation libraries for CRISPR-mediated gene repression and activation, *Elife* **5**, e19760 (2016).

18. B. Adamson, T. M. Norman, M. Jost, M. Y. Cho, J. K. Nuñez, Y. Chen, J. E. Villalta, L. A. Gilbert, M. A. Horlbeck, M. Y. Hein, R. A. Pak, A. N. Gray, C. A. Gross, A. Dixit, O. Parnas, A. Regev, J. S. Weissman, A Multiplexed Single-Cell CRISPR Screening Platform Enables Systematic Dissection of the Unfolded Protein Response, *Cell* **167**, 1867–1882.e21 (2016).

19. K. K. Ray, R. S. Wright, D. Kallend, W. Koenig, L. A. Leiter, F. J. Raal, J. A. Bisch, T. Richardson, M. Jaros, P. L. J. Wijngaard, J. J. P. Kastelein, Two phase 3 trials of inclisiran in

patients with elevated LDL cholesterol, *N. Engl. J. Med.* **382**, 1507-1519 (2020).

20. B. B. Knowles, C. C. Howe, D. P. Aden, Human hepatocellular carcinoma cell lines secrete the major plasma proteins and hepatitis B surface antigen, *Science* **209**, 497–499 (1980).

21. H. Scharnagl, R. Schinker, H. Gierens, M. Nauck, H. Wieland, W. März, Effect of atorvastatin, simvastatin, and lovastatin on the metabolism of cholesterol and triacylglycerides in HepG2 cells., *Biochem. Pharmacol.* **62**, 1545–1555 (2001).

22. J. Liu, F. Zhang, C. Li, M. Lin, M. R. Briggs, Synergistic Activation of Human LDL Receptor Expression by SCAP Ligand and Cytokine Oncostatin M, *Arterioscler. Thromb. Vasc. Biol.* **23**, 90–96 (2003).

23. G. Dubuc, A. Chamberland, H. Wassef, J. Davignon, N. G. Seidah, L. Bernier, A. Prat, Statins Upregulate PCSK9, the Gene Encoding the Proprotein Convertase Neural Apoptosis-Regulated Convertase-1 Implicated in Familial Hypercholesterolemia, *Arterioscler. Thromb. Vasc. Biol.* **24**, 1454–1459 (2004).

24. T. A. Lagace, D. E. Curtis, R. Garuti, M. C. McNutt, S. W. Park, H. B. Prather, N. N. Anderson, Y. K. Ho, R. E. Hammer, J. D. Horton, Secreted PCSK9 decreases the number of LDL receptors in hepatocytes and in livers of parabiotic mice., *J. Clin. Invest.* **116**, 2995–3005 (2006).

25. M. A. Mandegar, N. Huebsch, E. B. Frolov, E. Shin, A. Truong, M. P. Olvera, A. H. Chan, Y. Miyaoka, K. Holmes, C. I. Spencer, L. M. Judge, D. E. Gordon, T. V. Eskildsen, J. E. Villalta, M. A. Horlbeck, L. A. Gilbert, N. J. Krogan, S. P. Sheikh, J. S. Weissman, L. S. Qi, P. L. So, B. R. Conklin, CRISPR Interference Efficiently Induces Specific and Reversible Gene Silencing in Human iPSCs, *Cell Stem Cell* **18**, 541–553 (2016).

26. A. W. Alberts, J. Chen, G. Kuron, V. Hunt, J. Huff, C. Hoffman, J. Rothrock, M. Lopez, H.

Joshua, E. Harris, A. Patchett, R. Monaghan, S. Currie, E. Stapley, G. Albers-Schonberg, O. Hensens, J. Hirshfield, K. Hoogsteen, J. Liesch, J. Springer, Mevinolin: A highly potent competitive inhibitor of hydroxymethylglutaryl-coenzyme A reductase and a cholesterol-lowering agent, *Proc. Natl. Acad. Sci. U. S. A.* **77**, 3957–3961 (1980).

27. M. S. Brown, J. R. Faust, J. L. Goldstein, I. Kaneko, A. Endo, Induction of 3-hydroxy-3-methylglutaryl coenzyme A reductase activity in human fibroblasts incubated with compactin (ML-236B), a competitive inhibitor of the reductase, *J. Biol. Chem.* **253**, 1121–1128 (1978).

28. S. Benjannet, D. Rhainds, R. Essalmani, J. Mayne, L. Wickham, W. Jin, M.-C. Asselin, J. Hamelin, M. Varret, D. Allard, M. Trillard, M. Abifadel, A. Tebon, A. D. Attie, D. J. Rader, C. Boileau, L. Brissette, M. Chrétien, A. Prat, N. G. Seidah, NARC-1/PCSK9 and its natural mutants: zymogen cleavage and effects on the low density lipoprotein (LDL) receptor and LDL cholesterol., *J. Biol. Chem.* **279**, 48865–48875 (2004).

29. S. Rashid, D. E. Curtis, R. Garuti, N. N. Anderson, Y. Bashmakov, Y. K. Ho, R. E. Hammer, Y. A. Moon, J. D. Horton, Decreased plasma cholesterol and hypersensitivity to statins in mice lacking Pcsk9, *Proc. Natl. Acad. Sci. U. S. A.* **102**, 5374–5379 (2005).

30. J. C. Chan, D. E. Piper, Q. Cao, D. Liu, C. King, W. Wang, J. Tang, Q. Liu, J. Higbee, Z. Xia, Y. Di, S. Shetterly, Z. Arimura, H. Salomonis, W. G. Romanow, S. T. Thibault, R. Zhang, P. Cao, X. P. Yang, T. Yu, M. Lu, M. W. Retter, G. Kwon, K. Henne, O. Pan, M. M. Tsai, B. Fuchslocher, E. Yang, L. Zhou, K. J. Lee, M. Daris, J. Sheng, Y. Wang, W. D. Shen, W. C. Yeh, M. Emery, N. P. Walker, B. Shan, M. Schwarz, S. M. Jackson, A proprotein convertase subtilisin/kexin type 9 neutralizing antibody reduces serum cholesterol in mice and nonhuman primates, *Proc. Natl. Acad. Sci. U. S. A.* **106**, 9820–9825 (2009).

31. P. Aisen, Transferrin receptor 1., *Int. J. Biochem. Cell Biol.* **36**, 2137–2143 (2004).

32. R. Coffey, T. Ganz, Iron homeostasis: An anthropocentric perspective, *J. Biol. Chem.* **292**, 12727–12734 (2017).

33. N. Zelcer, C. Hong, R. Boyadjian, P. Tontonoz, LXR regulates cholesterol uptake through Idol-dependent ubiquitination of the LDL receptor, *Science* **325**, 100–104 (2009).

34. M. Yoshinaga, Y. Nakatsuka, A. Vandenbon, D. Ori, T. Uehata, T. Tsujimura, Y. Suzuki, T. Mino, O. Takeuchi, Regnase-1 Maintains Iron Homeostasis via the Degradation of Transferrin Receptor 1 and Prolyl-Hydroxylase-Domain-Containing Protein 3 mRNAs, *Cell Rep.* **19**, 1614–1630 (2017).

35. H. Mi, A. Muruganujan, D. Ebert, X. Huang, P. D. Thomas, PANTHER version 14: more genomes, a new PANTHER GO-slim and improvements in enrichment analysis tools, *Nucleic Acids Res.* **47**, D419–D426 (2019).

36. T. M. Teslovich, K. Musunuru, A. V. Smith, A. C. Edmondson, I. M. Stylianou, M. Koseki, J. P. Pirruccello, S. Ripatti, D. I. Chasman, C. J. Willer, C. T. Johansen, S. W. Fouchier, A. Isaacs, G. M. Peloso, M. Barbalic, S. L. Ricketts, J. C. Bis, Y. S. Aulchenko, G. Thorleifsson, M. F. Feitosa, J. Chambers, M. Orho-Melander, O. Melander, T. Johnson, X. Li, X. Guo, M. Li, Y. Shin Cho, M. Jin Go, Y. Jin Kim, J.-Y. Lee, T. Park, K. Kim, X. Sim, R. Twee-Hee Ong, D. C. Croteau-Chonka, L. A. Lange, J. D. Smith, K. Song, J. Hua Zhao, X. Yuan, J. Luan, C. Lamina, A. Ziegler, W. Zhang, R. Y. L. Zee, A. F. Wright, J. C. M. Witteman, J. F. Wilson, G. Willemsen, H.-E. Wichmann, J. B. Whitfield, D. M. Waterworth, N. J. Wareham, G. Waeber, P. Vollenweider, B. F. Voight, V. Vitart, A. G. Uitterlinden, M. Uda, J. Tuomilehto, J. R. Thompson, T. Tanaka, I. Surakka, H. M. Stringham, T. D. Spector, N. Soranzo, J. H. Smit, J. Sinisalo, K. Silander, E. J. G. Sijbrands, A. Scuteri, J. Scott, D. Schlessinger, S. Sanna, V. Salomaa, J. Saharinen, C. Sabatti, A. Ruokonen, I. Rudan, L. M. Rose, R. Roberts, M. Rieder, B.

M. Psaty, P. P. Pramstaller, I. Pichler, M. Perola, B. W. J. H. Penninx, N. L. Pedersen, C. Pattaro, A. N. Parker, G. Pare, B. A. Oostra, C. J. O'Donnell, M. S. Nieminen, D. A. Nickerson, G. W. Montgomery, T. Meitinger, R. McPherson, M. I. McCarthy, W. McArdle, D. Masson, N. G. Martin, F. Marroni, M. Mangino, P. K. E. Magnusson, G. Lucas, R. Luben, R. J. F. Loos, M.-L. Lokki, G. Lettre, C. Langenberg, L. J. Launer, E. G. Lakatta, R. Laaksonen, K. O. Kyvik, F. Kronenberg, I. R. König, K.-T. Khaw, J. Kaprio, L. M. Kaplan, Å. Johansson, M.-R. Jarvelin, A. Cecile J. W. Janssens, E. Ingelsson, W. Igl, G. Kees Hovingh, J.-J. Hottenga, A. Hofman, A. A. Hicks, C. Hengstenberg, I. M. Heid, C. Hayward, A. S. Havulinna, N. D. Hastie, T. B. Harris, T. Haritunians, A. S. Hall, U. Gyllensten, C. Guiducci, L. C. Groop, E. Gonzalez, C. Gieger, N. B. Freimer, L. Ferrucci, J. Erdmann, P. Elliott, K. G. Ejebe, A. Döring, A. F. Dominiczak, S. Demissie, P. Deloukas, E. J. C. de Geus, U. de Faire, G. Crawford, F. S. Collins, Y. I. Chen, M. J. Caulfield, H. Campbell, N. P. Burtt, L. L. Bonnycastle, D. I. Boomsma, S. M. Boekholdt, R. N. Bergman, I. Barroso, S. Bandinelli, C. M. Ballantyne, T. L. Assimes, T. Quertermous, D. Altshuler, M. Seielstad, T. Y. Wong, E.-S. Tai, A. B. Feranil, C. W. Kuzawa, L. S. Adair, H. A. Taylor Jr, I. B. Borecki, S. B. Gabriel, J. G. Wilson, H. Holm, U. Thorsteinsdottir, V. Gudnason, R. M. Krauss, K. L. Mohlke, J. M. Ordovas, P. B. Munroe, J. S. Kooner, A. R. Tall, R. A. Hegele, J. J. P. Kastelein, E. E. Schadt, J. I. Rotter, E. Boerwinkle, D. P. Strachan, V. Mooser, K. Stefansson, M. P. Reilly, N. J. Samani, H. Schunkert, L. A. Cupples, M. S. Sandhu, P. M. Ridker, D. J. Rader, C. M. van Duijn, L. Peltonen, G. R. Abecasis, M. Boehnke, S. Kathiresan, Biological, clinical and population relevance of 95 loci for blood lipids, *Nature* **466**, 707–713 (2010).

37. P. Natarajan, G. M. Peloso, S. M. Zekavat, M. Montasser, A. Ganna, M. Chaffin, A. V. Khera, W. Zhou, J. M. Bloom, J. M. Engreitz, J. Ernst, J. R. O'Connell, S. E. Ruotsalainen, M.

Alver, A. Manichaikul, W. C. Johnson, J. A. Perry, T. Poterba, C. Seed, I. L. Surakka, T. Esko, S. Ripatti, V. Salomaa, A. Correa, R. S. Vasan, M. Kellis, B. M. Neale, E. S. Lander, G. Abecasis, B. Mitchell, S. S. Rich, J. G. Wilson, L. A. Cupples, J. I. Rotter, C. J. Willer, S. Kathiresan, NHLBI TOPMed Lipids Working Group, Deep-coverage whole genome sequences and blood lipids among 16,324 individuals, *Nat. Commun.* **9**, 3391 (2018).

38. D. J. Liu, G. M. Peloso, H. Yu, A. S. Butterworth, X. Wang, A. Mahajan, D. Saleheen, C. Emdin, D. Alam, A. C. Alves, P. Amouyel, E. Di Angelantonio, D. Arveiler, T. L. Assimes, P. L. Auer, U. Baber, C. M. Ballantyne, L. E. Bang, M. Benn, J. C. Bis, M. Boehnke, E. Boerwinkle, J. Bork-Jensen, E. P. Bottinger, I. Brandslund, M. Brown, F. Busonero, M. J. Caulfield, J. C. Chambers, D. I. Chasman, Y. E. Chen, Y.-D. I. Chen, R. Chowdhury, C. Christensen, A. Y. Chu, J. M. Connell, F. Cucca, L. A. Cupples, S. M. Damrauer, G. Davies, I. J. Deary, G. Dedoussis, J. C. Denny, A. Dominiczak, M.-P. Dubé, T. Ebeling, G. Eiriksdottir, T. Esko, A.-E. Farmaki, M. F. Feitosa, M. Ferrario, J. Ferrieres, I. Ford, M. Fornage, P. W. Franks, T. M. Frayling, R. Frikke-Schmidt, L. G. Fritsche, P. Frossard, V. Fuster, S. K. Ganesh, W. Gao, M. E. Garcia, C. Gieger, F. Giulianini, M. O. Goodarzi, H. Grallert, N. Grarup, L. Groop, M. L. Grove, V. Gudnason, T. Hansen, T. B. Harris, C. Hayward, J. N. Hirschhorn, O. L. Holmen, J. Huffman, Y. Huo, K. Hveem, S. Jabeen, A. U. Jackson, J. Jakobsdottir, M.-R. Jarvelin, G. B. Jensen, M. E. Jørgensen, J. W. Jukema, J. M. Justesen, P. R. Kamstrup, S. Kanoni, F. Karpe, F. Kee, A. V Khera, D. Klarin, H. A. Koistinen, J. S. Kooner, C. Kooperberg, K. Kuulasmaa, J. Kuusisto, M. Laakso, T. Lakka, C. Langenberg, A. Langsted, L. J. Launer, T. Lauritzen, D. C. M. Liewald, L. A. Lin, A. Linneberg, R. J. F. Loos, Y. Lu, X. Lu, R. Mägi, A. Malarstig, A. Manichaikul, A. K. Manning, P. Mäntyselkä, E. Marouli, N. G. D. Masca, A. Maschio, J. B. Meigs, O. Melander, A. Metspalu, A. P. Morris, A. C. Morrison, A. Mulas, M. Müller-Nurasyid, P. B. Munroe, M. J.

Neville, J. B. Nielsen, S. F. Nielsen, B. G. Nordestgaard, J. M. Ordovas, R. Mehran, C. J. O'Donnell, M. Orho-Melander, C. M. Molony, P. Muntendam, S. Padmanabhan, C. N. A. Palmer, D. Pasko, A. P. Patel, O. Pedersen, M. Perola, A. Peters, C. Pisinger, G. Pistis, O. Polasek, N. Poulter, B. M. Psaty, D. J. Rader, A. Rasheed, R. Rauramaa, D. F. Reilly, A. P. Reiner, F. Renström, S. S. Rich, P. M. Ridker, J. D. Rioux, N. R. Robertson, D. M. Roden, J. I. Rotter, I. Rudan, V. Salomaa, N. J. Samani, S. Sanna, N. Sattar, E. M. Schmidt, R. A. Scott, P. Sever, R. S. Sevilla, C. M. Shaffer, X. Sim, S. Sivapalaratnam, K. S. Small, A. V Smith, B. H. Smith, S. Somayajula, L. Southam, T. D. Spector, E. K. Speliotes, J. M. Starr, K. E. Stirrups, N. Stitziel, K. Strauch, H. M. Stringham, P. Surendran, H. Tada, A. R. Tall, H. Tang, J.-C. Tardif, K. D. Taylor, S. Trompet, P. S. Tsao, J. Tuomilehto, A. Tybjaerg-Hansen, N. R. van Zuydam, A. Varbo, T. V Varga, J. Virtamo, M. Waldenberger, N. Wang, N. J. Wareham, H. R. Warren, P. E. Weeke, J. Weinstock, J. Wessel, J. G. Wilson, P. W. F. Wilson, M. Xu, H. Yaghootkar, R. Young, E. Zeggini, H. Zhang, N. S. Zheng, W. Zhang, Y. Zhang, W. Zhou, Y. Zhou, M. Zoledziewska, J. M. M. Howson, J. Danesh, M. I. McCarthy, C. A. Cowan, G. Abecasis, P. Deloukas, K. Musunuru, C. J. Willer, S. Kathiresan, G. Abecasis, P. Deloukas, K. Musunuru, C. J. Willer, S. Kathiresan, Exome-wide association study of plasma lipids in >300,000 individuals, *Nat. Genet.* **49**, 1758–1766 (2017).

39. C. Bycroft, C. Freeman, D. Petkova, G. Band, L. T. Elliott, K. Sharp, A. Motyer, D. Vukcevic, O. Delaneau, J. O'Connell, A. Cortes, S. Welsh, A. Young, M. Effingham, G. McVean, S. Leslie, N. Allen, P. Donnelly, J. Marchini, The UK Biobank resource with deep phenotyping and genomic data, *Nature* **562**, 203–209 (2018).

40. A. Loregger, J. K. Nelson, N. Zelcer, Assaying Low-Density-Lipoprotein (LDL) Uptake into Cells, *Methods Mol. Biol.* **1583**, 53–63 (2017).

41. A. Mazein, S. Watterson, W. Y. Hsieh, W. J. Griffiths, P. Ghazal, A comprehensive machine-readable view of the mammalian cholesterol biosynthesis pathway, *Biochem. Pharmacol.* **86**, 56–66 (2013).

42. R. B. Rose, J. H. Bayle, J. A. Endrizzi, J. D. Cronk, G. R. Crabtree, T. Alber, Structural basis of dimerization, coactivator recognition and MODY3 mutations in HNF-1α, *Nat. Struct. Biol.* **7**, 744–748 (2000).

43. A. Delaforest, F. Di Furio, R. Jing, A. Ludwig-Kubinski, K. Twaroski, A. Urick, K. Pulakanti, S. Rao, S. A. Duncan, HNF4A regulates the formation of hepatic progenitor cells from human iPSC-derived endoderm by facilitating efficient recruitment of RNA pol II, *Genes (Basel)* **10**, 21 (2019).

44. K. Wang, A. X. Holterman, Pathophysiologic role of hepatocyte nuclear factor 6, *Cell. Signal.* **24**, 9–16 (2012).

45. U. Wellner, J. Schubert, U. C. Burk, O. Schmalhofer, F. Zhu, A. Sonntag, B. Waldvogel, C. Vannier, D. Darling, A. Zur Hausen, V. G. Brunton, J. Morton, O. Sansom, J. Schüler, M. P. Stemmler, C. Herzberger, U. Hopt, T. Keck, S. Brabletz, T. Brabletz, The EMT-activator ZEB1 promotes tumorigenicity by repressing stemness-inhibiting microRNAs, *Nat. Cell Biol.* **11**, 1487–1495 (2009).

46. C. L. Gao, J. G. Zhu, Y. P. Zhao, X. H. Chen, C. B. Ji, C. M. Zhang, C. Zhu, Z. K. Xia, Y. Z. Peng, X. R. Guo, Mitochondrial dysfunction is induced by the overexpression of UCP4 in 3T3-L1 adipocytes, *Int. J. Mol. Med.* **25**, 71–80 (2010).

47. F. Quazi, R. S. Molday, Differential phospholipid substrates and directional transport by ATP-binding cassette proteins ABCA1, ABCA7, and ABCA4 and disease-causing mutants, *J. Biol. Chem.* **288**, 34414–34426 (2013).

48. J. E. Kung, N. Jura, The pseudokinase TRIB 1 toggles an intramolecular switch to regulate COP 1 nuclear export, *EMBO J.* **38**, e99708 (2019).

49. J. M. Murphy, Y. Nakatani, S. A. Jamieson, W. Dai, I. S. Lucet, P. D. Mace, Molecular Mechanism of CCAAT-Enhancer Binding Protein Recruitment by the TRIB1 Pseudokinase, *Structure* **23**, 2111–2121 (2015).

50. S. Soubeyrand, A. Martinuk, R. McPherson, TRIB1 is a positive regulator of hepatocyte nuclear factor 4-Alpha, *Sci. Rep.* **7**, 5574 (2017).

51. R. C. Bauer, M. Sasaki, D. M. Cohen, J. Cui, M. A. Smith, B. O. Yenilmez, D. J. Steger, D. J. Rader, Tribbles-1 regulates hepatic lipogenesis through posttranscriptional regulation of C/EBPα, *J. Clin. Invest.* **125**, 3809–3818 (2015).

52. R. Burkhardt, S. A. Toh, W. R. Lagor, A. Birkeland, M. Levin, X. Li, M. Robblee, V. D. Fedorov, M. Yamamoto, T. Satoh, S. Akira, S. Kathiresan, J. L. Breslow, D. J. Rader, Trib1 is a lipid- and myocardial infarction-associated gene that regulates hepatic lipogenesis and VLDL production in mice, *J. Clin. Invest.* **120**, 4410–4414 (2010).

53. A. Motley, N. A. Bright, M. N. J. Seaman, M. S. Robinson, Clathrin-mediated endocytosis in AP-2-depleted cells, *J. Cell Biol.* **162**, 909–918 (2003).

54. S. F. Parsons, G. Mallinson, C. H. Holmes, J. M. Houlihan, K. L. Simpson, W. J. Mawby, N. K. Spurr, D. Warne, A. N. Barclay, D. J. Anstee, The Lutheran blood group glycoprotein, another member of the immunoglobulin superfamily, is widely expressed in human tissues and is developmentally regulated in human liver, *Proc. Natl. Acad. Sci. U. S. A.* **92**, 5496–5500 (1995).

55. S. K. Mishra, P. A. Keyel, M. A. Edeling, A. L. Dupin, D. J. Owen, L. M. Traub, Functional dissection of an AP-2 β2 appendage-binding sequence within the autosomal recessive hypercholesterolemia protein, *J. Biol. Chem.* **280**, 19270–19280 (2005).

56. A. Radhakrishnan, J. L. Goldstein, J. G. McDonald, M. S. Brown, Switch-like Control of SREBP-2 Transport Triggered by Small Changes in ER Cholesterol: A Delicate Balance, *Cell Metab.* **8**, 512–521 (2008).

57. J. D. Horton, N. A. Shah, J. A. Warrington, N. N. Anderson, S. W. Park, M. S. Brown, J. L. Goldstein, Combined analysis of oligonucleotide microarray data from transgenic and knockout mice identifies direct SREBP target genes., *Proc. Natl. Acad. Sci. U. S. A.* **100**, 12027–12032 (2003).

58. Scandinavian Simvastatin Survival Study Group, Randomised trial of cholesterol lowering in 4444 patients with coronary heart disease: the Scandinavian Simvastatin Survival Study (4S), *Lancet* **344**, 1383–1389 (1994).

59. N. G. Lintner, K. F. McClure, D. Petersen, A. T. Londregan, D. W. Piotrowski, L. Wei, J. Xiao, M. Bolt, P. M. Loria, B. Maguire, K. F. Geoghegan, A. Huang, T. Rolph, S. Liras, J. A. Doudna, R. G. Dullea, J. H. D. Cate, Selective stalling of human translation through small-molecule engagement of the ribosome nascent chain., *PLoS Biol.* **15**, e2001882 (2017).

60. W. Li, F. R. Ward, K. F. McClure, S. T.-L. Chang, E. Montabana, S. Liras, R. G. Dullea, J. H. D. Cate, Structural basis for selective stalling of human ribosome nascent chain complexes by a drug-like molecule, *Nat. Struct. Mol. Biol.* **26**, 501–509 (2019).

61. H. E. Careskey, R. A. Davis, W. E. Alborn, J. S. Troutt, G. Cao, R. J. Konrad, Atorvastatin increases human serum levels of proprotein convertase subtilisin/kexin type 9, *J. Lipid Res.* **49**, 394–398 (2008).

62. T. Suzuki, M. Terasaki, C. Takemoto-Hori, T. Hanada, T. Ueda, A. Wada, K. Watanabe, Structural compensation for the deficit of rRNA with proteins in the mammalian mitochondrial ribosome. Systematic analysis of protein components of the large ribosomal subunit from

mammalian mitochondria, *J. Biol. Chem.* **276**, 21724–21736 (2001).

63. P. J. Thul, L. Akesson, M. Wiking, D. Mahdessian, A. Geladaki, H. Ait Blal, T. Alm, A. Asplund, L. Björk, L. M. Breckels, A. Bäckström, F. Danielsson, L. Fagerberg, J. Fall, L. Gatto, C. Gnann, S. Hober, M. Hjelmare, F. Johansson, S. Lee, C. Lindskog, J. Mulder, C. M. Mulvey, P. Nilsson, P. Oksvold, J. Rockberg, R. Schutten, J. M. Schwenk, A. Sivertsson, E. Sjöstedt, M. Skogs, C. Stadler, D. P. Sullivan, H. Tegel, C. Winsnes, C. Zhang, M. Zwahlen, A. Mardinoglu, F. Pontén, K. Von Feilitzen, K. S. Lilley, M. Uhlén, E. Lundberg, A subcellular map of the human proteome, *Science* **356**, eaal3321 (2017).

64. H. Li, B. Dong, S. W. Park, H.-S. Lee, W. Chen, J. Liu, Hepatocyte nuclear factor 1alpha plays a critical role in PCSK9 gene transcription and regulation by the natural hypocholesterolemic compound berberine, *J. Biol. Chem.* **284**, 28885–28895 (2009).

65. A.-X. Guo, J.-J. Cui, L.-Y. Wang, J.-Y. Yin, The role of CSDE1 in translational reprogramming and human diseases, *Cell Commun. Signal.* **18**, 14 (2020).

66. M. Dinur, R. Kilav, A. Sela-Brown, H. Jacquemin-Sablon, T. Naveh-Many, In vitro evidence that upstream of N-ras participates in the regulation of parathyroid hormone messenger ribonucleic acid stability, *Mol. Endocrinol.* **20**, 1652–1660 (2006).

67. K. S. Moore, N. Yagci, F. Van Alphen, N. A. Paolini, R. Horos, N. M. Held, R. H. Houtkooper, E. Van Den Akker, A. B. Meijer, P. A. C. T'Hoen, M. Von Lindern, Csde1 binds transcripts involved in protein homeostasis and controls their expression in an erythroid cell line, *Sci. Rep.* **8**, 2628 (2018).

68. T. C. Chang, A. Yamashita, C. Y. A. Chen, Y. Yamashita, W. Zhu, S. Durdan, A. Kahvejian, N. Sonenberg, A. Bin Shyu, UNR, a new partner of poly(A)-binding protein, plays a key role in translationally coupled mRNA turnover mediated by the c-fos major coding-region determinant,

Genes Dev. **18**, 2010–2023 (2004).

69. G. M. Wilson, M. Z. Vasa, R. G. Deeley, Stabilization and cytoskeletal-association of LDL receptor mRNA are mediated by distinct domains in its 3' untranslated region, *J. Lipid Res.* **39**, 1025–1032 (1998).

70. M. A. Horlbeck, A. Xu, M. Wang, N. K. Bennett, C. Y. Park, D. Bogdanoff, B. Adamson, E. D. Chow, M. Kampmann, T. R. Peterson, K. Nakamura, M. A. Fischbach, J. S. Weissman, L. A. Gilbert, Mapping the Genetic Landscape of Human Cells, *Cell* **174**, 953–967.e22 (2018).

71. H. Li, W. Chen, Y. Zhou, P. Abidi, O. Sharpe, W. H. Robinson, F. B. Kraemer, J. Liu, Identification of mRNA binding proteins that regulate the stability of LDL receptor mRNA through AU-rich elements, *J. Lipid Res.* **50**, 820–831 (2009).

72. K. Bjune, L. Wierød, S. Naderi, Triciribine increases LDLR expression and LDL uptake through stabilization of LDLR mRNA, *Sci. Rep.* **8**, 16174 (2018).

73. T. Bakheet, M. Frevel, B. R. G. Williams, W. Greer, K. S. A. Khabar, ARED: Human AU-rich element-containing mRNA database reveals an unexpectedly diverse functional repertoire of encoded proteins, *Nucleic Acids Res.* **29**, 246–254 (2001).

74. C. Liu, Y. S. Kim, J. Kim, J. Pattison, A. Kamaid, Y. I. Miller, Modeling hypercholesterolemia and vascular lipid accumulation in LDL receptor mutant zebrafish, *J. Lipid Res.* **59**, 391–399 (2018).

75. R. S. Wu, I. I. Lam, H. Clay, D. N. Duong, R. C. Deo, S. R. Coughlin, A Rapid Method for Directed Gene Knockout for Screening in G0 Zebrafish., *Dev. Cell* **46**, 112-125.e4 (2018).

76. A. B. Singh, H. Li, C. F. K. Kan, B. Dong, M. R. Nicolls, J. Liu, The critical role of mRNA destabilizing protein heterogeneous nuclear ribonucleoprotein D in 3′ untranslated region-mediated decay of low-density lipoprotein receptor mRNA in liver tissue, *Arterioscler. Thromb.*

Vasc. Biol. **34**, 8–16 (2014).

77. B. Paigen, A. Morrow, C. Brandon, D. Mitchell, P. Holmes, Variation in susceptibility to atherosclerosis among inbred strains of mice, *Atherosclerosis* **57**, 65–73 (1985).

78. P. M. Nishina, J. Verstuyft, B. Paigen, Synthetic low and high fat diets for the study of atherosclerosis in the mouse, *J. Lipid Res.* **31**, 859–869 (1990).

79. A. H. Lichtman, S. K. Clinton, K. Iiyama, P. W. Connelly, P. Libby, M. I. Cybulsky, Hyperlipidemia and Atherosclerotic Lesion Development in LDL Receptor–Deficient Mice Fed Defined Semipurified Diets With and Without Cholate, *Arterioscler. Thromb. Vasc. Biol.* **19**, 1938–1944 (1999).

80. G. S. Getz, C. A. Reardon, Diet and murine atherosclerosis, *Arterioscler. Thromb. Vasc. Biol.* **26**, 242–249 (2006).

81. M. von Scheidt, Y. Zhao, Z. Kurt, C. Pan, L. Zeng, X. Yang, H. Schunkert, A. J. Lusis, Applications and Limitations of Mouse Models for Understanding Human Atherosclerosis, *Cell Metab.* **25**, 248–261 (2017).

82. M. M. Bjørklund, A. K. Hollensen, M. K. Hagensen, F. Dagnæs-Hansen, C. Christoffersen, J. G. Mikkelsen, J. F. Bentzon, Induction of atherosclerosis in mice and hamsters without germline genetic engineering, *Circ. Res.* **114**, 1684–1689 (2014).

83. N. Matsuzawa, T. Takamura, S. Kurita, H. Misu, T. Ota, H. Ando, M. Yokoyama, M. Honda, Y. Zen, Y. Nakanuma, K. I. Miyamoto, S. Kaneko, Lipid-induced oxidative stress causes steatohepatitis in mice fed an atherogenic diet, *Hepatology* **46**, 1392–1403 (2007).

84. R. Collins, C. Reith, J. Emberson, J. Armitage, C. Baigent, L. Blackwell, R. Blumenthal, J. Danesh, G. D. Smith, D. DeMets, S. Evans, M. Law, S. MacMahon, S. Martin, B. Neal, N. Poulter, D. Preiss, P. Ridker, I. Roberts, A. Rodgers, P. Sandercock, K. Schulz, P. Sever, J.

Simes, L. Smeeth, N. Wald, S. Yusuf, R. Peto, Interpretation of the evidence for the efficacy and safety of statin therapy, *Lancet* **388**, 2532–2561 (2016).

85. B. T. Emmer, E. J. Sherman, P. J. Lascuna, S. E. Graham, C. J. Willer, D. Ginsburg, Genome-scale CRISPR screening for modifiers of cellular LDL uptake, *PLOS Genet.* **17**, e1009285 (2021).

86. M. N. Trinh, M. S. Brown, J. L. Goldstein, J. Han, G. Vale, J. G. McDonald, J. Seemann, J. T. Mendell, F. Lu, Last step in the path of LDL cholesterol from lysosome to plasma membrane to ER is governed by phosphatidylserine, *Proc. Natl. Acad. Sci. U. S. A.* **117**, 18521–18529 (2020).

87. C. Knouff, S. Malloy, J. Wilder, M. K. Altenburg, N. Maeda, Doubling Expression of the Low Density Lipoprotein Receptor by Truncation of the 3′-Untranslated Region Sequence Ameliorates Type III Hyperlipoproteinemia in Mice Expressing the Human ApoE2 Isoform, *J. Biol. Chem.* **276**, 3856–3862 (2001).

88. E. Bjornsson, K. Gunnarsdottir, G. H. Halldorsson, A. Sigurdsson, G. A. Arnadottir, H. Jonsson, E. F. Olafsdottir, S. Niehus, B. Kehr, G. Sveinbjörnsson, S. Gudmundsdottir, A. Helgadottir, K. Andersen, G. Thorleifsson, G. I. Eyjolfsson, I. Olafsson, O. Sigurdardottir, J. Saemundsdottir, I. Jonsdottir, O. T. Magnusson, G. Masson, H. Stefansson, D. F. Gudbjartsson, G. Thorgeirsson, H. Holm, B. V Halldorsson, P. Melsted, G. L. Norddahl, P. Sulem, U. Thorsteinsdottir, K. Stefansson, Lifelong Reduction in LDL (Low-Density Lipoprotein) Cholesterol due to a Gain-of-Function Mutation in LDLR, *Circ. Genomic Precis. Med.* **14**, e003029 (2021).

89. W. Kong, J. Wei, P. Abidi, M. Lin, S. Inaba, C. Li, Y. Wang, Z. Wang, S. Si, H. Pan, S. Wang, J. Wu, Y. Wang, Z. Li, J. Liu, J. D. Jiang, Berberine is a novel cholesterol-lowering drug

working through a unique mechanism distinct from statins, *Nat. Med.* **10**, 1344–1351 (2004).

90. M. Dandan, J. Han, S. Mann, R. Kim, H. Mohammed, E. Nyangau, M. Hellerstein, Turnover Rates of the Low-Density Lipoprotein Receptor and PCSK9: Added Dimension to the Cholesterol Homeostasis Model, *Arterioscler. Thromb. Vasc. Biol.* **41**, 2866–2876 (2021).

91. A. B. Singh, C. F. K. Kan, V. Shende, B. Dong, J. Liu, A novel posttranscriptional mechanism for dietary cholesterol-mediated suppression of liver LDL receptor expression, *J. Lipid Res.* **55**, 1397–1407 (2014).

92. H. Ju Lee, D. Bartsch, C. Xiao, S. Guerrero, G. Ahuja, C. Schindler, J. J. Moresco, J. R. Yates, F. Gebauer, H. Bazzi, C. Dieterich, L. Kurian, D. Vilchez, A post-transcriptional program coordinated by CSDE1 prevents intrinsic neural differentiation of human embryonic stem cells, *Nat. Commun.* **8**, 1456 (2017).

93. O. Boussadia, M. Niepmann, L. Créancier, A.-C. Prats, F. Dautry, H. Jacquemin-Sablon, Unr Is Required In Vivo for Efficient Initiation of Translation from the Internal Ribosome Entry Sites of both Rhinovirus and Poliovirus, *J. Virol.* **77**, 3353–3359 (2003).

94. V. Dormoy-Raclet, J. Markovits, A. Jacquemin-Sablon, H. Jacquemin-Sablon, Regulation of Unr expression by 5′- and 3′-untranslated regions of its mRNA through modulation of stability and IRES mediated translation, *RNA Biol.* **2**, e27–35 (2005).

95. K. E. Duncan, C. Strein, M. W. Hentze, The SXL-UNR Corepressor Complex Uses a PABP-Mediated Mechanism to Inhibit Ribosome Recruitment to msl-2 mRNA, *Mol. Cell* **36**, 571–582 (2009).

96. S. Ray, E. C. Anderson, Stimulation of translation by human Unr requires cold shock domains 2 and 4, and correlates with poly(A) binding protein interaction, *Sci. Rep.* **6**, 22461 (2016).

97. H. Guo, Y. Li, L. Shen, T. Wang, X. Jia, L. Liu, T. Xu, M. Ou, K. Hoekzema, H. Wu, M. A. Gillentine, C. Liu, H. Ni, P. Peng, R. Zhao, Y. Zhang, C. Phornphutkul, A. P. A. Stegmann, C. E. Prada, R. J. Hopkin, J. T. Shieh, K. McWalter, K. G. Monaghan, P. M. van Hasselt, K. van Gassen, T. Bai, M. Long, L. Han, Y. Quan, M. Chen, Y. Zhang, K. Li, Q. Zhang, J. Tan, T. Zhu, Y. Liu, N. Pang, J. Peng, D. A. Scott, S. R. Lalani, M. Azamian, G. M. S. Mancini, D. J. Adams, M. Kvarnung, A. Lindstrand, A. Nordgren, J. Pevsner, I. A. Osei-Owusu, C. Romano, G. Calabrese, O. Galesi, J. Gecz, E. Haan, J. Ranells, M. Racobaldo, M. Nordenskjold, S. Madan-Khetarpal, J. Sebastian, S. Ball, X. Zou, J. Zhao, Z. Hu, F. Xia, P. Liu, J. A. Rosenfeld, B. B. A. de Vries, R. A. Bernier, Z. Q. D. Xu, H. Li, W. Xie, R. B. Hufnagel, E. E. Eichler, K. Xia, Disruptive variants of CSDE1 associate with autism and interfere with neuronal development and synaptic transmission, *Sci. Adv.* **5**, eaax2166 (2019).

98. L. Wurth, P. Papasaikas, D. Olmeda, N. Bley, G. T. Calvo, S. Guerrero, D. Cerezo-Wallis, J. Martinez-Useros, M. García-Fernández, S. Hüttelmaier, M. S. Soengas, F. Gebauer, UNR/CSDE1 Drives a Post-transcriptional Program to Promote Melanoma Invasion and Metastasis, *Cancer Cell* **30**, 694–707 (2016).

99. P. Gennemark, K. Walter, N. Clemmensen, D. Rekić, C. A. M. Nilsson, J. Knöchel, M. Hölttä, L. Wernevik, B. Rosengren, D. Kakol-Palm, Y. Wang, R. Z. Yu, R. S. Geary, S. J. Riney, B. P. Monia, R. Isaksson, R. Jansson-Löfmark, C. S. J. Rocha, D. Lindén, E. Hurt-Camejo, R. Crooke, L. Tillman, T. Rydén-Bergsten, B. Carlsson, U. Andersson, M. Elebring, A. Tivesten, N. Davies, An oral antisense oligonucleotide for PCSK9 inhibition, *Sci. Transl. Med.* **13**, eabe9117 (2021).

100. K. Musunuru, A. C. Chadwick, T. Mizoguchi, S. P. Garcia, J. E. DeNizio, C. W. Reiss, K. Wang, S. Iyer, C. Dutta, V. Clendaniel, M. Amaonye, A. Beach, K. Berth, S. Biswas, M. C.

Braun, H.-M. Chen, T. V Colace, J. D. Ganey, S. A. Gangopadhyay, R. Garrity, L. N. Kasiewicz, J. Lavoie, J. A. Madsen, Y. Matsumoto, A. M. Mazzola, Y. S. Nasrullah, J. Nneji, H. Ren, A. Sanjeev, M. Shay, M. R. Stahley, S. H. Y. Fan, Y. K. Tam, N. M. Gaudelli, G. Ciaramella, L. E. Stolz, P. Malyala, C. J. Cheng, K. G. Rajeev, E. Rohde, A. M. Bellinger, S. Kathiresan, In vivo CRISPR base editing of PCSK9 durably lowers cholesterol in primates, *Nature* **593**, 429–434 (2021).

101. K. F. McClure, D. W. Piotrowski, D. Petersen, L. Wei, J. Xiao, A. T. Londregan, A. S. Kamlet, A.-M. Dechert-Schmitt, B. Raymer, R. B. Ruggeri, D. Canterbury, C. Limberakis, S. Liras, P. DaSilva-Jardine, R. G. Dullea, P. M. Loria, B. Reidich, C. T. Salatto, H. Eng, E. Kimoto, K. Atkinson, A. King-Ahmad, D. Scott, K. Beaumont, J. R. Chabot, M. W. Bolt, K. Maresca, K. Dahl, R. Arakawa, A. Takano, C. Halldin, Liver-Targeted Small-Molecule Inhibitors of Proprotein Convertase Subtilisin/Kexin Type 9 Synthesis, *Angew. Chemie Int. Ed.* **56**, 16218–16222 (2017).

102. J. J. V McMurray, M. Packer, A. S. Desai, J. Gong, M. P. Lefkowitz, A. R. Rizkala, J. L. Rouleau, V. C. Shi, S. D. Solomon, K. Swedberg, M. R. Zile, Angiotensin–Neprilysin Inhibition versus Enalapril in Heart Failure, *N. Engl. J. Med.* **371**, 993–1004 (2014).

103. D. G. Gibson, L. Young, R.-Y. Chuang, J. C. Venter, C. A. Hutchison, H. O. Smith, Enzymatic assembly of DNA molecules up to several hundred kilobases., *Nat. Methods* **6**, 343–345 (2009).

104. J. S. Chorba, A. M. Galvan, K. M. Shokat, Stepwise processing analyses of the single-turnover PCSK9 protease reveal its substrate sequence specificity and link clinical genotype to lipid phenotype, *J. Biol. Chem.* **293**, 1875–1886 (2018).

105. J. H. Kim, S.-R. Lee, L.-H. Li, H.-J. Park, J.-H. Park, K. Y. Lee, M.-K. Kim, B. A. Shin, S.-

Y. Choi, V. Thiel, Ed. High Cleavage Efficiency of a 2A Peptide Derived from Porcine Teschovirus-1 in Human Cell Lines, Zebrafish and Mice, *PLoS One* **6**, e18556 (2011).

106. D. G. Gibson, H. O. Smith, C. A. Hutchison, J. C. Venter, C. Merryman, Chemical synthesis of the mouse mitochondrial genome, *Nat. Methods* An oral antisense oligonucleotide for PCSK9 inhibition **7**, 901–903 (2010).

107. H. Mi, A. Muruganujan, X. Huang, D. Ebert, C. Mills, X. Guo, P. D. Thomas, Protocol Update for large-scale genome and gene function analysis with the PANTHER classification system (v.14.0), *Nat. Protoc.* **14**, 703–721 (2019).

108. UniProt Consortium, UniProt: A worldwide hub of protein knowledge, *Nucleic Acids Res.* **47**, D506–D515 (2019).

109. C. Sudlow, J. Gallacher, N. Allen, V. Beral, P. Burton, J. Danesh, P. Downey, P. Elliott, J. Green, M. Landray, B. Liu, P. Matthews, G. Ong, J. Pell, A. Silman, A. Young, T. Sprosen, T. Peakman, R. Collins, UK Biobank: An Open Access Resource for Identifying the Causes of a Wide Range of Complex Diseases of Middle and Old Age, *PLoS Med.* **12**, e1001779 (2015).

110. P. R. Loh, G. Tucker, B. K. Bulik-Sullivan, B. J. Vilhjálmsson, H. K. Finucane, R. M. Salem, D. I. Chasman, P. M. Ridker, B. M. Neale, B. Berger, N. Patterson, A. L. Price, Efficient Bayesian mixed-model analysis increases association power in large cohorts, *Nat. Genet.* **47**, 284–290 (2015).

111. P. Bartuzi, D. D. Billadeau, R. Favier, S. Rong, D. Dekker, A. Fedoseienko, H. Fieten, M. Wijers, J. H. Levels, N. Huijkman, N. Kloosterhuis, H. van der Molen, G. Brufau, A. K. Groen, A. M. Elliott, J. A. Kuivenhoven, B. Plecko, G. Grangl, J. McGaughran, J. D. Horton, E. Burstein, M. H. Hofker, B. van de Sluis, CCC- and WASH-mediated endosomal sorting of LDLR is required for normal clearance of circulating LDL., *Nat. Commun.* **7**, 10961 (2016).

112. J. M. Baker, F. M. Boyce, High-throughput functional screening using a homemade dual-glow luciferase assay, *J. Vis. Exp.* **88**, 50282 (2014).

113. J. S. Chorba, A. M. Galvan, K. M. Shokat, A High-Throughput Luciferase Assay to Evaluate Proteolysis of the Single-Turnover Protease PCSK9, *J. Vis. Exp.* **138**, 58265 (2018).

114. A. Padmanabhan, M. Alexanian, R. Linares-Saldana, B. González-Terán, G. Andreoletti, Y. Huang, A. J. Connolly, W. Kim, A. Hsu, Q. Duan, S. A. B. Winchester, F. Felix, J. A. Perez-Bermejo, Q. Wang, L. Li, P. P. Shah, S. M. Haldar, R. Jain, D. Srivastava, BRD4 (Bromodomain-Containing Protein 4) Interacts with GATA4 (GATA Binding Protein 4) to Govern Mitochondrial Homeostasis in Adult Cardiomyocytes, *Circulation* **142**, 2338–2355 (2020).

115. M. I. Love, W. Huber, S. Anders, Moderated estimation of fold change and dispersion for RNA-seq data with DESeq2, *Genome Biol.* **15**, 550 (2014).

116. M. D. Robinson, D. J. McCarthy, G. K. Smyth, edgeR: a Bioconductor package for differential expression analysis of digital gene expression data, *Bioinformatics* **26**, 139–140 (2010).

117. A. T. L. Lun, Y. Chen, G. K. Smyth, It's DE-licious: A Recipe for Differential Expression Analyses of RNA-seq Experiments Using Quasi-Likelihood Methods in edgeR, *Methods Mol. Biol.* **1418**, 391–416 (2016).

118. M. V. Kuleshov, M. R. Jones, A. D. Rouillard, N. F. Fernandez, Q. Duan, Z. Wang, S. Koplev, S. L. Jenkins, K. M. Jagodnik, A. Lachmann, M. G. McDermott, C. D. Monteiro, G. W. Gundersen, A. Ma'ayan, Enrichr: a comprehensive gene set enrichment analysis web server 2016 update, *Nucleic Acids Res.* **44**, W90–97 (2016).

119. Z. Gu, R. Eils, M. Schlesner, Complex heatmaps reveal patterns and correlations in

multidimensional genomic data., *Bioinformatics* **32**, 2847–2849 (2016).

120. J. P. T. Higgins, S. Green (editors), Cochrane Handbook for Systematic Reviews of Interventions Version 5.1.0, *Cochrane Collab.* (2011).

Acknowledgments

We thank Max Horlbeck for guidance with the CRISPRi system, Jonathan D. Brown for helpful discussion on *in vivo* experimental designs, Rachel Yang for assistance with histologic imaging, and Paul Cheng and Richard Baylis for helpful discussion on histologic insights and *in vivo* experimental planning. Plasmids for the CRISPRi system were a generous gift from Luke Gilbert and Jonathan Weissman. We thank the Gladstone Institutes Flow Cytometry core facility for their assistance with flow cytometry experiments. UK Biobank analyses were conducted using the UK Biobank resource under application 7089.

Funding: Ar. P. receives support from the Tobacco-Related Disease Research Program (578649), the A.P. Giannini Foundation (P0527061), NIH/NHLBI (K08 HL157700), the Michael Antonov Charitable Foundation Inc., and the Sarnoff Cardiovascular Research Foundation. T.N. is supported by the Japan Society for the Promotion of Science Overseas Research Fellowship. R.J. is supported by the NIH/NHLBI (R01 HL139783) and the Burroughs Wellcome Foundation. P.N. is supported by a Hassenfeld Scholar Award from the Massachusetts General Hospital, the NIH/NHLBI (R01 HL127564, R01 HL142711, R01 HL148565, and R01 HL148050), and the Fondation Leducq (TNE-18CVD04). B.L.B. is supported by NIH grants R01 DK119621 and P01 HL146366. D.S. is supported by NIH grants P01 HL098707, P01 HL146366, R01 HL057181 and R01 HL127240, the Roddenberry Foundation, the L.K. Whittier Foundation, the Younger Family Fund, and the NIH/National Center for Research Resources

grant C06 RR018928 to the Gladstone Institute. K.M.S. is supported by the Howard Hughes Medical Institute. J.S.C. is supported by the NIH/NHLBI (K08 HL124068, R03 HL145259, R01 HL146404, and R01 HL159457), a Pfizer ASPIRE Cardiovascular Award and the Harris Fund and Research Evaluation and Allocation Committee of the UCSF School of Medicine.

Author Contributions: Overall study design: J.S.C. Execution of *in vitro* screen and data processing: G.A.S. Genomic analyses: Ak.P., P.N. *In vitro* validation and synergy experiments, and analysis of mouse blood samples: J.S.C. Execution of zebrafish gene knockdowns: B.H.L., R.S.W. Oversight of zebrafish husbandry: R.S.W., B.L.B. Planning and execution of *in vivo* mouse experiments: Ar.P. Mouse handling, blood, and tissue collection and analysis: Ar.P., Y.C.L., T.N., N.S., V.Q.X. Processing of RNA-seq data: Ar.P., An.P. Histologic analysis of mouse samples: L.L., R.J. Critical data review and analysis: B.L.B, D.S., K.M.S. Preparation of manuscript: J.S.C. Critical review and revision of manuscript: All authors.

Competing Interests: P.N. reports investigator-initiated grant support from Amgen, Apple, AstraZeneca, Boston Scientific, and Novartis, personal fees from Apple, AstraZeneca, Blackstone Life Sciences, Foresite Labs, Novartis, and Roche/Genentech, is a co-founder of TenSixteen Bio, is a shareholder of geneXwell and TenSixteen Bio, and spousal employment at Vertex, all unrelated to the present work. R.S.W. is an employee of Amgen, Inc. D.S. is the scientific cofounder, shareholder, and director of Tenaya Therapeutics, unrelated to the present work. K.M.S. has consulting agreements for the following companies involving cash and/or stock compensation: Black Diamond Therapeutics, BridGene Biosciences, Denali Therapeutics, Dice Molecules, eFFECTOR Therapeutics, Erasca, Genentech/Roche, Janssen Pharmaceuticals, Kumquat Biosciences, Kura Oncology, Merck, Mitokinin, Petra Pharma, Revolution Medicines, Type6 Therapeutics, Venthera, Wellspring Biosciences (Araxes Pharma). J.S.C. has received

consulting fees from Gilde Healthcare and is an uncompensated scientific advisor to Eko, both unrelated to this work.

Data and Materials Availability: All data associated with this study are in the paper or supplementary materials. Alternative formats for the supporting data are available upon request from the corresponding author. All requests for raw and analyzed data, and materials, including plasmids or cell lines, generated in this study will be responded to promptly. UK Biobank data is available by application to the UK Biobank. The raw and processed sequencing data from the RNA-seq experiments have been deposited in the Gene Expression Omnibus (GEO) database under the accession number GSE206846.

Figure Legends

Figure 1: Genome-Wide CRISPR Interference Screen. *A)* Overall schematic of selection. See text for details. *B)* Volcano plot showing the statistical significance (Mann-Whitney test) of the guides recovered for each gene against the mean ρ phenotype of the 3 guides with the strongest effect. ρ is defined as the $\log_2$-fold enrichment for high LDLR abundance cells to the low LDLR abundance cells. Guides targeting known regulators of the LDLR are noted. *C)* Venn diagram showing the overlap between parallel LDLR and TFR screens. Six guides common to both had opposing abundance phenotypes in the respective screens and were included as specific hits. *D)* Venn diagram of hits between the LDLR screen (GWCS) and putative genes correlated with serum LDL from GWAS. The dotted line indicates a relaxed threshold for hit selection from LDLR screen, with only an additional 3 genes in the overlap. Overlap genes shown at right.

Figure 2: Validation of LDLR CRISPRi Hits. Heatmap showing receptor abundance (LDLR, TFR, and LDLR/TFR ratio) and function (LDL uptake) for dCas9-KRAB HepG2 cells transduced with sgRNA targeting the indicated gene, analyzed by flow cytometry. Hits are grouped according to directional effect on LDLR abundance, and then within groups, by effect on LDL uptake (with uptake from *FOXL3-OT1*, *CIT*, and *DHX15* sgRNAs not significantly different, at $p > 0.05$, from negative control sgRNA). *CSDE1* highlighted in blue. Control sgRNAs shown at right. Readouts show $\log_2$ fold change compared to transduction with negative control sgRNA and represent the weighted average of the effects from both sgRNAs targeting each gene. Viability indicates the relative number of cells surviving to flow cytometry in the

experiments. Functional classification of genes is shown visually in Fig. S3. Note that LDLR/TFR is a separately ascertained value from individual cells, and not a derived parameter from aggregate data. Only the hits for which two separate sgRNAs independently validated for receptor expression are shown, defined as $p < 0.05$ via Holm-Sidak corrected t-test. Data represent summary information from 3 to 4 independent experiments.

Figure 3: CRISPRi Knockdown Synergy with Statin and PF-846. Heatmap showing synergy score with statin (top) or PF-846 (bottom) for knockdowns of indicated validated genes with a single sgRNA for separate LDLR abundance and function experiments. Hits are grouped first according to overall effect on LDLR abundance, and secondarily by effect on LDL uptake, as in Fig. 2. *CSDE1* highlighted in blue. Data represent summary information from 4 independent experiments.

Figure 4: CSDE1 Mediates *LDLR* mRNA Decay. *A)* Relative LDLR abundance of CRISPRi HepG2 cells transduced with indicated sgRNAs and grown in the indicated media. *B)* Relative LDL uptake of dual-sgRNA CRISPRi HepG2 cells. The pie chart shows the relative contribution of LDLR-dependent ($CSDE1^{LDLR}$, blue with purple stripes) and LDLR-independent ($CSDE1^{non\text{-}LDLR}$, purple with magenta stripes) CSDE1-mediated mechanisms, as well as SREBP2-mediated mechanisms ($SREBP2^{LDLR}$, white with grey stripes) to LDL uptake. Data is normalized to the control cells in standard media (dashed line, data in Fig. S10B). *C)* Relative LDLR abundance of HepG2 cells overexpressing indicated CSDE1 isoforms. *D)* Relative expression of indicated mRNA targets in CRISPRi cells under sterol-depleted conditions. *E)* Relative expression of *LDLR* mRNA in CRISPRi cells after arrest of transcription with actinomycin D. Data normalized

at T=0 within the sgRNA evaluated to illustrate the change in time, and thus no comparison can be made at T=0. $t_{1/2}$ shown indicates data fit to a one-stage exponential decay equation and analyzed by extra sum-of-squares F test. *E)* Schematics (not to scale) of Luc2-$Prom_{LDLR}$ reporter constructs, illustrating *LDLR* promoter, start site (arrowhead), P2A ribosomal skipping sequence, AREs in 3' UTR, stop codon (red octagon), and indicated regions of the *LDLR* gene. *G, H, I*) Ratiometric luciferase outputs of CRISPRi cells transfected with indicated reporter constructs. Outputs normalized to negative control in *H* and *I*. *All panels)* Data represent summary information from 3-4 independent experiments.

Figure 5: CSDE1 Disruption Upregulates *Ldlr* mRNA and LDLR Function *in vivo*. *A)* Relative expression of hepatic eGFP, *Csde1,* and *Ldlr* transcripts in chow-fed mice transduced with indicated moderate-dose AAV8-shRNA. Matched two-way ANOVA with Holm-Sidak multiple comparisons test shown. *B)* Immunoblots of liver extracts from mice in *A*. Each lane represents an individual mouse. Quantification of protein, normalized to loading control, shown at right. Unpaired t-tests shown. *C)* Mean plasma cholesterol of Western diet-fed mice before and 2 weeks after transduction with moderate-dose AAV8-shRNA. Matched two-way ANOVA with Sidak multiple comparisons test shown. *D)* Mean LDL cholesterol, fractionated by gel filtration, from individual mice from *C*. *E)* Mean plasma cholesterol of Paigen diet-fed mice 2 weeks after transduction with low-dose AAV8-shRNA. *F)* Mean plasma cholesterol of mice in *E* 2 weeks after transduction with a second low-dose AAV8-shRNA. *G)* Mean cholesterol of fractions collected from gel filtration of plasma from individual mice in *F.* Immunoblots of fractions from representative mice against ApoB shown below. Note that fractions shown begin with the elution front from the size-exclusion column. Two-way ANOVA with Sidak's multiple

comparisons test shown to illustrate comparison between treatment arm within a given fraction. Error bars indicate standard error of the mean. *H)* Mean plasma cholesterol of *Pcsk9*-D377Y overexpressing and Paigen diet-fed mice 2 weeks after transduction with a second dose of low-dose AAV8-shRNA (8 weeks after first dose, for singly dosed mice). Note that *Pcsk9*-targeted mice were only given the first dose of AAV8. *I, J)* Leading upregulated *(I)* and downregulated *(J)* biological process GO terms in the differentially expressed genes (adj. $p < 0.05$, $\log_2FC > |1|$) in *Csde1* knockdown mice on the Paigen diet.

Figure 6: An Exploratory Map of Potential LDLR Regulatory Targets. Genes identified and validated in the screen are mapped by cellular localization and possible mechanisms of effect. Known downregulators are shown in cyan (including CSDE1 given the results presented in the current study) and known upregulators shown in magenta. Validated hits with observed effects on cell proliferation or viability are excluded.

Tables and Table Legends

Hit	Hit (NCBI Name)
ABCA1	ABCA1
ABCA4	ABCA4
ACAN	ACAN
ALKBH5	ALKBH5
AMMECR1L	AMMECR1L
ANO8	ANO8
BCAR1	BCAR1
C12orf45	C12orf45
C14orf79	CLBA1
C1orf210	C1orf210
C5orf34	C5orf34
C6orf132	C6orf132
C9orf40	C9orf40
C9orf92	C9orf92
CD164L2	CD164L2
CD276	CD276
CD96	CD96
CIT	CIT
CSDE1	CSDE1
CXCR2	CXCR2
CXXC11	FBXL19
CYB5R3	CYB5R3
DDX39B	DDX39B
DESI1	DESI1

DHX15	DHX15
DUOX1	DUOX1
EIF3D	EIF3D
ENG	ENG
ENTPD1	ENTPD1
ESRRG	ESRRG
EVA1B	EVA1B
FAM126A	FAM126A
FAM178B	FAM178B
FAM57A	TLCD3A
FBXW11	FBXW11
FDPS	FDPS
GXYLT1	GXYLT1
HMGCR	HMGCR
HMGCS1	HMGCS1
HNF1A	HNF1A
HNF4A	HNF4A
HPGDS	HPGDS
HRK	HRK
ICAM4	ICAM4
INTS8	INTS8
ITGA11	ITGA11
ITGA7	ITGA7
ITGAV	ITGAV
LDLR	LDLR
LGALS14	LGALS14
LOC100288524	FOXL3-OT1

LOC729159	NPAP1L
LYZ	LYZ
MARK2	MARK2
MATN1	MATN1
MFHAS1	MFHAS1
MRAP2	MRAP2
MRPL16	MRPL16
MRPL22	MRPL22
MSMO1	MSMO1
MYLIP	MYLIP
NCR2	NCR2
NDUFB5	NDUFB5
NDUFS8	NDUFS8
NINJ1	NINJ1
NLRP6	NLRP6
ONECUT1	ONECUT1
OR52A1	OR52A1
PCDH7	PCDH7
PCDHB4	PCDHB4
PCSK9	PCSK9
PHGR1	PHGR1
PIANP	PIANP
PID1	PID1
PLAC1L	OOSP2
PMVK	PMVK
POLD2	POLD2
POLD3	POLD3

PRIM1	PRIM1
PROL1	OPRPN
PTGDR2	PTGDR2
RARRES3	PLAAT4
REPS1	REPS1
RNF151	RNF151
RSG1	CPLANE2
SCUBE1	SCUBE1
SEC61G	SEC61G
SERPINA9	SERPINA9
SF3A2	SF3A2
SLC25A27	SLC25A27
SLC2A7	SLC2A7
SLC6A19	SLC6A19
SLURP1	SLURP1
SMURF1	SMURF1
SON	SON
SREBF2	SREBF2
SSR2	SSR2
SSUH2	SSUH2
ST6GALNAC4	ST6GALNAC4
STAC	STAC
STAG2	STAG2
TIMELESS	TIMELESS
TMEM217	TMEM217
TMEM86A	TMEM86A
TPRG1	TPRG1

TRMT10C	TRMT10C
TRPM1	TRPM1
TRPM7	TRPM7
TTC14	TTC14
TXNDC8	TXNDC8
WDR5	WDR5
WDR75	WDR75
ZBED6CL	ZBED6CL
ZBTB42	ZBTB42
ZC3H12A	ZC3H12A
ZEB1	ZEB1
ZNF595	ZNF595

Table 1: LDLR Specific CRISPRi Screen Hits. Hits are listed both by gene name in the genome-wide library *(17)* as well as NCBI name.

GENE	Variant rsID	BETA	P_BOLT_LMM	Consequence	IMPACT
HNF4A	rs1800961	0.0564144	0	missense_variant	MODERATE
BCAM	rs28399659	-0.0174111	7.70E-29	missense_variant	MODERATE
BCAM	rs200398713	-0.0803165	1.80E-28	splice_region_variant,intron_variant	LOW
BCAM	rs199922856	-0.342179	6.20E-28	missense_variant	MODERATE
BCAM	rs28399654	0.220592	6.10E-10	missense_variant	MODERATE
BCAM	rs3810141	0.020077	5.50E-07	stop_gained	HIGH
TIMELESS	rs2291738	0.00388393	0.00014	splice_region_variant,intron_variant	LOW
BCAM	rs149302547	-0.147327	0.005	missense_variant	MODERATE
BCAM	rs1135062	-0.0213642	0.0074	missense_variant	MODERATE
C6orf132	rs55772414	0.0116856	0.013	missense_variant	MODERATE
MSMO1	rs142496142	0.0432195	0.015	missense_variant	MODERATE

Table 2: Association of Nonsynonymous Variants in CRISPRi Screen Hits with Serum LDL-C in the UK Biobank. BETA indicates the linear regression standardized effect size, and P_BOLT_LMM indicates the linear mixed model p value using BOLT-LMM*(110)*.

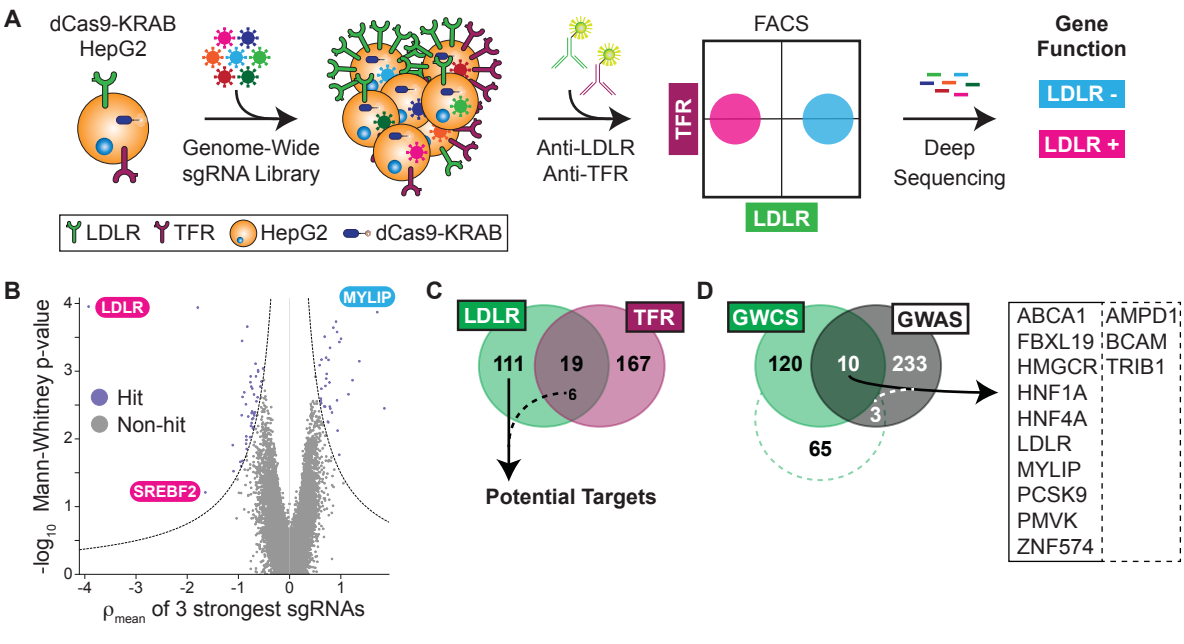
A
dCas9-KRAB
HepG2
Genome-Wide
sgRNA Library
Anti-LDLR
Anti-TFR
FACS
TFR
LDLR
Deep
Sequencing
Gene
Function
LDLR -
LDLR +
LDLR
TFR
HepG2
dCas9-KRAB
B
LDLR
MYLIP
SREBF2
Hit
Non-hit
-log10 Mann-Whitney p-value
ρmean of 3 strongest sgRNAs
C
LDLR
TFR
111
19
167
6
Potential Targets
D
GWCS
GWAS
120
10
233
3
65
ABCA1
FBXL19
HMGCR
HNF1A
HNF4A
LDLR
MYLIP
PCSK9
PMVK
ZNF574
AMPD1
BCAM
TRIB1

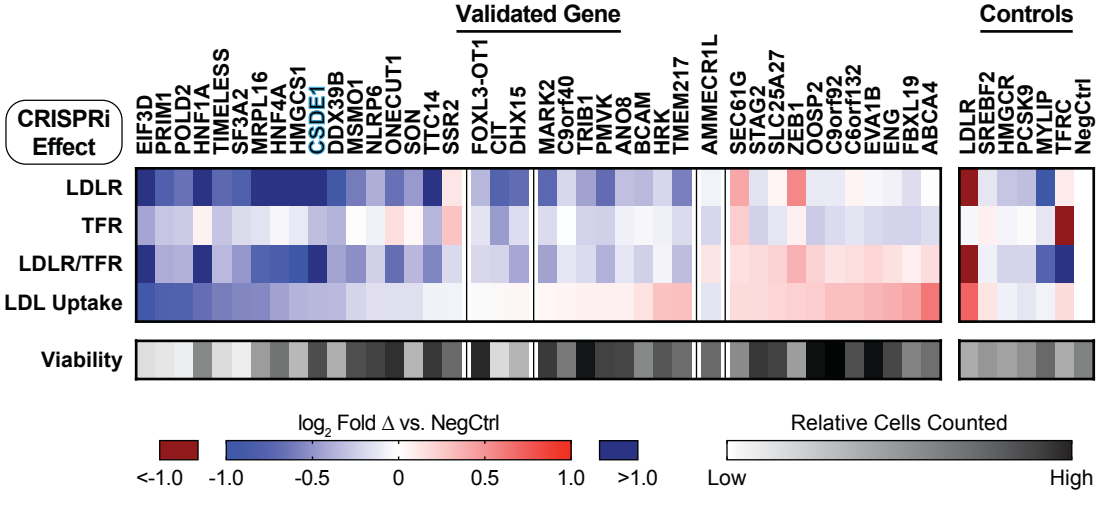
Validated Gene
Controls
CRISPRi Effect
EIF3D
PRIM1
POLD2
HNF1A
TIMELESS
SF3A2
MRPL16
HNF4A
HMGCS1
CSDE1
DDX39B
MSMO1
NLRP6
ONECUT1
SON
TTC14
SSR2
FOXL3-OT1
CIT
DHX15
MARK2
C9orf40
TRIB1
PMVK
ANO8
BCAM
HRK
TMEM217
AMMECR1L
SEC61G
STAG2
SLC25A27
ZEB1
OOSP2
C9orf92
C6orf132
EVA1B
ENG
FBXL19
ABCA4
LDLR
SREBF2
HMGCR
PCSK9
MYLIP
TFRC
NegCtrl
LDLR
TFR
LDLR/TFR
LDL Uptake
Viability
log2 Fold Δ vs. NegCtrl
<-1.0
-1.0
-0.5
0
0.5
1.0
>1.0
Relative Cells Counted
Low
High

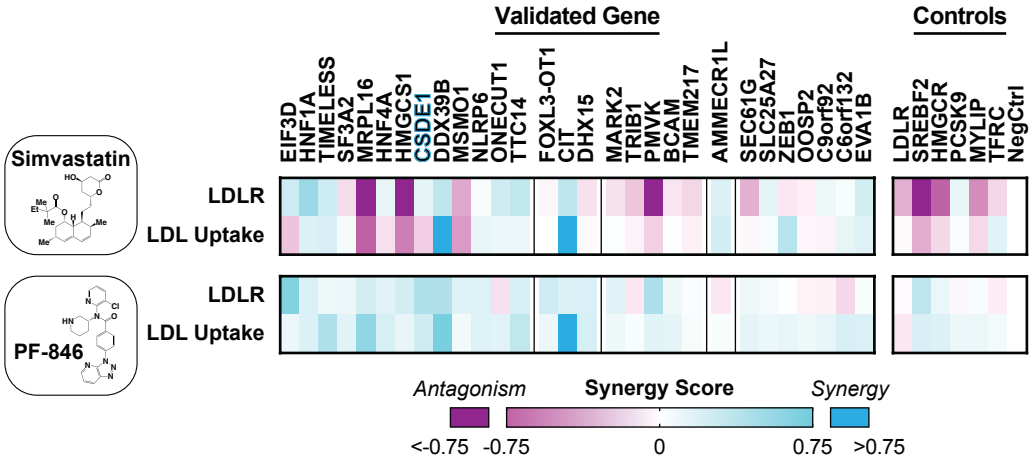
Validated Gene
Controls
EIF3D
HNF1A
TIMELESS
SF3A2
MRPL16
HNF4A
HMGCS1
CSDE1
DDX39B
MSMO1
NLRP6
ONECUT1
TTC14
FOXL3-OT1
CIT
DHX15
MARK2
TRIB1
PMVK
BCAM
TMEM217
AMMECR1L
SEC61G
SLC25A27
ZEB1
OOSP2
C9orf92
C6orf132
EVA1B
LDLR
SREBF2
HMGCR
PCSK9
MYLIP
TFRC
NegCtrl
Simvastatin
LDLR
LDL Uptake
PF-846
LDLR
LDL Uptake
Antagonism
Synergy Score
Synergy
<-0.75
-0.75
0
0.75
>0.75

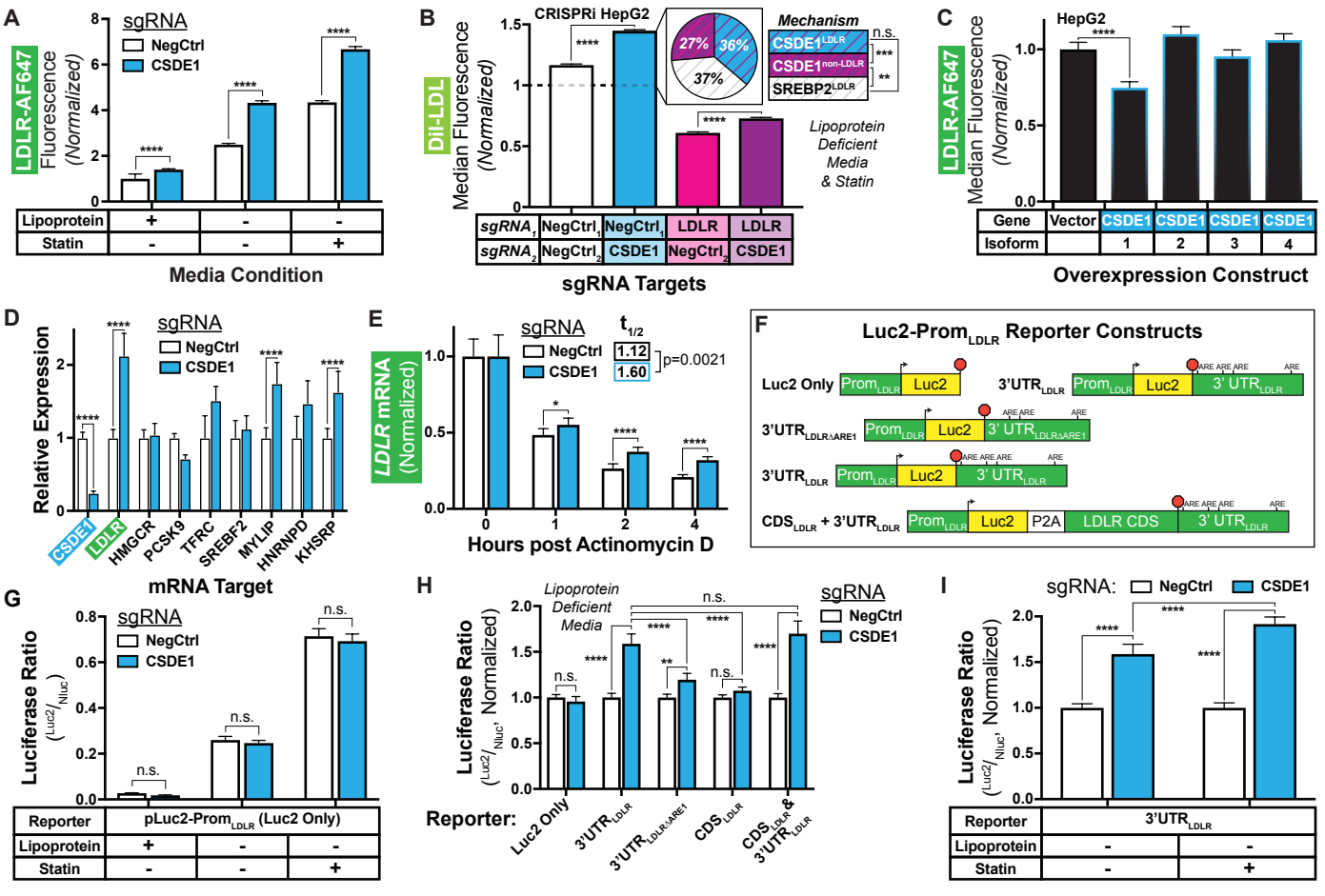
A
LDLR-AF647 Fluorescence (Normalized)
sgRNA
NegCtrl
CSDE1
Lipoprotein
Statin
Media Condition
B
Dil-LDL Median Fluorescence (Normalized)
CRISPRi HepG2
Mechanism
CSDE1 LDLR
CSDE1 non-LDLR
SREBP2 LDLR
n.s.
27%
36%
37%
Lipoprotein Deficient Media & Statin
sgRNA1
sgRNA2
NegCtrl1
NegCtrl2
LDLR
CSDE1
sgRNA Targets
C
LDLR-AF647 Median Fluorescence (Normalized)
HepG2
Gene
Vector
Isoform
Overexpression Construct
D
Relative Expression
sgRNA
NegCtrl
CSDE1
HMGCR
PCSK9
TFRC
SREBF2
MYLIP
HNRNPD
KHSRP
mRNA Target
E
LDLR mRNA (Normalized)
t1/2
1.12
1.60
p=0.0021
Hours post Actinomycin D
F
Luc2-Promoter LDLR Reporter Constructs
Luc2 Only
3'UTR LDLR
3'UTR LDLR ΔARE1
CDS LDLR + 3'UTR LDLR
Prom LDLR
Luc2
P2A
LDLR CDS
3' UTR LDLR
ARE
G
Luciferase Ratio (Luc2/Nluc)
Reporter
pLuc2-Prom LDLR (Luc2 Only)
Lipoprotein
Statin
H
Lipoprotein Deficient Media
Reporter:
Luc2 Only
3'UTR LDLR
3'UTR LDLR ΔARE1
CDS LDLR
CDS LDLR & 3'UTR LDLR
I
sgRNA: NegCtrl CSDE1
3'UTR LDLR

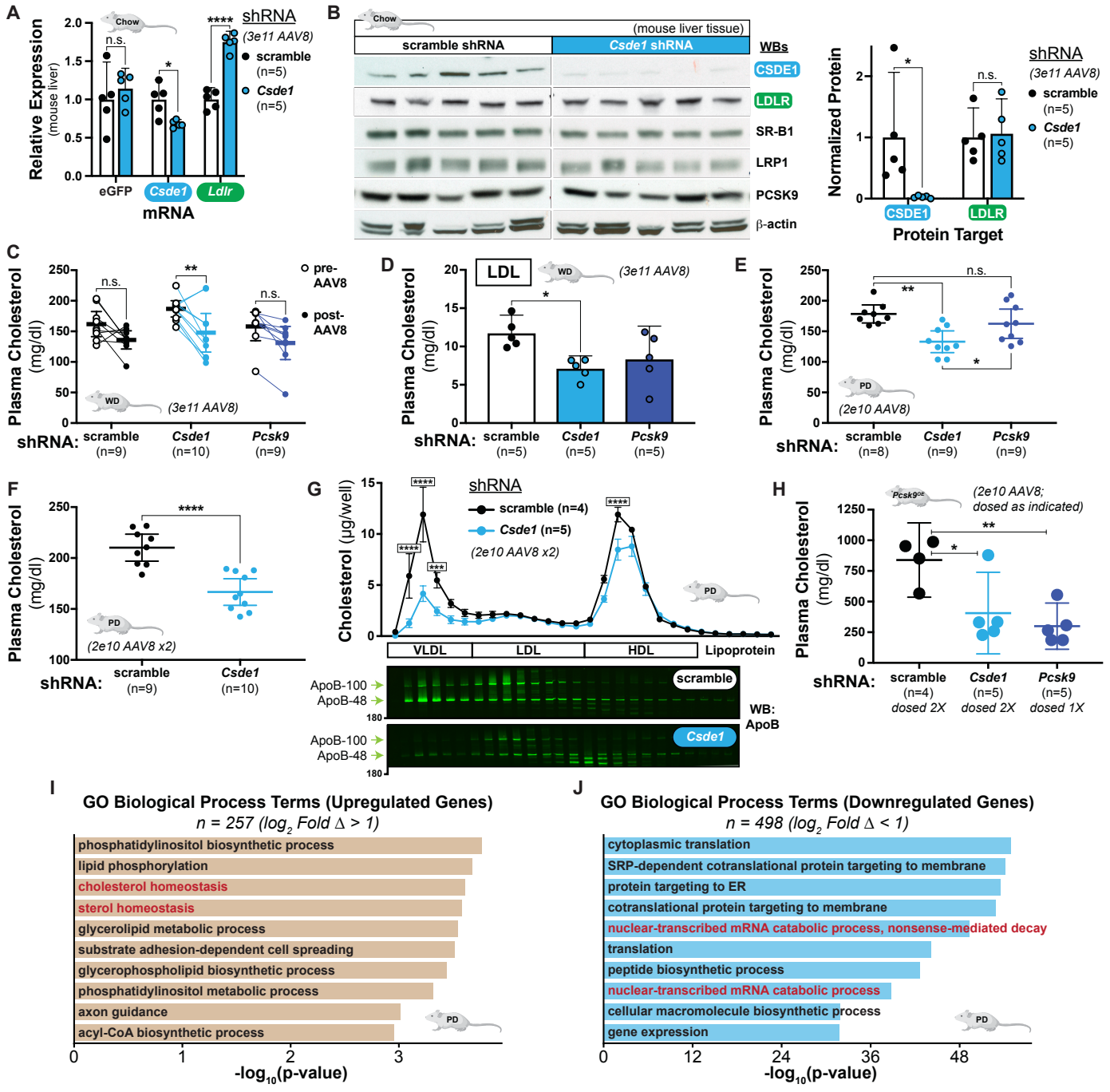
A
Chow
n.s.
*
****
shRNA
(3e11 AAV8)
scramble
(n=5)
Csde1
(n=5)
Relative Expression
(mouse liver)
2.0
1.5
1.0
0.5
0.0
eGFP
Csde1
Ldlr
mRNA
B
Chow
(mouse liver tissue)
scramble shRNA
Csde1 shRNA
WBs
CSDE1
LDLR
SR-B1
LRP1
PCSK9
β-actin
Normalized Protein
2
1
0
*
n.s.
shRNA
(3e11 AAV8)
scramble
(n=5)
Csde1
(n=5)
CSDE1
LDLR
Protein Target
C
pre-
AAV8
post-
AAV8
n.s.
**
n.s.
Plasma Cholesterol
(mg/dl)
250
200
150
100
50
0
WD
(3e11 AAV8)
shRNA:
scramble
(n=9)
Csde1
(n=10)
Pcsk9
(n=9)
D
LDL
WD
(3e11 AAV8)
*
Plasma Cholesterol
(mg/dl)
20
15
10
5
0
shRNA:
scramble
(n=5)
Csde1
(n=5)
Pcsk9
(n=5)
E
n.s.
**
*
Plasma Cholesterol
(mg/dl)
250
200
150
100
50
0
PD
(2e10 AAV8)
shRNA:
scramble
(n=8)
Csde1
(n=9)
Pcsk9
(n=9)
F
****
Plasma Cholesterol
(mg/dl)
250
200
150
100
PD
(2e10 AAV8 x2)
shRNA:
scramble
(n=9)
Csde1
(n=10)
G
shRNA
scramble (n=4)
Csde1 (n=5)
(2e10 AAV8 x2)
Cholesterol (µg/well)
15
10
5
0
****
****
***
PD
VLDL
LDL
HDL
Lipoprotein
ApoB-100
ApoB-48
180
scramble
Csde1
WB:
ApoB
H
Pcsk9OE
(2e10 AAV8;
dosed as indicated)
**
*
Plasma Cholesterol
(mg/dl)
1250
1000
750
500
250
0
shRNA:
scramble
(n=4)
dosed 2X
Csde1
(n=5)
dosed 2X
Pcsk9
(n=5)
dosed 1X
I
GO Biological Process Terms (Upregulated Genes)
n = 257 (log2 Fold Δ > 1)
phosphatidylinositol biosynthetic process
lipid phosphorylation
cholesterol homeostasis
sterol homeostasis
glycerolipid metabolic process
substrate adhesion-dependent cell spreading
glycerophospholipid biosynthetic process
phosphatidylinositol metabolic process
axon guidance
acyl-CoA biosynthetic process
PD
0
1
2
3
-log10(p-value)
J
GO Biological Process Terms (Downregulated Genes)
n = 498 (log2 Fold Δ < 1)
cytoplasmic translation
SRP-dependent cotranslational protein targeting to membrane
protein targeting to ER
cotranslational protein targeting to membrane
nuclear-transcribed mRNA catabolic process, nonsense-mediated decay
translation
peptide biosynthetic process
nuclear-transcribed mRNA catabolic process
cellular macromolecule biosynthetic process
gene expression
PD
0
12
24
36
48
-log10(p-value)

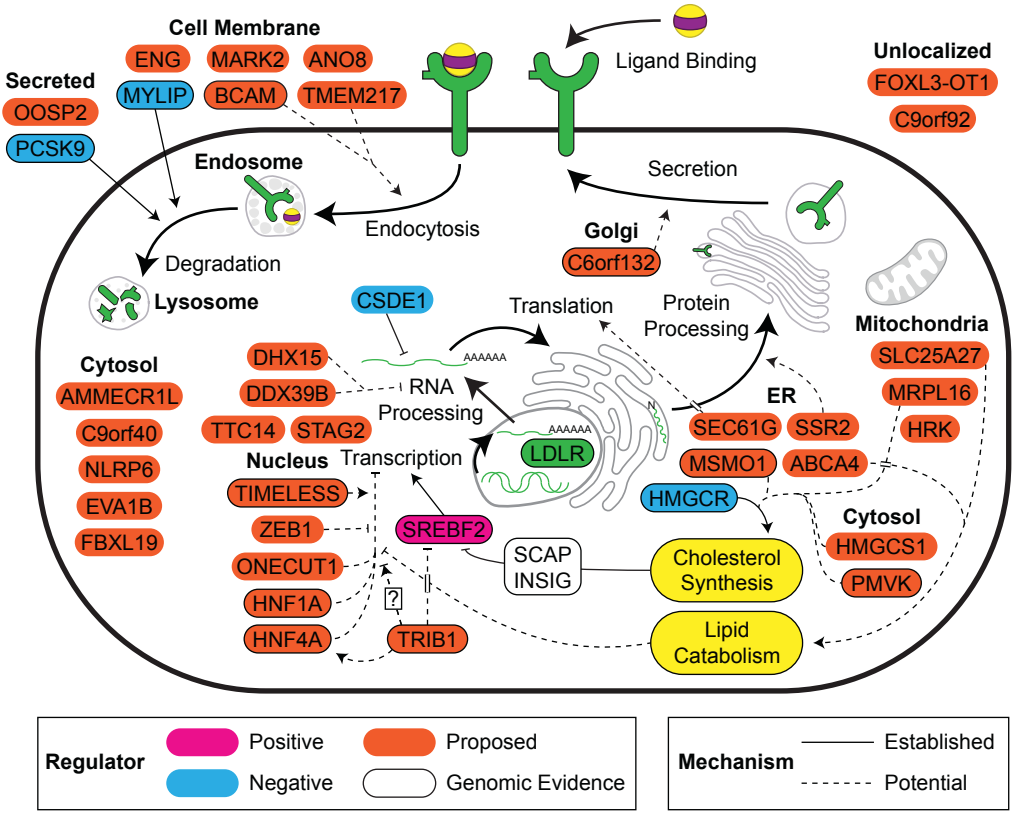
Cell Membrane
ENG
MARK2
ANO8
MYLIP
BCAM
TMEM217
Secreted
OOSP2
PCSK9
Ligand Binding
Unlocalized
FOXL3-OT1
C9orf92
Endosome
Endocytosis
Secretion
Degradation
Lysosome
Golgi
C6orf132
CSDE1
Translation
Protein Processing
Mitochondria
SLC25A27
MRPL16
HRK
Cytosol
AMMECR1L
C9orf40
NLRP6
EVA1B
FBXL19
DHX15
DDX39B
TTC14
STAG2
RNA Processing
ER
SEC61G
SSR2
MSMO1
ABCA4
HMGCR
LDLR
Nucleus
Transcription
TIMELESS
ZEB1
ONECUT1
HNF1A
HNF4A
?
TRIB1
SREBF2
SCAP
INSIG
Cholesterol Synthesis
Cytosol
HMGCS1
PMVK
Lipid Catabolism
Regulator
Positive
Negative
Proposed
Genomic Evidence
Mechanism
Established
Potential

Supplementary Materials

Table S10: Differentially Expressed Genes in Paigen Diet-Fed Mice by *in vivo* RNA Seq *(provided as an Excel file)*

Table S11: Enriched GO Terms in Paigen Diet-Fed Mice by *in vivo* RNA Seq *(provided as an Excel file)*

Table S12: Differentially Expressed Genes in Chow-Fed Mice by *in vivo* RNA Seq *(provided as an Excel file)*

Table S13: Enriched GO Terms in Chow-Fed Mice by *in vivo* RNA Seq *(provided as an Excel file)*

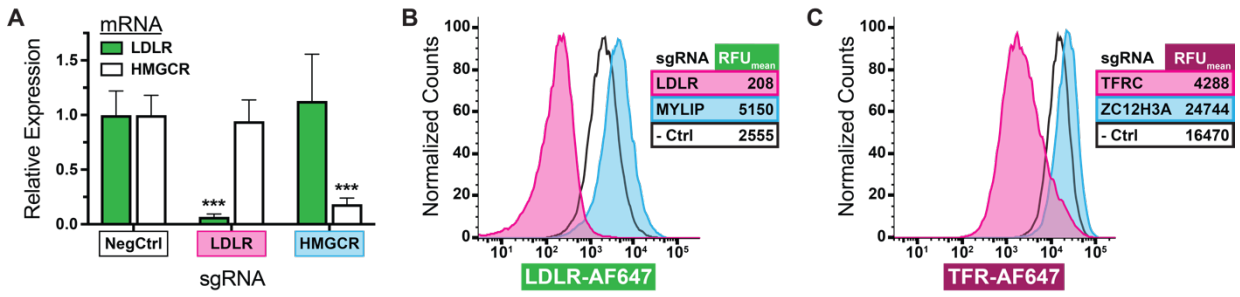

Supplementary Figure 1: Validation of dCas9-KRAB-HepG2 Cells. *A)* Relative expression, by RT-qPCR, of *LDLR* and *HMGCR* in engineered dCas9-KRAB HepG2 cells transduced with sgRNAs targeting the indicated genes. *B2M* used as RT-qPCR control. Error bars indicate 95% confidence intervals. *** = $p < 0.001$ by Holm-Sidak corrected t-test, comparing to negative control sgRNA of the same target. *B)* Flow cytometry analysis, by surface labeling with anti-LDLR-AF647, of dCas9-KRAB HepG2 cells transduced with sgRNAs targeting the indicated genes. Mean fluorescence shown in inset. *MYLIP* (IDOL) is an E3 ligase which ubiquitinates the LDLR, leading to lysosomal degradation *(26)*. *C)* Flow cytometry analysis as in *B* but transduced with indicated sgRNAs and labeled with anti-TFR-AF647. *ZC3H12A* (REG1) is an endoribonuclease that accelerates the degradation of TFR mRNA *(27)*.

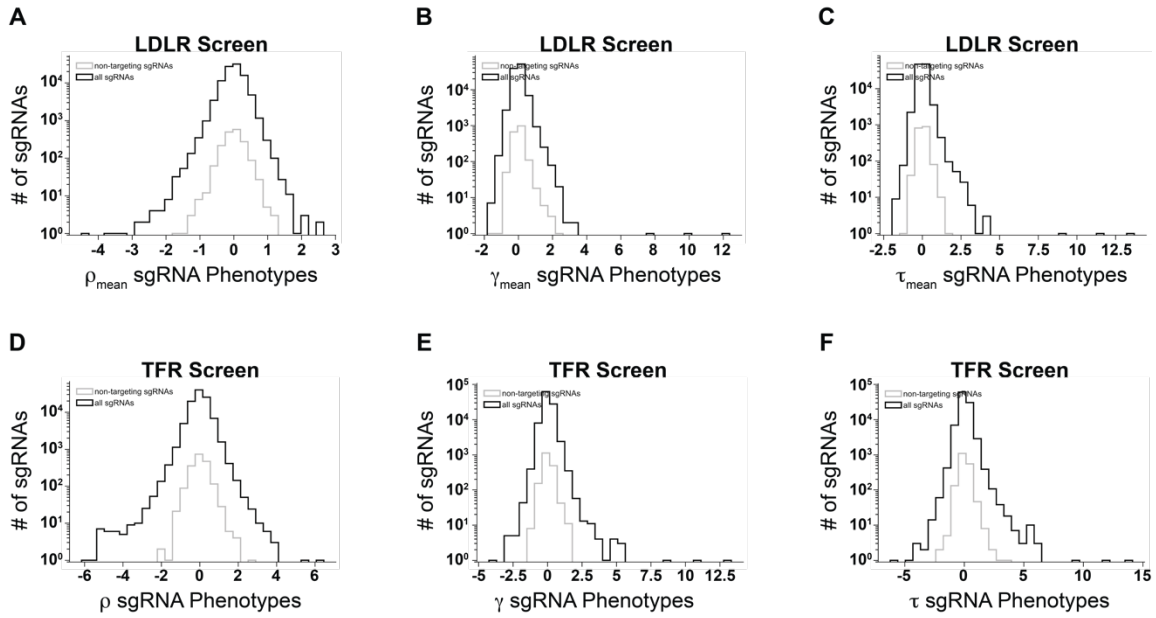

Supplementary Figure 2: Recovered sgRNAs from Screening Phenotypes. Distribution of number of guide RNAs recovered by phenotype in both LDLR *(A-C)* and TFR *(D-F)* screens. ρ *(A,D)* indicates $\log_2$ fold enrichment for sgRNA in high receptor abundance cells compared to low receptor abundance cells. γ *(B,E)* indicates $\log_2$ enrichment for sgRNA in low receptor abundance cells compared to unsorted population. τ *(C,F)* indicates $\log_2$ enrichment for sgRNA in high receptor abundance cells compared to unsorted population. Mean results are reported for the 3 replicates of the LDLR screen *(A-C)*.

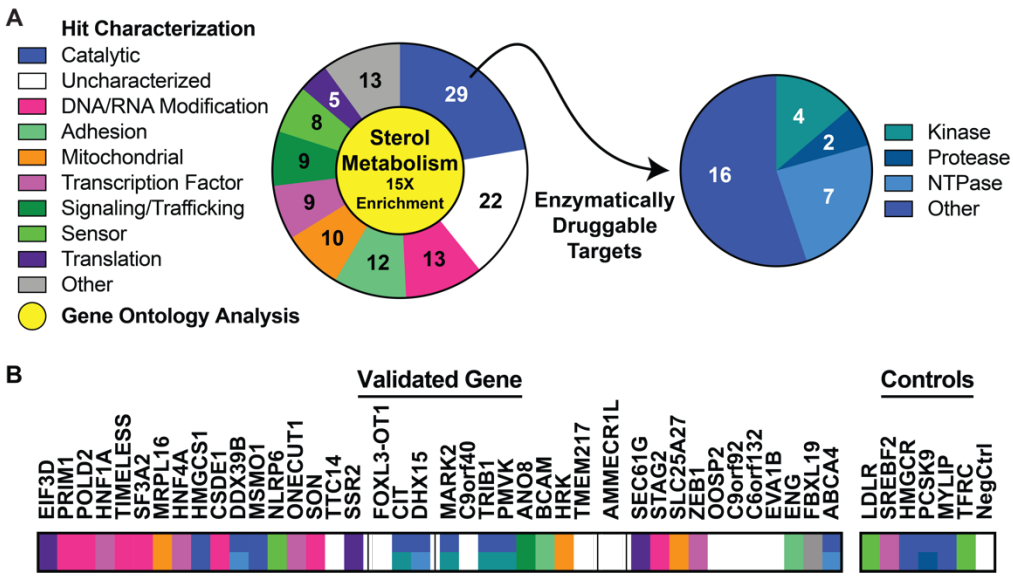

Supplementary Figure 3: Gene Ontology and Localization Analysis. *A)* Characterization of hits from the LDLR screen based on gene ontology (GO) and localization, along with results from GO enrichment analysis (yellow center). Note that multiple genes fall into more than one category. *B)* Primary classification of the 40 LDLR hits independently validated outside of the pooled screen and displayed, as in Fig. 2, according to the color codes in *A*.

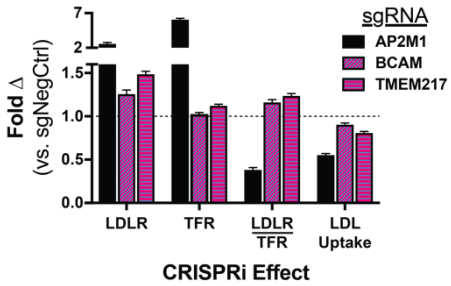

Supplementary Figure 4: Selective LDLR Effect of Transmembrane Proteins. Flow cytometric readout of receptor abundance and LDLR function assays, using CRISPRi knockdowns against genes thought to be involved in endocytosis. Data, which represents 3 to 4 independent experiments, are normalized to readout of negative control sgRNA within each experiment. Error bars represent 95% confidence intervals. Note the discontinuous Y axis.

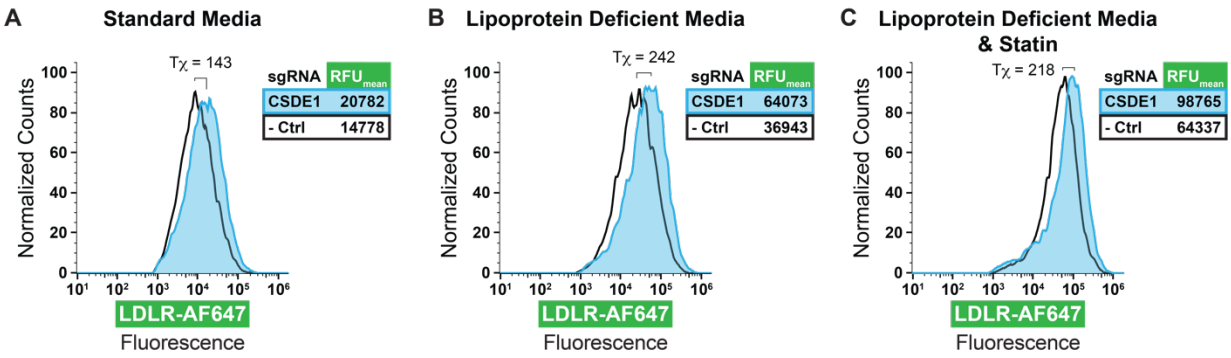

Supplementary Figure 5: Effect of Sterol Conditions on *CSDE1* Knockdown. Flow cytometry histograms showing AF647 conjugated anti-LDLR antibody labeling (as proxy for LDLR abundance) of engineered dCas9-KRAB HepG2 cells transduced with indicated sgRNAs and grown in standard growth media *(A)*, lipoprotein-deficient media *(B)*, or lipoprotein deficient media with a concomitant statin *(C)*. Tχ metric (FlowJo v10) *(105–107)* shown on graph, and mean fluorescence shown in insets. Data includes 3 independent experiments.

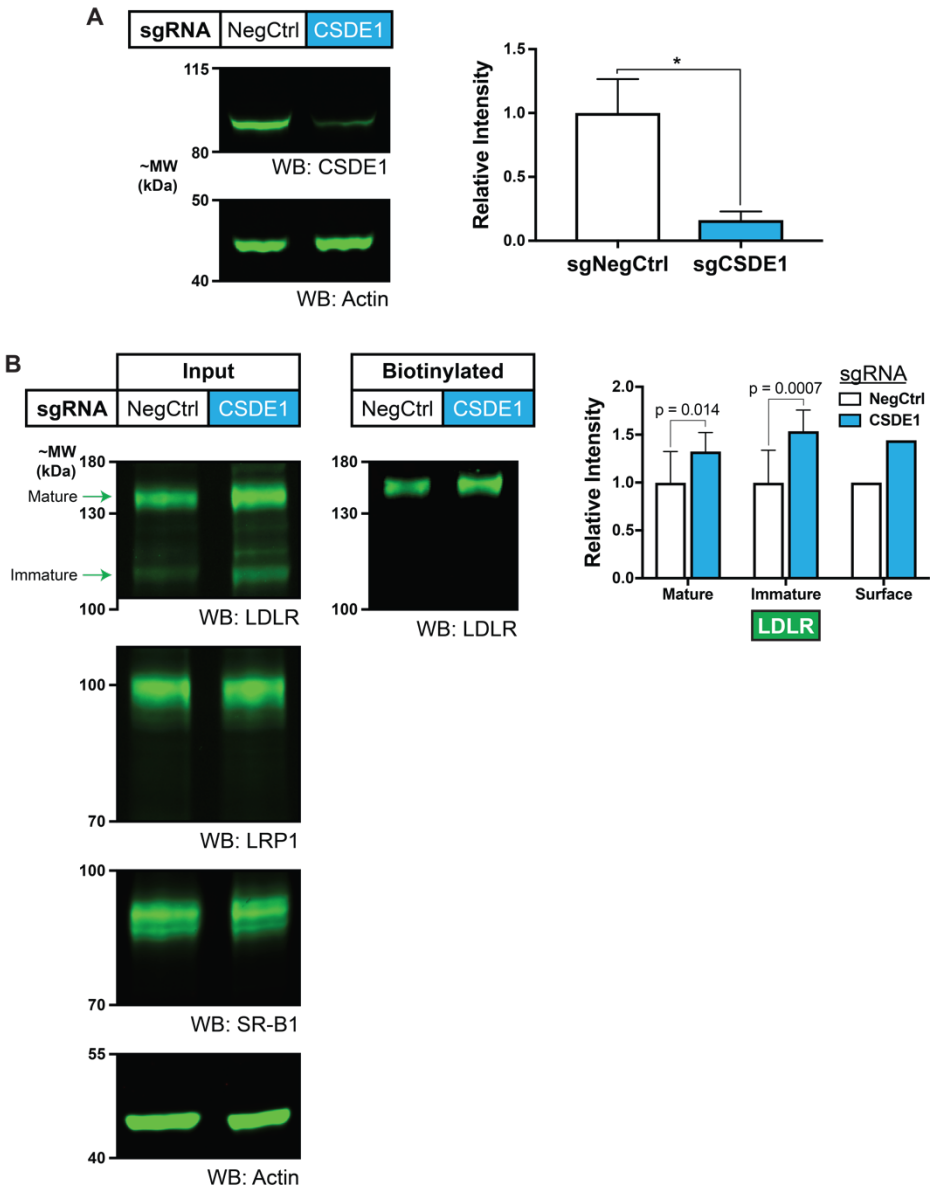

Supplementary Figure 6: Effect of CSDE1 Knockdown on Total and Cell Surface Proteins. *A)* Representative immunoblots of lysates of dCas9-KRAB HepG2 cells harboring indicated guide RNA. CSDE1 shown above and β-actin (loading control) shown below. Quantification of relative abundance of CSDE1 (normalized to loading control) shown at right. *B)* Representative immunoblots from same cells in *A* subjected to cell surface biotinylation assay. Input (total) and biotinylated (cell-surface) fractions shown. Quantification of relative abundance of LDLR (normalized to loading control) shown at right. No error bars are shown for surface LDLR quantification as the biological replicates were pooled to obtain the required amount of input for the pulldown. Data includes 3 independent experiments. * indicates $p < 0.05$ by Welch's t-test.

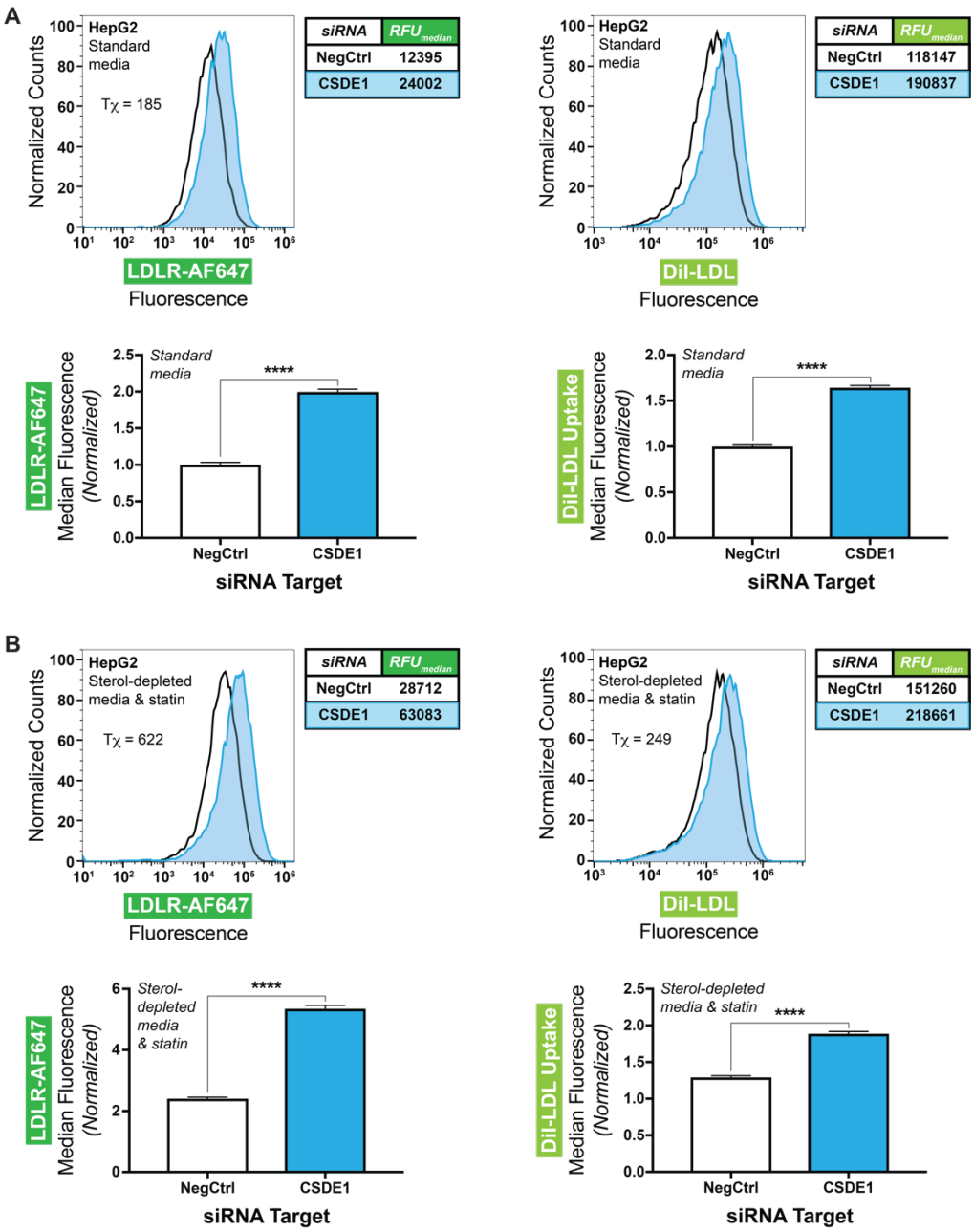

Supplementary Figure 7: Effect of siRNA Knockdown on HepG2 Cells. Flow cytometry histograms and graphical quantification of HepG2 cells treated with siRNA targeting *CSDE1* or a non-targeting control, showing AF647 conjugated anti-LDLR antibody labeling as proxy for LDLR abundance (left, dark green) or DiI conjugated LDL uptake (right, light green). Panels in *A* indicate cells grown with standard media, and panels in *B* indicate cells grown with sterol-depleted media supplemented with a statin. Tχ metric (FlowJo v10) *(105–107)* shown on histograms and median fluorescence shown in both insets and bar graphs. Error bars indicate 95% confidence intervals. **** indicates $p < 0.0001$ by Welch's t-test. Data includes 3 independent experiments.

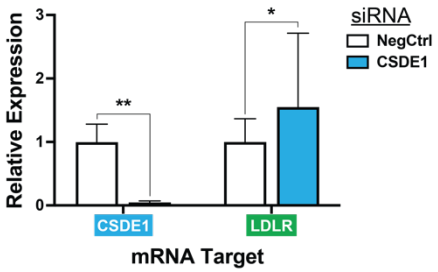

Supplementary Figure 8: Effect of siRNA Knockdown on Huh7 Cells. Relative expression, by RT-qPCR, of *CSDE1* and *LDLR* mRNA in Huh7 cells treated with siRNA targeting *CSDE1* or a non-targeting control. Error bars indicate 95% confidence intervals. ** indicates $p < 0.01$ and * indicates $p < 0.05$ by two-way matched ANOVA and Holm-Sidak multiple comparisons test. Data includes 3 independent experiments.

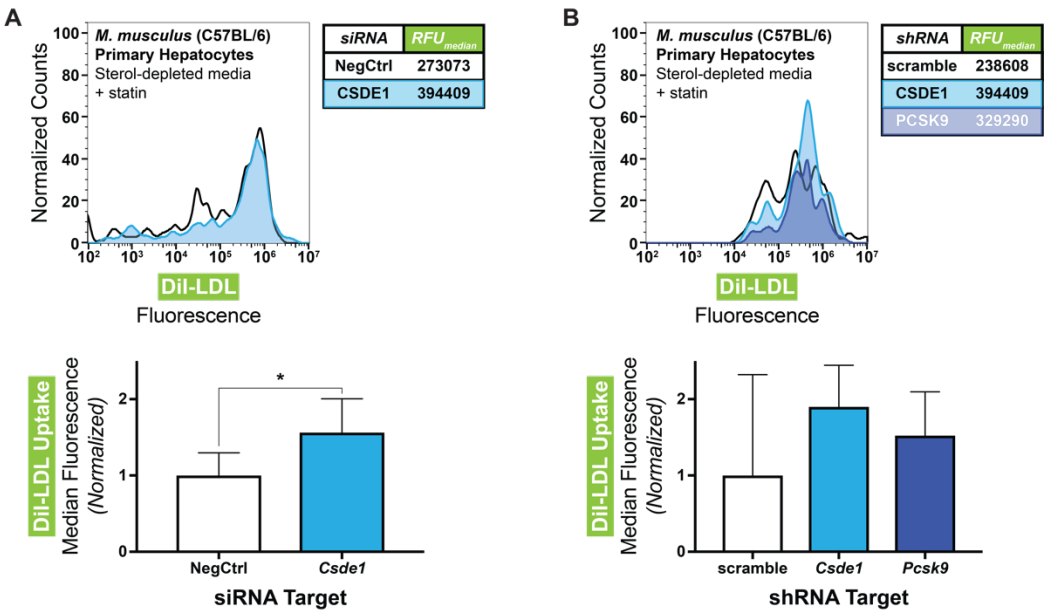

Supplementary Figure 9: Effect of *CSDE1* Knockdown on Primary Mouse Hepatocytes. Flow cytometry histograms and bar graphs showing DiI-conjugated LDL fluorescence of primary C57BL/6 mouse hepatocytes as proxy for functional LDL uptake. *A)* Mouse hepatocytes transfected with siRNA against Csde1 or a negative control. *B)* Mouse hepatocytes transduced with AAV8 vector encoding shRNA against either scramble control, *Csde1*, or *Pcsk9*. Error bars indicate 95% confidence intervals. * indicates $p < 0.05$ by Welch's t-test. Between group comparisons in *B* not statistically significant at $p > 0.05$ by ANOVA. Data includes 3 independent experiments.

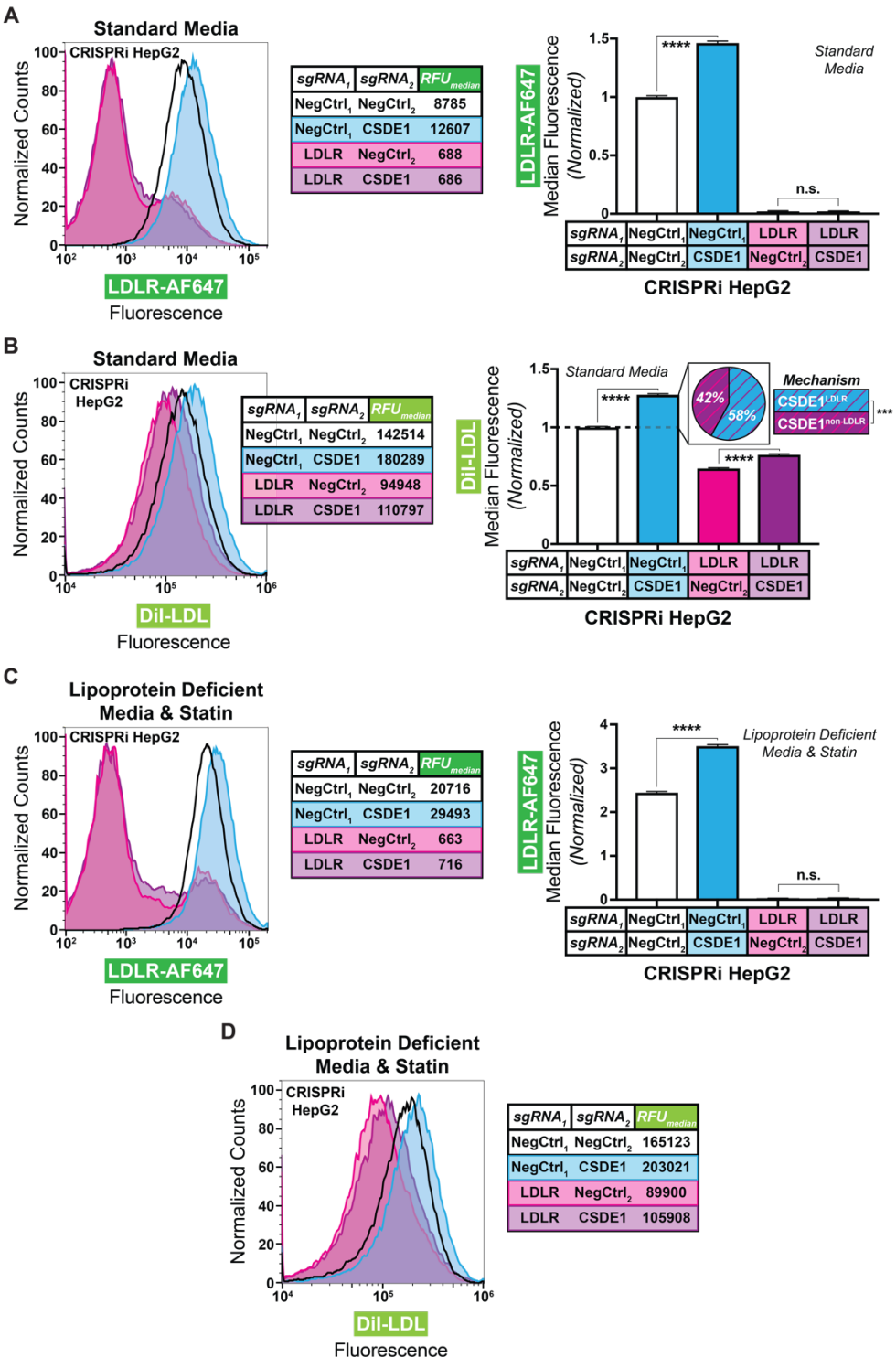

Supplementary Figure 10: Effect of Combined *CSDE1*/*LDLR* Knockdowns. Flow cytometry histograms and bar graphs showing AF647 conjugated anti-LDLR antibody labeling as proxy for LDLR abundance *(A,C)* or DiI conjugated LDL fluorescence as proxy for functional LDL uptake *(B,D)*. The CRISPRi HepG2 cells harbor two sgRNAs as indicated and are treated with either standard media *(A,B)* or sterol-depleted media with a concomitant statin *(C,D)*. Median

fluorescence also shown in insets. The pie chart *(B)* illustrates the relative contribution of LDLR-dependent ($CSDE1^{LDLR}$, blue with purple stripes) and LDLR-independent ($CSDE1^{non\text{-}LDLR}$, purple with magenta stripes) mechanisms to the increase in LDL uptake mediated by *CSDE1* knockdown. Data in bar graphs is normalized to the value of the control ($NegCtrl_1$/$NegCtrl_2$) CRISPRi cells in the standard media condition (dashed line). Error bars indicate 95% confidence intervals. n.s. indicates non-significant at $p > 0.05$, *** indicates $p < 0.001$, and **** indicates $p < 0.0001$ by one-way ANOVA with Tukey's multiple comparisons test or, for the comparison of mechanisms in *B*, unpaired t-test. Note that in this figure, all between group comparisons are significant at $p < 0.05$ unless indicated, as the annotation has been omitted to improve clarity. Data includes 3 independent experiments.

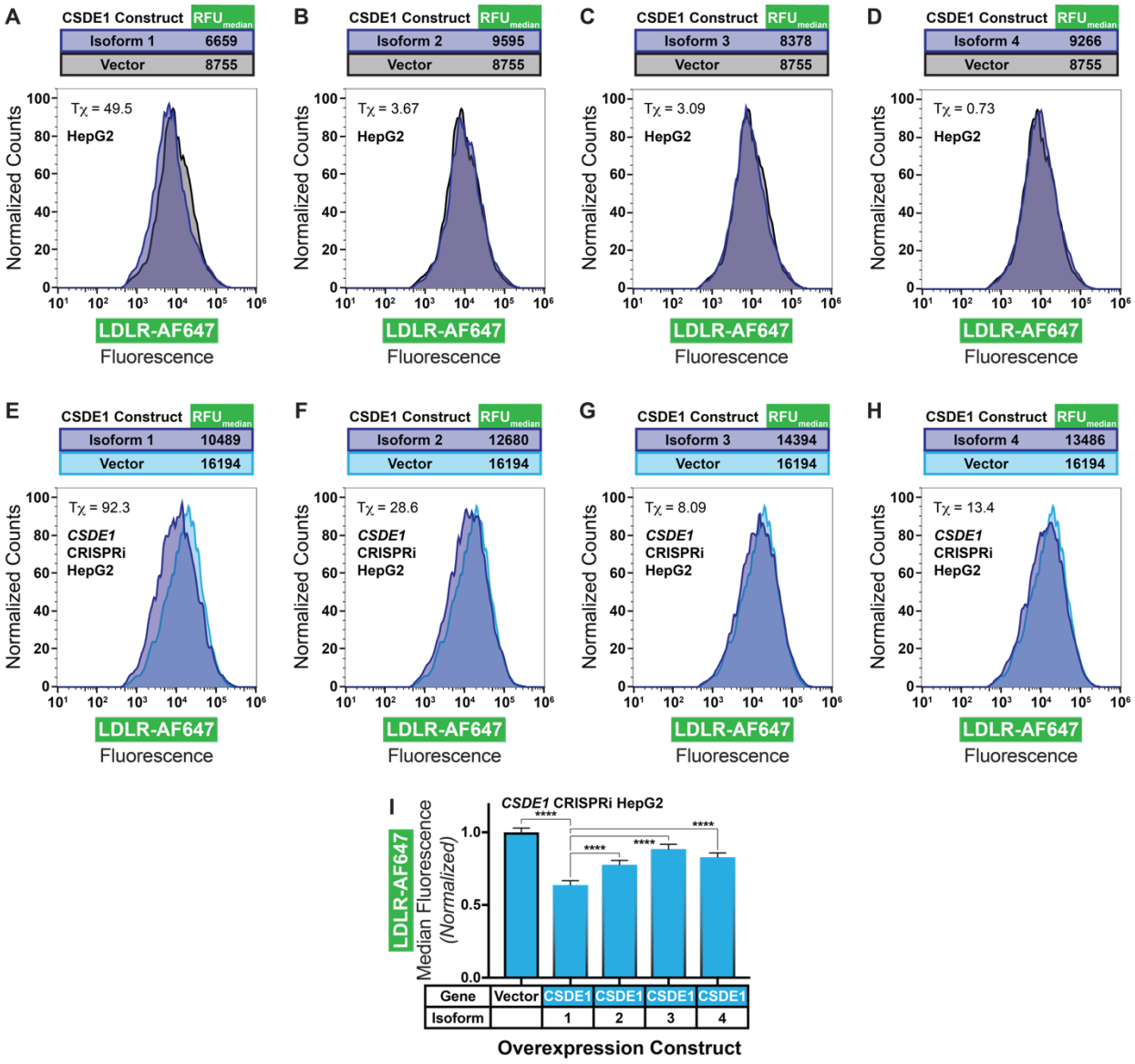

Supplementary Figure 11: Effect of *CSDE1* Overexpression. Flow cytometry histograms showing AF647 conjugated anti-LDLR antibody labeling (as proxy for LDLR abundance) of HepG2 cells *(A-D)* or engineered dCas9-KRAB HepG2 cells transduced with *CSDE1* targeting sgRNA *(E-H)* and transfected with an overexpression construct encoding the indicated CSDE1 isoform or vector alone. Tχ metric (FlowJo v10) *(105–107)* shown on graphs, and median fluorescence shown above. Quantified relative LDLR abundance of the data from *E-H* shown in *I*, with one-way ANOVA with Tukey's multiple comparisons test shown. Error bars indicate 95% confidence intervals. **** = $p < 0.0001$. Data from 3 independent experiments.

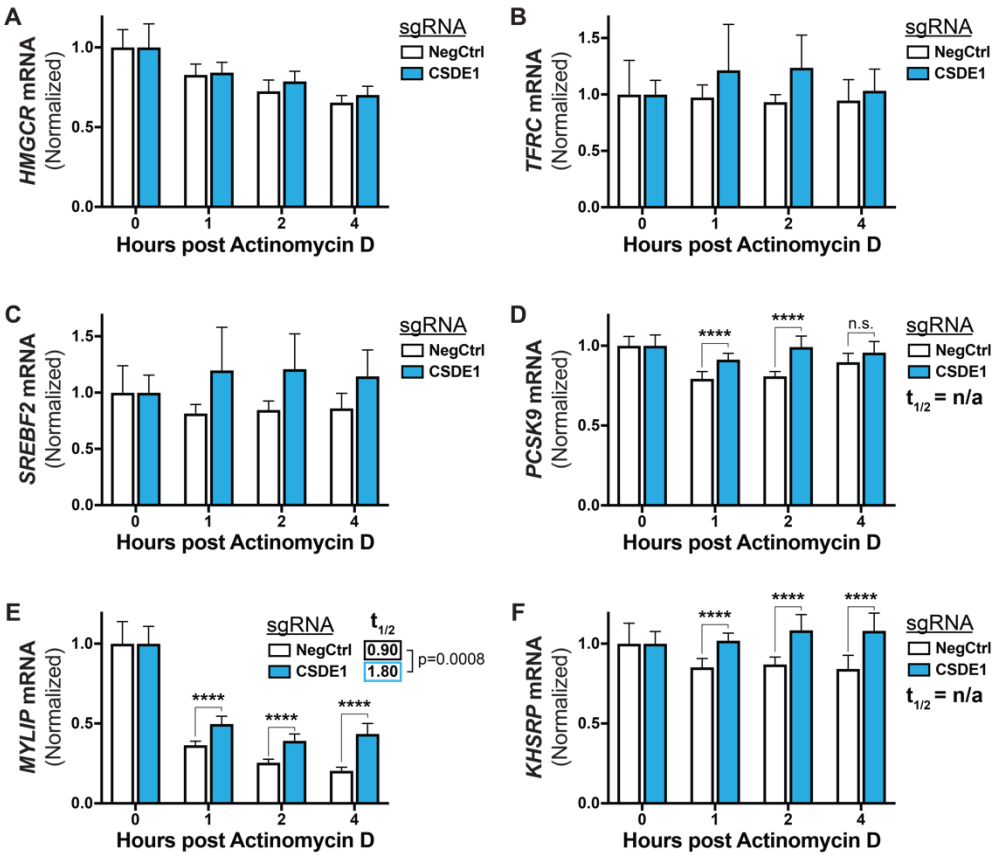

Supplementary Figure 12: Effect of *CSDE1* Knockdown on Decay of Non-*LDLR* Transcripts. Relative expression, by RT-qPCR, of *HMGCR (A), TFRC (B), SREBF2 (C), PCSK9 (D), MYLIP (E),* or *KHSRP (F)* mRNA in dCas9-KRAB HepG2 cells transduced with indicated sgRNAs and subjected to arrest of transcription with actinomycin D. Data are normalized to results at T=0 within the sgRNA evaluated to illustrate the change in time, and therefore no comparison can be drawn between sgRNAs at T=0. Data represent summary results from 3 to 6 independent experiments. Error bars = 95% confidence intervals. **** indicates $p < 0.0001$ by unpaired t-tests with Holm-Sidak correction. All unlabeled pairwise comparisons are nonsignificant at $p > 0.05$. Extra sum-of-square F test shown for one-stage exponential decay equation in *E*.

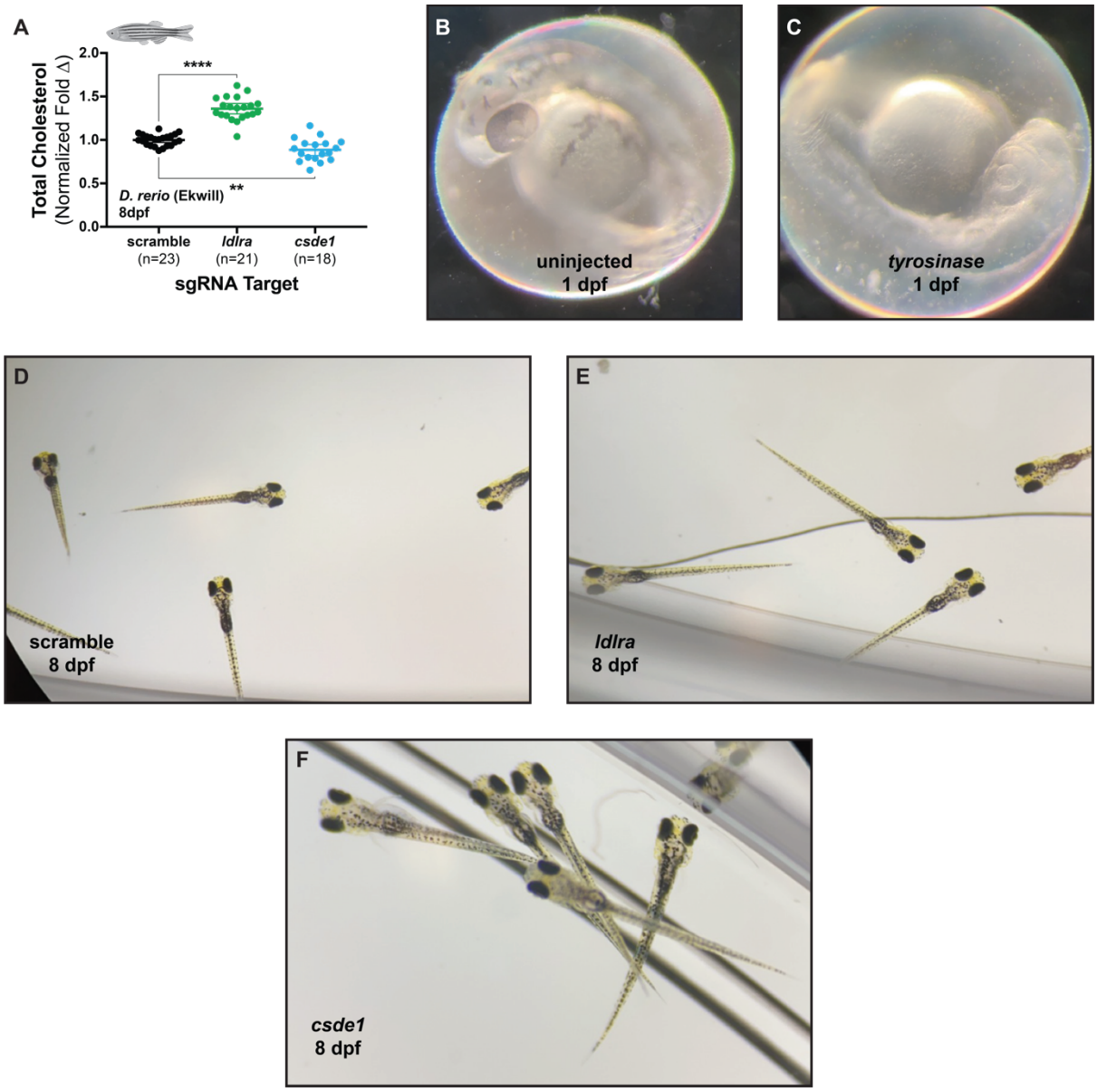

Supplementary Figure 13: Zebrafish Cas9-sgRNA Saturation Gene Disruption. *A)* Total cholesterol, in µg cholesterol per mg of total protein, of homogenates of 8 days post fertilization (dpf) zebrafish larvae fed a high-cholesterol diet and subjected to Cas9 mediated gene disruption of indicated target. Data are normalized to the scramble control of a particular experiment. Each point represents a homogenate consisting of 10 larvae. Data represent summary information from 4 independent experiments. One-way ANOVA with Holm-Sidak's multiple comparisons test shown. *B,C)* Representative microscopic images of zebrafish larvae at 1 day post fertilization without *(B)* or with *(C)* injected Cas9 and redundant guides against tyrosinase control performed concomitantly with each zebrafish experiment. Albinism is the readout for successful injections. *D-F)* Representative microscopic images of zebrafish larvae at 8 dpf and with injected Cas9 and guides against scramble controls *(D)*, *ldlra (E)*, and *csde1 (F)*.

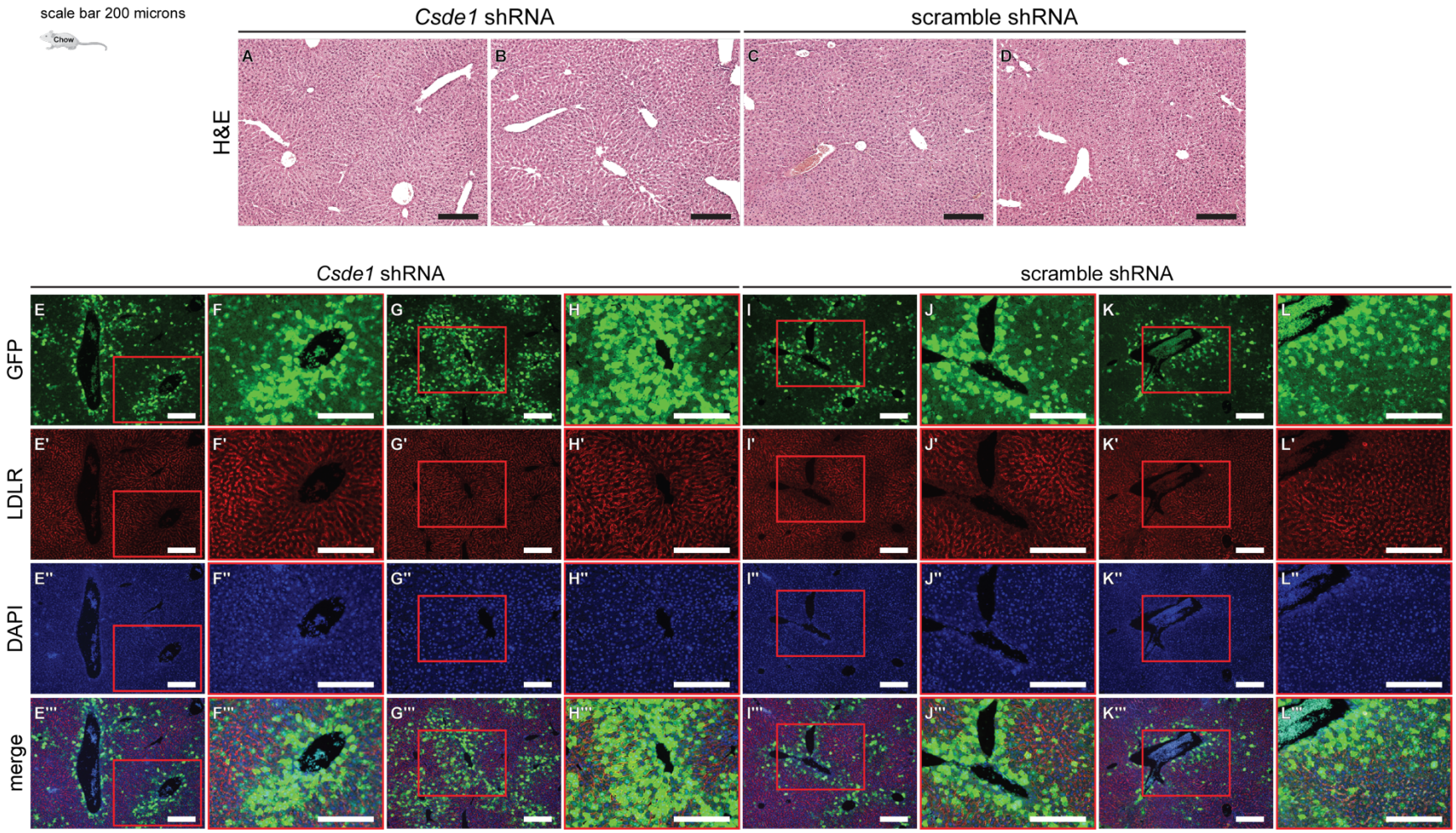
scale bar 200 microns
Chow
Csde1 shRNA
scramble shRNA
H&E
A
B
C
D
Csde1 shRNA
scramble shRNA
GFP
LDLR
DAPI
merge
E
F
G
H
I
J
K
L
E'
F'
G'
H'
I'
J'
K'
L'
E''
F''
G''
H''
I''
J''
K''
L''
E'''
F'''
G'''
H'''
I'''
J'''
K'''
L'''

Supplementary Figure 14: Histology and Immunohistochemistry of AAV8-treated Chow-Fed Mice. *A-D)* Representative histologic images from hematoxylin & eosin staining of mouse liver tissue. Two mice from each treatment arm shown. *E-L)* Representative immunohistochemical images from GFP and LDLR costained mouse liver tissue. 4',6-diamidino-2-phenylindole (DAPI) and merged images also shown. Two mice from each treatment arm shown. *All panels)* Scale bar at 200 μm.

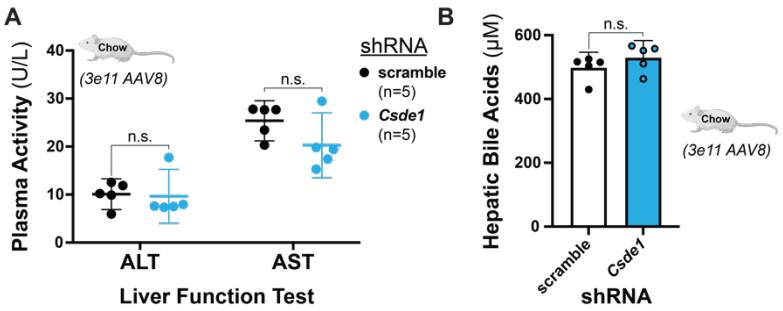

Supplementary Figure 15: Additional Effects of *in vivo Csde1* Disruption in Chow-Fed Mice. *A)* Mean plasma alanine and aspartate aminotransferase activities (ALT and AST, respectively) in chow-fed C57BL/6 mice 1 week after transduction with moderate dose AAV8-shRNA. *B)* Mean total bile acids in liver tissue in same mice from *A*. *Both panels)* Pairwise comparison analyzed by unpaired t-test. Error bars indicate 95% confidence intervals.

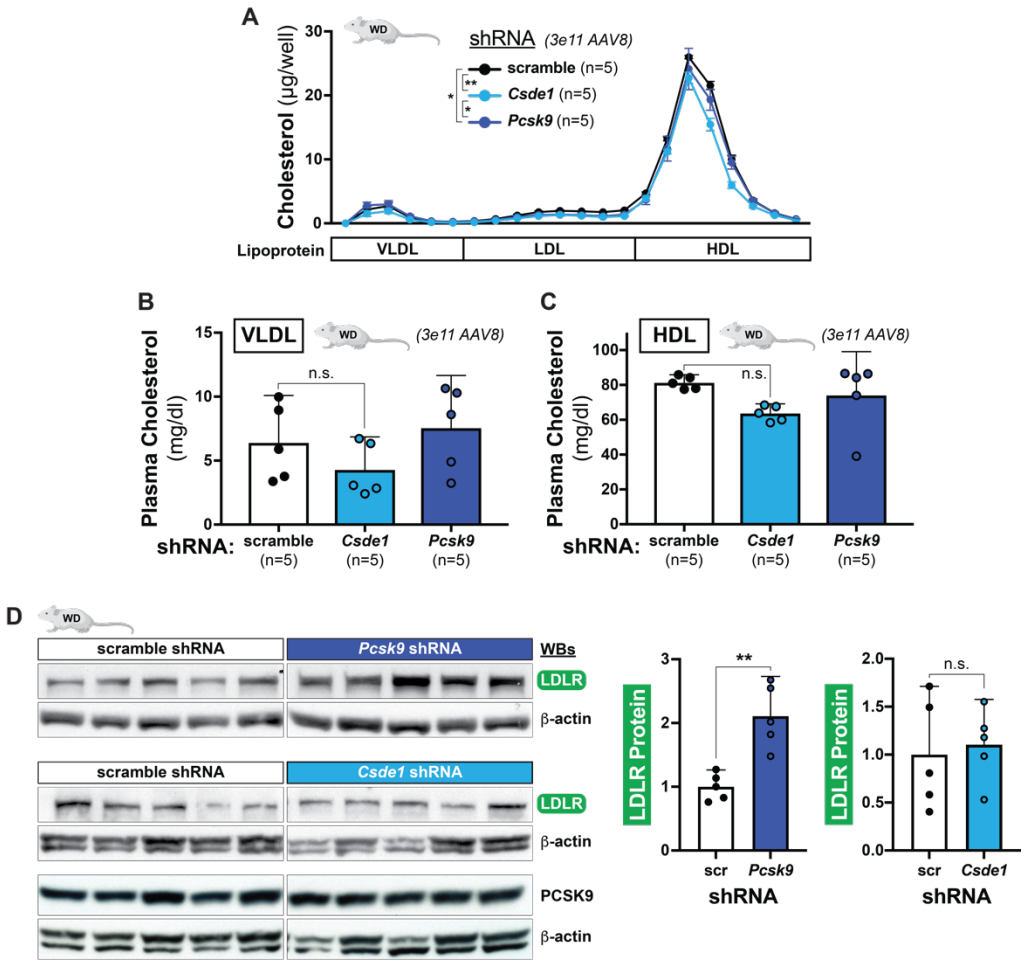

Supplementary Figure 16: Additional Effects of *in vivo Csde1* Disruption in Western Diet-Fed Mice. *A)* Mean cholesterol of gel filtration fractions collected from individual Western diet-fed mice transduced with moderate dose AAV8-shRNA. Matched one-way ANOVA with Geisser-Greenhouse correction and Tukey's multiple comparisons test shown. Error bars indicate standard error of the mean. *B, C)* Mean total cholesterol of VLDL *(B)* and HDL containing fractions *(C)* from gel filtration experiment of Western diet-fed mice in *A*. Data analyzed by one-way ANOVA with Tukey's multiple comparisons test. *D)* Immunoblots of mouse liver lysate from the Western diet-fed mice. Quantification of LDLR blots shown in graphs at right. Pairwise comparisons by unpaired t-test. *All panels)* * = $p < 0.05$, ** = $p < 0.01$. Error bars indicate 95% confidence intervals except as noted in *A*.

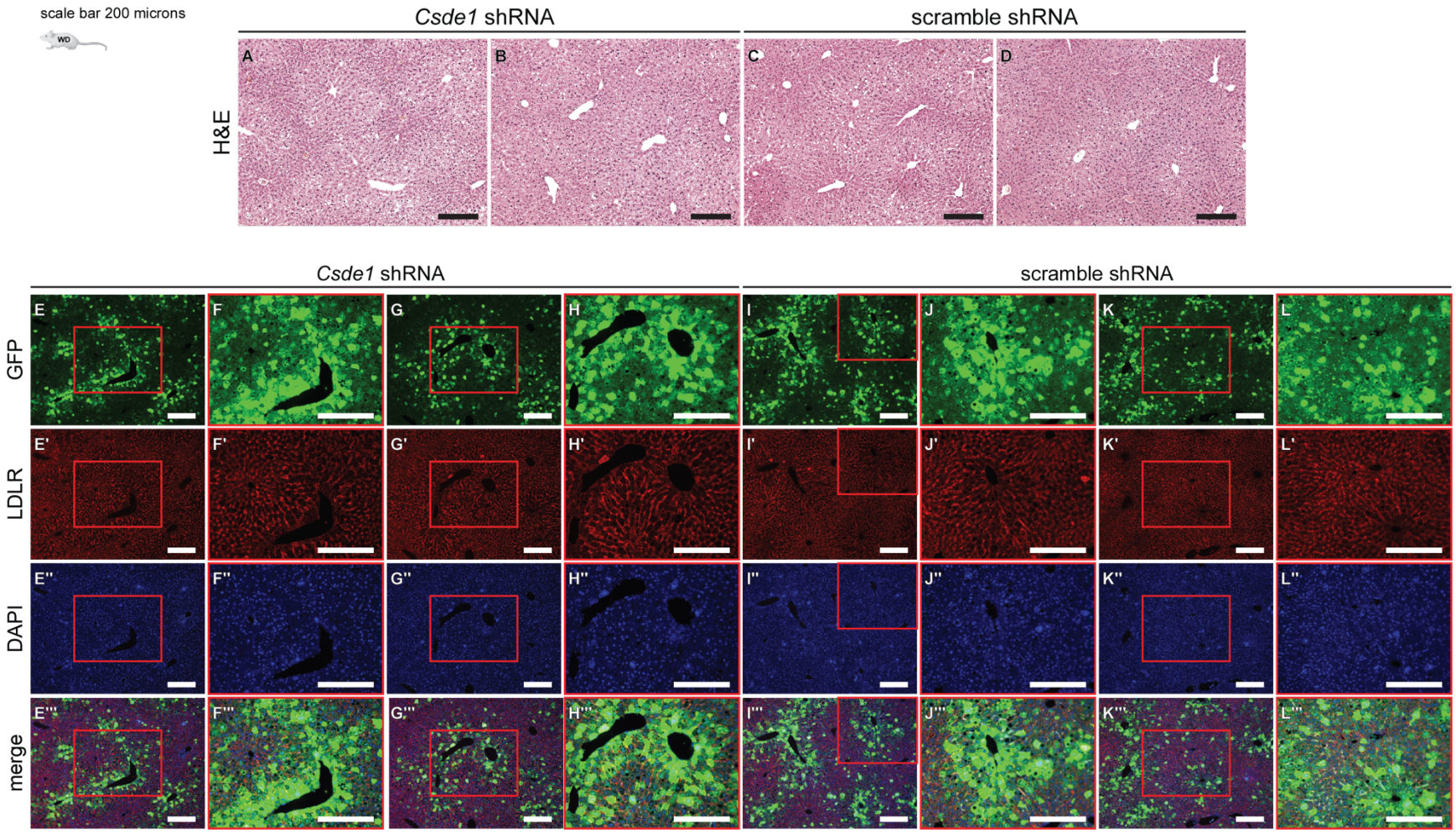
scale bar 200 microns
WD
Csde1 shRNA
scramble shRNA
H&E
A
B
C
D
Csde1 shRNA
scramble shRNA
GFP
LDLR
DAPI
merge
E
F
G
H
I
J
K
L
E'
F'
G'
H'
I'
J'
K'
L'
E''
F''
G''
H''
I''
J''
K''
L''
E'''
F'''
G'''
H'''
I'''
J'''
K'''
L'''

Supplementary Figure 17: Histology and Immunohistochemistry of AAV8-treated Western Diet-Fed Mice. *A-D)* Representative histologic images from hematoxylin & eosin staining of mouse liver tissue. Two mice from each treatment arm shown. *E-L)* Representative immunohistochemical images from GFP and LDLR costained mouse liver tissue. DAPI and merged images also shown. Two mice from each treatment arm shown. *All panels)* Scale bar at 200 μm.

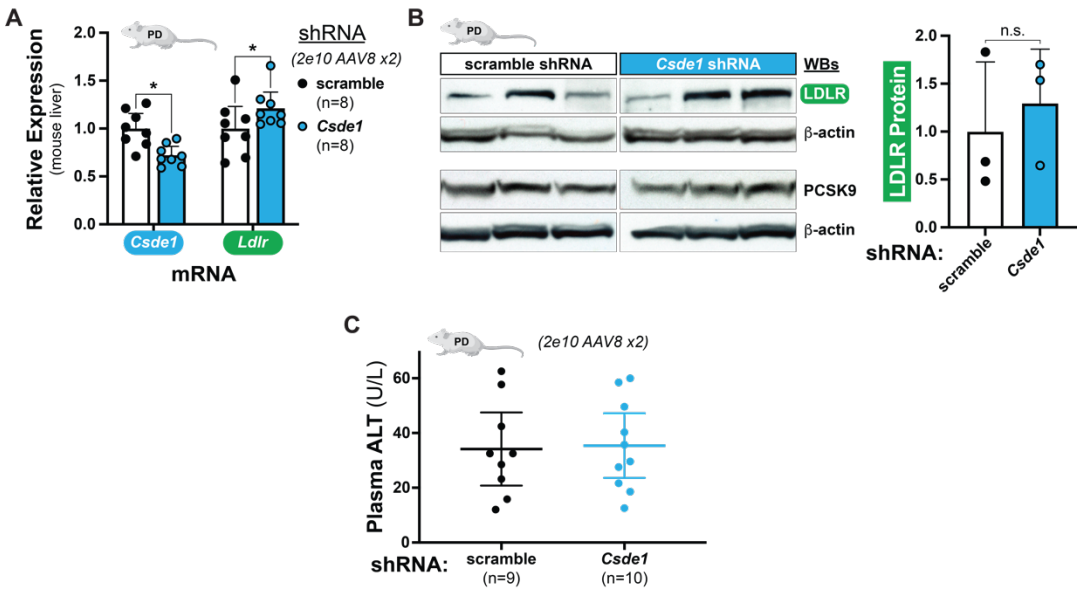

Supplementary Figure 18: Additional Effects of *in vivo Csde1* Disruption in Paigen Diet-Fed Mice. *A)* Relative expression, by RT-qPCR, of hepatic *Csde1* and *Ldlr* transcripts in Paigen diet-fed mice transduced with indicated low-dose AAV8-shRNA. Data analyzed by matched two-way ANOVA with Holm-Sidak multiple comparisons test. *B)* Immunoblots of mouse liver lysate from the Paigen diet-fed mice. Quantification of LDLR blot shown in graph at right. Pairwise comparisons by unpaired t-test. Error bars indicate standard deviation. *C)* Mean plasma ALT activity in Paigen diet-fed C57BL/6 mice 2 weeks after second transduction with low-dose AAV8-shRNA. Data analyzed by unpaired t-test. *Both panels)* * = $p < 0.05$. Error bars indicate 95% confidence intervals except as noted in *B*.

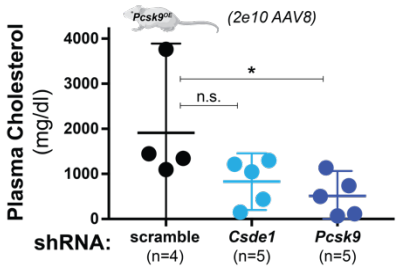

Supplementary Figure 19: Additional Effects of *in vivo Csde1* Disruption in *Pcsk9*-D377Y Overexpressing Paigen Diet-Fed Mice. Mean plasma cholesterol of *Pcsk9*-D377Y overexpressing and Paigen diet-fed mice 2 weeks after transduction with low-dose AAV8-shRNA. One- way ANOVA with Dunnet's multiple comparisons test shown. * = $p < 0.05$. Error bars indicate 95% confidence intervals.

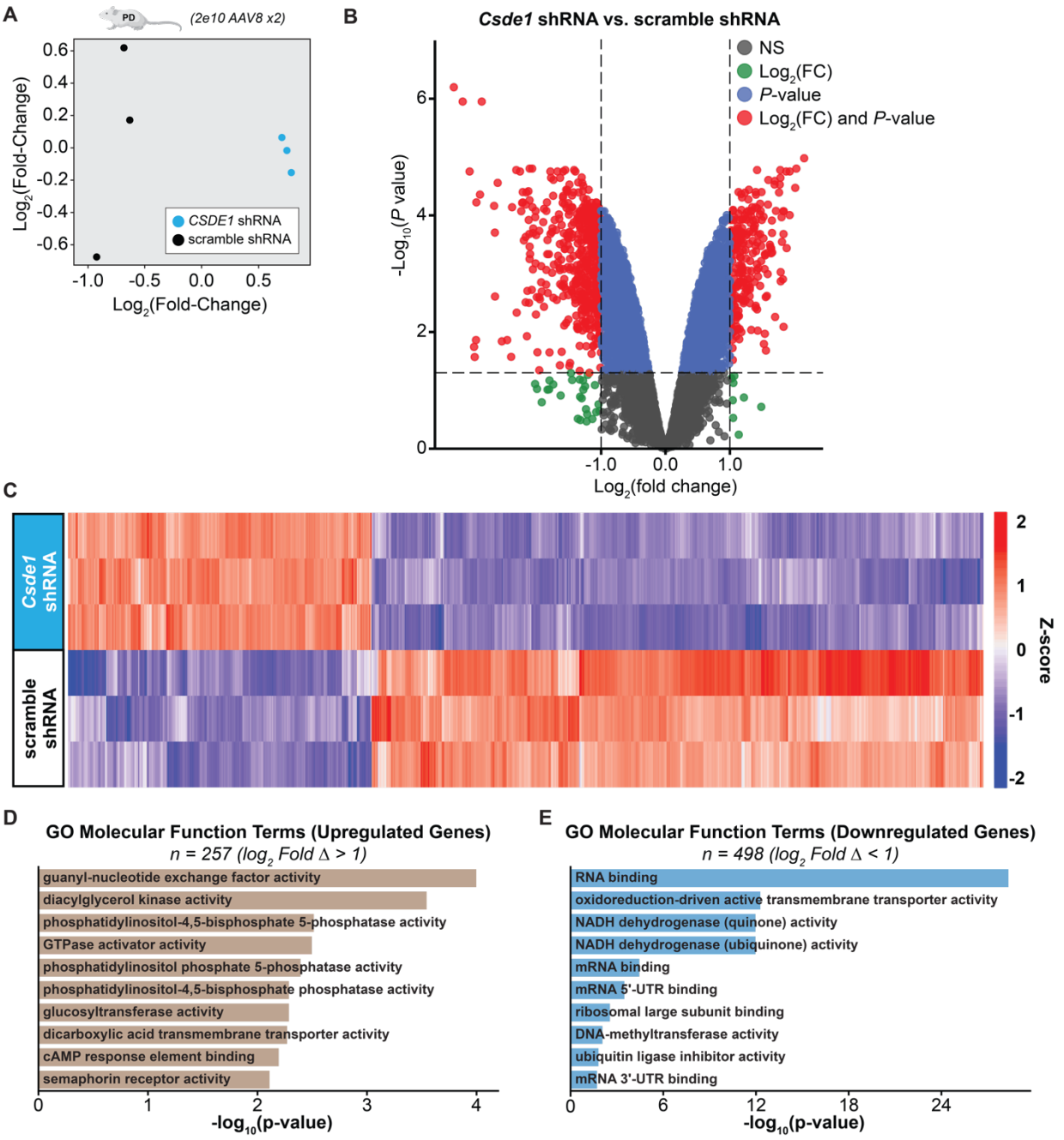

Supplementary Figure 20: RNA-seq Analysis of *Csde1* Disruption in Paigen Diet-Fed Mice. *A)* Unsupervised cluster analysis of individual mice analyzed for differential gene analysis. Each data point represents an individual mouse. *B)* Volcano plot showing differentially expressed genes between *Csde1* and scramble shRNA treatment arms in Paigen-diet fed mice, filtered for effects of viral transduction. Statistical significance is shown on the y axis and strength of effect is shown on the x axis. Comparison made among the 3 mice in each arm with the highest *eGFP* transcript expression, as a proxy for transduction efficiency. Genes reaching threshold significance for p-value (adj. $p < 0.05$, blue), $\log_2$ fold change ($> |1|$, green), both (red), or neither (grey) annotated accordingly. *C)* Heatmap of differentially expressed genes ($\log_2$ fold change >

|1|, adj. $p < 0.05$) of the individual mice analyzed by RNA-seq. Mice transduced with AAV8-scramble-shRNA at the bottom and those transduced with AAV8-*Csde1*-shRNA at the top. Each row represents an individual mouse. *D,E)* Leading upregulated *(D)* and downregulated *(E)* molecular function GO terms in the differentially expressed genes (adj. $p < 0.05$, $\log_2FC < |1|$) in *Csde1* knockdown mice on the Paigen diet.

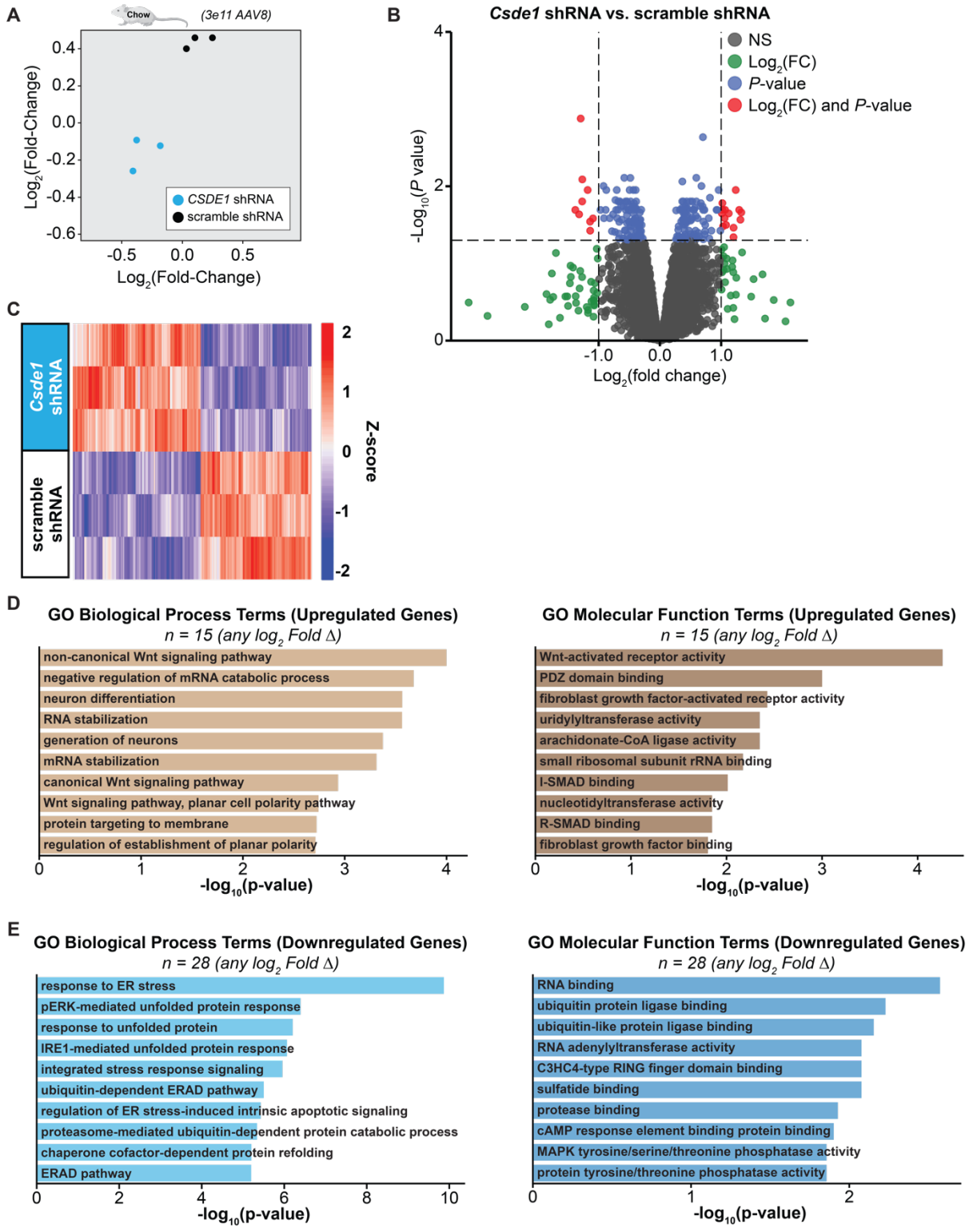

Supplementary Figure 21: RNA-seq Analysis of *Csde1* Disruption in Chow-Fed Mice. *A)* Unsupervised cluster analysis of individual mice analyzed for differential gene analysis. Each data point represents an individual mouse. *B)* Volcano plot showing differentially expressed genes between *Csde1* and scramble shRNA treatment arms in chow-fed mice. Statistical

significance is shown on the y axis and strength of effect is shown on the x axis. Comparison made among the 3 mice in each arm. Genes reaching threshold significance for p-value (adj. $p < 0.05$, blue), $\log_2$ fold change ($> |1|$, green), both (red), or neither (grey) annotated accordingly. *C)* Heatmap of all differentially expressed genes (adj. $p < 0.05$) of the individual mice analyzed by RNA-seq. Mice transduced with AAV8-scramble-shRNA at the bottom and those transduced with AAV8-*Csde1*-shRNA at the top. Each row represents an individual mouse. *D,E)* Leading upregulated *(D)* and downregulated *(E)* biological process (left) and molecular function (right) GO terms in the differentially expressed genes (adj. $p < 0.05$, any $\log_2$FC) in *Csde1* knockdown mice on the chow diet.

Metric	Value
Age (y)	56.9 (7.9)
Sex	179,963 (46.1%)
European ancestry	376,358 (96.4%)
Cholesterol (mg/dl)	
Total	221.1 (44.3)
HDL	56.1 (14.8)
LDL	138.1 (33.7)
Triglycerides (mg/dl)	132.6 [93.6-191.5]
Statin Rx	64,004 (16.4%)
BMI (kg/m^2)	27.4 (4.8)
Systolic blood pressure (mmHg)	140.2 (19.7)
Diastolic blood pressure (mmHg)	82.3 (10.7)
Current smoker	39,736 (10.2%)
Diabetes mellitus type 2	25,349 (6.5%)
Coronary artery disease	18,204 (4.8%)

Supplementary Table 7: Baseline Characteristics of UK Biobank Participants in Genomic Association Analyses. Continuous values are presented as mean (standard deviation) except for triglycerides which is given as median (Q1-Q3) due to the skewness of the triglyceride distribution. Categorical data are presented as count (percentage). BMI = body-mass index; HDL = high-density lipoprotein; LDL = low-density lipoprotein.